Study on the mechanism of metal nano-oxide induced stress on 'Type 2 Pneumocytes' cultured *in vitro.*

THESIS

Submitted in partial fulfillment of the requirements for the degree of

DOCTOR OF PHILOSOPHY

by

Ansie Martin

Supervisor

Prof. Angshuman Sarkar

Co-Supervisor

Prof. Samit Chattopadhyay

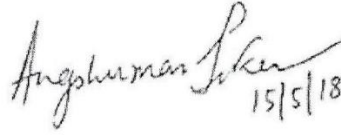BIRLA INSTITUTE OF TECHNOLOGY AND SCIENCE, PILANI

2018

BIRLA INSTITUTE OF TECHNOLOGY AND SCIENCE, PILANI

CERTIFICATE

This is to certify that the thesis entitled 'Studies on The Mechanism of Metal Nano-Oxide Induced Stress in Type 2 Pneumocytes Cultured *in vitro*'. submitted by Ansie Martin. ID No. 2012PHXF0009G for the award of Ph.D. of the Institute embodies original work done by her under our supervision.

Signature of Supervisor

15|5|18

Dr. Angshuman Sarkar, Ph. D.
Associate Professor
BITS Pilani KK Birla Goa Campus
Zuarinagar, Goa, Pin-403726

Name in capital letters: ANGSHUMAN SARKAR. Ph.D.

Designation: Associate Professor.
Department of Biological Sciences
Birla Institute of Technology & Science. Pilani.
K K Birla Goa Campus

Signature of Co-Supervisor

16|5|18

Name in capital letters: SAMIT CHATTOPADHYAY. Ph.D.

Designation: Director.

Indian Institute of Chemical Biology. Kolkata.
4. Raja. Raja Subodh Chandra Mallick Rd.
Poddar Nagar. Jadavpur. Kolkata.
West Bengal 700032

निदेशक
Director
केन्द्रीय रासायनिक जीवविज्ञान संस्थान
(वैज्ञानिक तथा औद्योगिक अनुसंधान परिषद्)
Indian Institute of Chemical Biology
(Council of Scientific & Industrial Research)
4, राजा एस. सी. मल्लिक रोड, जादवपुर
4, Raja S. C. Mullick Road Jadavpur
कोलकाता/Kolkata-700 032

Ph.D.!

If you can't fly then run, run then walk, walk then crawl, but whatever you do you have to keep moving forward.

- *Martin Luther King Jr.*

ACKNOWLEDGEMENTS

Happiness cannot be traveled to, owned, earned, worn or consumed. Happiness is the spiritual experience of living every minute with love, grace and gratitude.

- *Denis Waitley*

To begin with, I would sincerely acknowledge with gratitude, the invaluable guidance and friendship of my supervisor Prof. Angshuman Sarkar. His consistent patience and motivation was indispensable in helping me complete my Ph.D. Not only did he provide the much-needed insight at every step of my academic progress, but also encouraged me greatly to think freely and implement my ideas. This has led me to develop techniques and discover some very novel molecular routes in the field of nanotoxicology. Beyond just intellectual mentorship, Prof. Angshuman Sarkar has been a healer, a friend and a trustworthy confidant in times of great need. I have had the misfortune of losing my elder brother Capt. Allen Martin, whilst he was on duty in September 2013. The following year in October 2014, I lost my beloved mother, Mrs. Flora Martin to Alzheimers. And my grief just escalated when I lost my dear father, Prof. J. Y. Martin to kidney failure in Aug 2016. These were incredibly tough times in my life, where let alone completing my Ph.D, I got highly dysfunctional. I could not think straight for years. The depression was unbearable, and I have had many chronic health issues that had come about because of it, from time to time.

My father, used to be my strength, still is, and he urged me to finish my education, despite the illness, the deaths and the

court cases that were troubling our family. Many people had taken advantage of the severity facing my family and I was left very torn between my responsibilities towards my family and completing my education. Without my father, I would not have been alive, let alone continued with my education. He forgave me, he made so many sacrifices for me. At his own cost, he cared for me in ways I might never even understand in this life time. I am blessed to have had him as my father and today when I have learned to pick up my pieces and move on, I only have the deepest of gratitude and joy whenever I remember all my family members.

Prof. Angshuman Sarkar has kindly been very accommodating of my setbacks with respect to my health issues including providing me time for any number of therapy sessions I needed to recover from my depression. Today as I stand on the verge of completion of this Ph.D which for me has also been a huge emotional investment, I feel hugely, indebted to my father, Prof. J. Y. Martin and to Prof. Angshuman Sarkar.

I thank Prof. Samit Chattopadhyay, my co-supervisor for his valuable support and guidance. I extend my humble gratitude to my Doctoral Advisory Committee (DAC) members, Prof. Meenal Kowshik and Prof. Sumit Biswas. They have inspired me to work harder, evaluated my research proposal and guided me, throughout my research work. I would also like to thank Prof. Meenal Kowshik and Prof. Judith M Braganca for all their support and encouragement whilst they were the head of the department. Dr. Sumit Biswas has been warm and supportive throughout my stay at BITS, I particularly thank him for his kindness.

To

My Family,

Dad, Mom and Ally

TABLE OF CONTENTS

LIST OF FIGURES AND TABLES

Review of Literature

Chapter 1: Differences and similarities in cellular responses of A549 cells to ZnO and TiO$_2$ nanoparticle exposure.

ABBREVIATIONS

µm – micrometer

A2M-alpha-2 macroglobulin

A549 - adenocarcinomic human alveolar basal epithelial cells

ADP - adenosine diphosphate

$Al(NO_3)_3$ – aluminum nitrate

Al_2O_3 – aluminum oxide

ALI – air liquid interface

apoA1- apolipoprotein A1

ATF - activating transcription factor

ATG – autophagy related protein

ATM - ataxia telangiectasia mutated protein

ATP - adenosine triphosphate

ATR - ATM and RAD3-related protein

AURK – aurora kinase

Bak – Bcl-2 homologous antagonist killer protein

BAL – broncho alveolar lavage fluid

BARC - Bhabha Atomic Research Centre, Mumbai

Bax – Bcl-2-associated X protein

Bcl2 – B cell lymphoma 2 encoded gene family member

BER – base excision repair

Bi_2O_3 – bismuth (III) oxide

BITS - Birla Institute of Technology and Science

BRCA1 - breast cancer type 1 susceptibility protein

BSA – bovine serum albumin

Ca^{2+} - calcium ion

CALM - clathrin assembly lymphoid myeloid leukemia protein

Calpain - calcium-activated neutral proteases

CBPI - cytokinesis-block proliferation index

CCMB - Centre for Cellular and Molecular Biology, Hyderabad

CCNB1 – cyclin B1

CCTCC - Conference on Current Trends in Computational Chemistry

Cdc – cell division control

Cdc42 - cell division control protein 42

CDK – cyclin dependent kinase

CDRI - Central Drug Research Institute, Lucknow

CeO_2 – cerium oxide

Chap – Chapter

CHOP - CCAAT-enhancer-binding protein homologous protein

Cm – centimeter

CO_2 – carbon dioxide

Co_3O_4 – cobalt (II, III) oxide

CoO – cobalt monoxide

CORAL – correlations and logic

CPS – counts per second

Cr_2O_3 – chromium (III) oxide

Cu – copper

Cu^{2+} - cupric ion

CuO – cupric oxide

CUR – curcumin

DAPI - 4',6-diamidino-2-phenylindole

DCFDA - 2',7' –dichlorofluorescin diacetate

DLS – dynamic light scattering

DMEM - dulbecco's modified eagle medium

DNA - deoxyribonucleic acid

E.Coli – Escherichia coli

ECL – electrochemiluminescence

EDTA - ethylenediaminetetraacetic acid

EGFR – epidermal growth factor receptor

eIF2α – α sub unit of the eukaryotic initiation factor

EMT – epithelial to mesenchymal transition

ER – endoplasmic reticulum

Et al – '*et al*ia' meaning and others

FACS – fluorescence-activated cell sorting

FBS- fetal bovine serum

Fe – iron

Fe_2O_3 – ferric oxide

G2/M – transition from second growth phase to mitotic phase

G2/S – transition between synthesis and gap 2 phase, also known as the second growth phase

GADD45 - growth arrest and DNA damage-inducible 45 protein

GAPDH - glyceraldehyde 3-phosphate dehydrogenase

GCN2 - general control nonderepressible protein kinase

GDP - guanosine diphosphate

GM-CSF - granulocyte-macrophage colony-stimulating factor

GPCR – G-protein-coupled receptor

G-Protein – proteins capable of binding to guanine nucleotides

Grb - growth factor receptor-bound protein

GRP - glucose-regulated protein

GTP - guanosine-5'-triphosphate

h – hour

H2AX – genes coding for histone 2A

H_2O – water / hydrogen oxide

H_2O_2 – hydrogen peroxide

HMGB1 - high mobility group box 1

HRI - heme-regulated eIF2α kinase

Hsp70 - heat shock protein of 70KDa

ICCB - International Congress of Cell Biology

ICDD - International center for Diffraction Data

IFN – interferon

IgG1-immunoglobulin G1

IL – interleukin

ISR – integrated stress response

JAK – janus kinase

JC1 - tetraethylbenzimidazolylcarbocyanine iodide

JNK - c-Jun N-terminal kinase

KDa – kilo dalton

La_2O_3 – lanthanum oxide

Lamp - lysosomal-associated membrane protein 1

LC3 - microtubule-associated protein 1A/1B-light chain 3

LD – Lethal death

LDH – lactate dehydrogenase

LINE - long interspersed nuclear elements

M – molarity

MAP kinase – mitogen activated protein kinase

Me-Ox – metal oxide

MgO – magnesium oxide

mi-RNA – micro RNA

ml – milliliter

mM – milli molarity

MMP - matrix metalloproteinase

MMS – methyl methane sulfonate

Mn_3O_4 – manganese (II, III) oxide

mRNA – messenger RNA

MSH - MutS protein homolog

MT – microtubule

NaCl – sodium chloride

NADPH - nicotinamide adenine dinucleotide phosphate

Nano – dimension in the scale of 10^{-9} meters

NER – nucleotide excision repair

NFκB1 – Nuclear factor kappa B subunit 1

Ng – nanogram

Ni – nickel

NIH – National Institute of Health

NiO – nickel oxide

Nm – nanomaterial

NOX – NADPH dependent oxidases

NP – nanoparticle

NR4A - orphan nuclear receptors

NRF - nuclear factor erythroid 2–related factor 2

NRF2 - nuclear factor erythroid 2 (NFE2)-related factor 2

P53 - transformation-related protein 53

PAGE – polyacrylamide gel electrophoresis

PBS – phosphate buffered saline

PCNA - proliferating cell nuclear antigen

PCR – polymerase chain reaction

p-eIF2α – phosphorylated form of α sub unit in eukaryotic initiation factor

PERK - protein kinase R (PKR)-like endoplasmic reticulum kinase

pH – potential of hydrogen

PHACTR1 - phosphatase and actin regulator 1

PI – propidium iodide

PI3K - phosphatidylinositol-4,5-bisphosphate 3-kinase

PIKK - phosphatidylinositol 3-kinase-related kinases

PKR - double stranded RNA (dsRNA)-activated protein kinase

PLGA – poly lactic-co-glycolic acid

Prx – peroxiredoxin

PVDF - polyvinylidene fluoride

QSAR – quantitative structure activity-based relationship

Rac - Ras-related C3 botulinum toxin

Rad - DNA recombinase

Rho - Ras homolog gene family member

RNA – ribonuclear acid

RNAse – ribonuclease

RNS – reactive nitrogen species

ROS – reactive oxygen species

RTK – receptor tyrosine kinase

Sb_2O_3 – antimony trioxide

SDS – sodium dodecyl sulphate

SEM – scanning electron microscopy

Ser – serine

SiO_2 – silicon dioxide

SiO_2 – silicon dioxide

SnO_2 – stannic oxide

SOD – superoxide dismutase

STAT – signal transducer and activator of transcription

TBE – tris borate EDTA buffer

TBS – Tris buffered saline

TBST – Tris buffered saline with Tween20

TEM – transmission electron microscopy

TiO_2 - titanium dioxide

TNF - tumor necrosis factor

TPX2 - targeting protein for Xklp2

UCP - mitochondrial uncoupling proteins

UFP – ultra fine particles

UPR – unfolded protein response

USA – United States of America

UV – ultraviolet

V_2O_3 – vanadium (III) oxide

Vitro – vitreous; in a test tube/glass

Vivo- within the living

WO_3 – tungsten oxide

XBP - X-box binding protein

Xklp2 - xenopus centrosomal kinesin-like protein

XRD – X-ray powder diffraction

Zn – zinc

ZnO – zinc oxide

ABSTRACT

We live in a world of exponential nano ingenuity. Exposure of engineered nanoparticles becomes inevitable and thus there is an increasing concern on nanomaterial safety and induced toxicity. Owing to small size and high surface area, nanoparticles are more penetrable and reactive with biological tissue than their bulk counterparts. Decades of research has shown nanotoxicity implements vastly different mechanisms and as such with any type of nanomaterial, it is important to understand the course of molecular events following their exposure.

Metal oxide nanoparticles are the largest class of manufactured nanomaterials, owing to their wide range of application. The exposure is pronounced at industries and manufacturing facilities that discharge waste including aerosolized suspensions. A large part of atmospheric presentation as vehicular effluents also adds to environmental pollution. Such a widely encountered exposure can present risk of toxicity. Nanotoxicity from metal oxides has been documented to realize alterations in cellular morphology, DNA damage, internalization, modulation of protein synthesis and ultimately causes cellular death. Although thus far there is no comprehensive study that elucidates molecular mechanisms of toxicity induced by metal nano oxides in pulmonary tissue. Especially for alveolar cells that are highly susceptible to aerosolized nanoparticles as they form the first line of entry into the human body.

This PhD thesis aimed to understand the mechanism of toxicity induced by metal nano oxides on alveolar type II cells. A systematic approach has been carried out with a less lethal (TiO_2) and a highly lethal (ZnO) metal oxide nanoparticle in understanding the differences between cellular responses to their exposure. Alveolar type II cells, A549 cell line is outlined for the scope of this thesis, which are widely studied as *in vitro* models. This study

has discovered some very novel findings in the field of nanotoxicology. These are involvement of cellular filopodia, HMGB1, Hsp70, cdc42, EMT and p-eIF2α in increasing the dose and time dependent tolerance of cells to nanoparticles. This can be used in the future, as crucial targets for designing stress revival strategies and in the discovery of new drug leads. Further internalization of nanoparticles is found to be common. While the generation of reactive oxygen species is found to be a significant contributor to the mechanism of toxicity. A direct proportionality has been discovered which presents an opportunity to build mathematical models and aid in accurate predictions. Such an effort led to the development of a quantitative structure-activity based relationship that could be used in the future to screen many metal oxides for the degree of stress that they might impart on meeting biological interfaces. This may alleviate the need for expensive and time-consuming processes for screening and lab testing.

Protein corona is also discovered as an accurate descriptor of metal oxide induced stress in alveolar type II cells. This discovery, sheds light on the possible interplay of accumulation of nanoparticles on the cell surface to generation of ROS. Further the DLS aided estimation of protein corona, is in tandem with the trend in toxicity established. These findings put forward a simple DLS estimation of nanoparticle incubated with cell media or a ROS assay as screening tests in design of nanoparticles to ensure their safety and efficacy while in use. The nature of ensuing cell death that is encountered when cellular stress overwhelms the cellular defenses is also proven to be highly dynamic in nature. It is experimentally validated and shown to switch between necrosis, apoptosis and autophagy depending upon the intensity and time of exposing agent. A detailed model is built to predict the mechanism that follows upon cell-nanoparticle interactions. These are attributed to be (i) low ROS mediated mitogenic response, (ii) high ROS mediated oxidative stress and (iii) overwhelming stress resulting in cell death.

REVIEW OF LITERATURE

Learn everything you can, anytime you can, from anyone you can. There will always come a time you will be grateful you did.

- *Sarah Caldwell*

Nanotechnology is an exponentially growing field and nanoparticles (NPs having dimensions less than 100nm; Panariti *et al*., 2012, Teow *et al*., 2011) with their unique physical and chemical properties (Bombin *et al*., 2015), are increasingly landing wide range of applications; such as, fields including biomedical (Saptarshi *et al*., 2013), electronic, industrial, cosmetic (Nel *et al*., 2006), paints, food additives (Teow *et al*., 2011) etc. Metal oxides particularly, are being developed for diagnostics, electronic sensing and computing. They are the largest class of commercially produced nanomaterials (Djurisic *et al*., 2015). Some of the applications also include robust memory devices, robotic navigation, optics, data security, solid state switches, low threshold lasers, solar cells, photo voltaic cells, cosmetic formulations, bulk fillers, molecular nano electronics and nano motors. The enormous flexibility of functionalization and fabrication renders an ever-growing number of tailored applications feasible such as targeted gene therapy and improved bioavailability of pharmaceutical drugs. Enhanced contrast and sensitivity in Imaging has also added to the explosion of global demand for nano-scale ingenuity resulting in the ever-increasing use of nano-scale metal oxide particles (Falcaro *et al*., 2016, Ramos *et al*., 2017). As such human exposure becomes inevitable.

With the unprecedented human exposure of nanoparticles, risks to human health also increase owing to the high penetrating potential and high reactivity of nanoparticles (Yin *et al*., 2015). Nanoparticles are more toxic than fine particles (Horie *et al*., 2011). Owing to differences in properties as compared to their bulk counterparts such as, increased surface area per unit volume, electrical conductivity, hardness, enhanced chemical and biological activity (Karlsson *et al*., 2008) etc. Ultra-fine particles (UFPs; nano-scale) can prove to be more toxic to human health in the form of environmental and occupational exposure. High presence of metal oxide nanoparticles at sites surrounding factories as compared to clean areas (Rogaczewska and Matczak, 1984) has been correlated with increase in pulmonary

diseases including exacerbation of bronchial asthma (Weinchenthal *et al.*, 2007). Pulmonary toxicity can manifest into emphysema, edema, fibrosis and oxidant injury often involving cells localized in the alveolar lining (Castranova *et al.*, 1988).

The alveolar lining is comprised of two types of cells specific to lungs; type I and II. Type I alveolar cells are narrow and elongated cells which make up for 96% of the alveolar surface area. These long cells minimize the length between alveolar space and capillaries of the lung, hence maximizing exchange of gases. In comparison, alveolar cells; type II are round shaped cells comprising only 4% of the epithelial surface area. Although they make up 60% of alveolar epithelial cells by number (Crapo *et al.*, 1983).

A major function of type II alveolar cells (type II pneumocytes) is the synthesis and secretion of lipoprotein surfactants (Sanders *et al.*, 1975), that deflated the surface energy and tension at the liquid-air barrier of the pulmonary alveolus (Pattle *et al.*, 1958, Clements *et al.*, 1957) realizing enhanced stability, thereby alleviating edema (Clements *et al.*, 1958). Alveolar tissue also significantly improves the potential of macrophages in phagocytosing of foreign particles including invading bacteria (O'Neill *et al.*, 1984). Surfactants further help the pulmonary tissue in protection from inhaled material that may prove noxious (Wallace *et al.*, 1985).

Another crucial function of type II pneumocytes is its capacity for xenobiotic processing of external entities including environmental accumulates and drugs (Minchin *et al.*, 1983, Bend *et al.*, 1985). Cytochrome P-450-dependent mono-oxygenase set of enzymes are a larger route for processing of foreign material in pulmonary tissue. It aids the mono-oxygenation of a renowned sets of lipophilic material in the presence of NADPH and oxygen (Gillette *et al.*, 1972). Jones *et al.*, 1982 also reports that type II cells eliminate large quantities of water and sodium through the cytoplasmic membrane and realizes an important

role by maintaining a dry alveolus. Na^+ - H^+ interchange realizes passive transport of sodium from the alveolus to the lateral side utilizing the active Na^+- K^+ pump (Mason *et al*., 1982) directing the flow of water while keeping the alveoli dry. Ultimately these type II pneumocytes de-differentiate into type I alveolar cells proceeding oxidant injury with type II increased proliferation and incorporation in thymidine. This resilience of type II cells is due to the presence of Na^+ Ascorbate co-transport system that aids in the accumulation of antioxidant vitamin C in these cells (Castranova *et al*., 1983).

Thus, any toxic substance that could alter or deter the potential of type II cells in building and releasing surfactants, impair its capacity for xenobiotic metabolism, transepithelial sodium transport or Vitamin C accumulation may adversely affect lung function (Catranova *et al*., 1988).

A549 cells as an *in vitro* model for testing pulmonary toxicity

There have been multitudes of nano-toxicity studies carried out using A549 cells as an *in vitro* model. A549 cells are a continuous human lung adenocarcinoma epithelial cell line initiated in 1973 by D. J. Giard through explant culture of lung carcinomatous tissue from a 58-year-old Caucasian male. A549 cells can synthesize lecithin with a high percentage of desaturated fatty acids utilizing the cytidine diphosphocholine pathway like type II pneumocyte (Lieber *et al*., 1976). Ultrastructural characteristics of A549 cells were like the in-situ type II pneumocyte and were unchanged by fatty acid supplementation. The morphology, composition and biosynthesis of phosphatidylcholine in A549 cells are consistent with that reported for type 2 cells (Nardone *et al*., 1979). A549 cells are also an established model for metabolic and macromolecular processing typical of alveolar type II cells (Foster *et al*., 1998). Therefore, A549 cells is not only an established model to study

alveolar type II cellular responses but their relative ease of culture allows for carrying out vast numbers of comparative experiments in a short duration of time. Any promising result could certainly be followed by *in vivo* and animal studies, if necessary, for future development of therapeutic strategies.

Not only does use of a robust model of study aid accuracy of prediction but the knowledge of a complete characterisation of nanoparticles along with the processes following contact with living systems are crucial in understanding it's possible toxicological effects (Elsaesser *et al*., 2012). In lieu of this knowledge there have been many reports elucidating the mechanism of metal oxide nanoparticle toxicity particularly on lung systems and alveolar tissues (Huang *et al*., 2010). Cytotoxicity is a multi-factorial process. Size and surface area are obvious determinants of the level of cytotoxicity (Sahu *et al*., 2016, Sohaebuddin *et al*., 2010). Chemical identity of the metal species in the oxide and its ensuing interactions at the cellular level also govern the level of cell death (Ivask *et al*., 2015, Lu *et al*., 2015). Adsorption ability of the particles themselves greatly affect the viability and proliferation especially for exposure to lesser toxic metal oxide nanoparticles (Horie *et al*., 2009). Cellular absorption of ions also seems preferential.

One report described that although not uniform, distribution of metal ions largely localized in perinuclear and cytoplasmic space with the trend of Cu>Zn>Fe>Ni (Lu *et al*., 2015). All nanoparticles adsorb proteins they encounter in tissues and fluids at the port of entry. The specific features of this adsorption kinetics depend on the surface characteristics of particles, including surface chemistry and surface energy, and may be modulated by intentional modification or functionalisation of the surfaces (Ito *et al*., 2005). Djurisic *et al*., 2015 broadly describes some of the more widely studied mechanisms of nanoparticle toxicity namely, ROS generation, metal ion release, accumulation on cell membrane and internalization. The process of toxicity is dynamic, and any statistical models developed to

predict toxicity need to consider the contributions of various mechanisms leading to cell

death. There is also thus a need for discovery of multi-disciplinary parameters to aid as descriptors in effectively understanding the progression of cellular stress.

Though there are many research reports available for understanding the effects of metal oxide nanoparticles on human alveolar cell lines but there is no conglomeration of the plethora of interactions following metal oxide nanoparticle exposure on A549 cells. There are no standard procedures or recommendations that elucidate experimental conditions and attitude to assess nano-toxicity. Further there is redundancy of results through various studies. The knowledge of cell-nanoparticle interactions, even those at sub-lethal doses are essential in devising novel strategies of stress recovery which could essentially change the fate of cell from death to survival. Thus, this review article is built as a sincere effort to summarize relevant, comprehensive and up to date information governing the cellular responses to metal oxide nanoparticle exposure on A549 cells.

Metal Oxide NPs and regulation of cellular morphology:

One of the first responses includes a change in cellular morphology. Structural aspects of a cell can provide valuable information about the stress it is responding to (Johar *et al*., 2017). Small guanosine 5'-triphosphate (GTP)-binding proteins such as Rho A, Rac 1, and Cdc42 are critical for triggering actin reorganization and thus modulating cellular morphology. Small GTPases (smGTPases) cycle between an active GTP bound state and an inactive GDP bound state. They play an important role in the regulation of cellular motility, cell structure and adhesion through dynamic cross talk of the actin cytoskeleton (Bishop *et al*., 2000, Sarkar *et al*., 2007).

Some other documentation of morphology modulations include SiO_2 NPs induced reduction in cell motility (Gonzalez *et al*., 2015). The report also showed an increase in microtubule dynamics, consistent with reduced levels of MT (microtubule) acetylation. Okoturo Evans *et al*., 2013, further describes structural re-organization and regulation of actin cytoskeleton (PHACTR1) upon SiO_2 exposure, leading to detrimental changes in cell morphology. SiO_2 treatment also regulated nuclear morphology (Seagrave *et al*., 2000).

TiO_2 were abundantly internalized through endocytic pathway though they did not induce cytotoxic effects or ultrastructural lesions (Moschini *et al*., 2013). The same report described that CuO NPs induced severe ultrastructural and cell membrane damages. Park S *et al*., 2007 suggests although TiO_2 is less cytotoxic than Zn exposure, it caused more morphological damage

Metal Oxide NPs and Oxidative Stress:

Free radicals are generated naturally as by-products of mitochondrial respiration and transition metal ion-catalyzed Fenton-type reactions (Vallyathan *et al*., 1997). Neutrophils and macrophages also induce oxidative outburst as a defense mechanism towards environmental pollutants, tumor cells, and microbes (Manke *et al*., 2013). Oxidative stress results when generation of Reactive oxygen species (ROS) exceed cell's anti-oxidant capacity (Martindale *et al*., 2002). ROS elicits a whole array of cellular responses from mitogenic proliferation, cell cycle arrest to cell death depending on the level of exposure dose.

Nel *et al* 2006, describes three tiers to quantitatively describe the level of total oxidative stress experienced by a cell. Tier 1 involves expression of anti-oxidant defense systems. Tier 2 engages inflammatory responses through cytokines and chemokines. Finally,

Tier 3 is the realization of cytotoxicity. Lloyd 2013, describes how superoxide radical is converted to H_2O_2 catalyzed by superoxide dismutase, which further gets converted to water using catalase and glutathione peroxidase. These antioxidant enzymes convert excess ROS into less harmful substances. Molecules classified as 'ROS' have a single unpaired electron in their outer energy orbital or are highly charged species causing alterations in any cellular molecules they encounter, thus eventually leading to damage and loss of biological function.

Nanoparticles can generate ROS upon irradiation or molecular dissociation. Depletion of glutathione along with induction of lipid peroxidation, upregulation of catalase and superoxide dismutase indicate increase in ROS generation (Boyles *et al*., 2016).

Several metal oxide nanoparticles have been reported to generate ROS. NiO nanoparticles have been proven to cause oxidative stress (Horie *et al*., 2011). Also, cellular uptake of NiO results in release of nickel ions (Horie *et al*., 2009). ZrO_2 and Fe_2O_3 also induce ROS (Soto *et al*., 2008). However, Fe_2O_3 is one of the least lethal nanoparticles, its induced ROS is inconsequential compared to that of highly toxic candidates such as CuO (Pandey *et al*., 2016) and ZnO (Lai *et al*., 2015). CuO NPs induced oxidative stress in a concentration dependent manner (Akhtar *et al*., 2016). It was also supported by glutathione depletion and lipid peroxidation. Saptarshi *et al*., 2015 described that ZnO NPs induced upregulation of heme oxygenase 1, a prominent redox stress marker. ZnO NPs also rendered a reduction in the expression of superoxide dismutase (SOD), Bcl-2, ATP synthase, and Complex IV (Kim *et al*., 2014), part of cellular anti-oxidant defense mechanisms. HO-1, lipid peroxidation and alpha-tocopherol were also induced by ZnO exposure in the pulmonary tissue (Akhtar *et al*., 2012). It was also shown that accumulated ZnO particles in the lung continuously released Zn^{2+} ion, thus increasing oxidative stress with time (Fukui *et al*., 2012). CUR/BSA particles alleviated some cytotoxic effects of CuO exposure indicating its higher intracellular accumulation as compared to CuO and thereby suppressing Cu^{2+} release and

ROS generation (Zhang *et al*., 2016). Moschini *et al*., 2013 described that CuO NPs induced oxidative stress caused severe mitochondrial, ultrastructural and cell membrane damages. Its cellular uptake was mediated by endocytosis in organelles including lysosome, mitochondria and nucleus (Wang *et al*., 2012). Further, mitochondrial depolarization was also observed.

SnO_2 (Tammina *et al*., 2017) and SiO_2 NPs (Berg *et al*., 2013, Horie *et al*., 2014, Guadagnini *et al*., 2015) also caused oxidative stress and induced expression of anti-oxidant defenses.

TiO_2 induced oxidative stress as per intensity and duration of exposure (Kim *et al*., 2010). TiO_2 was shown to have abundantly internalized through endocytic pathway though they did not induce cytotoxic effects or ultrastructural lesions (Stoccoro *et al*., 2017). Singh *et al*., 2007 reports uptake of TiO_2 as membrane bound aggregates. Despite their aggregation, they were capable of oxidant generation. TiO_2 NPs are examples of the few low solubility, low toxicity inducing particles which can elicit oxidative stress (Monteiller *et al*., 2007). TiO_2 exposure induced ROS prevented ATP synthesis (Tang *et al*., 2013) and lipid deformation in A549 cells (Kuku *et al*., 2017).

Co_3O_4 is more toxic than TiO_2 (Alinovi *et al*., 2017). This study suggests that higher oxidative stress generated in response to more lethal nanoparticles hampers energy homeostasis and impairs the ability to repair the resulting damage, probably preventing autophagy. High toxicity NPs cause dysfunction in the autophagic progression (Kermanizadeh *et al*., 2017). The more toxic ZnO exposure also induced both apoptotic and autophagic pathway though eventually the formation of autolysosome was blocked.

Cytokine release on Metal oxide NP exposure:

Cytokines are cell secreted molecules that trigger specific interactions. Cytokines are named after their source and function such as lymphokine- cytokines made by lymphocytes, monokine- cytokines made by monocytes, chemokine- cytokines with chemotactic activities, and interleukin- cytokines made by one leukocyte and acting on other leukocytes. Cytokines may act on the cells that secrete them; autocrine action, on nearby cells; paracrine action or in some cases on distant cells; endocrine action (Zhang *et al*., 2007). Pro-inflammatory cytokines like IL-1β, IL-6, and TNF-α are produced by macrophages and upregulate inflammatory processes in response to physiological injury or pathological stimulus.

Cytokine release directs cell-cell interaction and therefore understanding the role of nanoparticle mediated cytokine responses are emerging as an essential component of nanoparticle safety testing. High levels of cytokines are released upon treatment with nanoparticles, which is usually associated with stress, toxicity, adverse reactions and low therapeutic efficacy; hence, cytokines might be utilized to partially predict the nanoparticle immuno-toxicity (Elsabahy *et al*., 2013).

Many NP- cell interactions elicit inflammatory responses, indicative of cell stress. Some reported studies are listed below. Guadagnini *et al*., 2015 places SiO_2 NPs as a positive control for pro-inflammatory responses as compared to PLGA NPs. Particularly, IL-8 release was prominent (O-Evans *et al*., 2013).

Fe_2O_3 exposure also resulted in cytokine release such as IL-6 and IL-8 (Boyles *et al*., 2016). The same study showed ZrO_2 could induce iL-6 release. Stringer *et al*., 1996, demonstrated that TiO_2 could not induce IL-8 release in the dose range of 1-6 ng/ml. At non-lethal doses of La_2O_3 exposure on A549 cells, the inflammatory effects on bronchoalveolar lavage fluid (BAL) resulted in an increased lung weight and severe proteinosis (Lim *et al*.,

2015). ZnO NPs caused upregulation of mRNA for the pro-inflammatory cytokine IL-8 with increased release of IL-8 (Saptarshi *et al*., 2013) at small doses of exposure. Though at elevated doses of exposure ZnO causes decreased IL-8 release and mitochondrial membrane potential (Vandebriel *et al*., 2012) along with an elevated Ca^{2+} concentration. Song J *et al*., 2013 further, described an upregulation of IL-1 levels upon ZnO treatment. Further, ZnO NP exposure even upregulated pro-inflammatory markers such as IL-8, IL-6 and GM-CSF at Air-Liquid Interface conditions (Lenz *et al*., 2013).

Pro inflammatory immune responses including IL-8 and nuclear factor kappa B induction was observed to CuO exposure with the air-liquid interface (ALI) system (Frijns *et al*., 2017). Belts and spherical TiO_2 NPs showed release of IL-2, IL-6, IL-8, IL-4, IFN-γ, and TNF-α, though cytokine levels settled comparatively early for spheres than belts (M-Reyes *et al*., 2015). Singh *et al*., 2007 reports internalized TiO_2 aggregates being capable of IL-8 release. TiO_2 NPs also elicit IL-6 cytokine release (Ursini *et al*., 2014) and IL-8 release (Wilson *et al*., 2012).

Metal Oxide NPs induced DNA damage:

The cell goes through several DNA damaging processes each day due to both exogenous and endogenous activities. Endogenous sources include replication errors, DNA base mismatches, topoisomerase-DNA complexes, spontaneous base deamination, abasic sites, oxidative damage and DNA methylation. Exogenous factors consist of ionizing radiation, UV radiation, chemical agents include alkylating agents, aromatic amines, polycyclic aromatic hydrocarbon, reactive electrophiles, toxins and environmental stress (Chatterjee *et al*., 2017).

Genome modulation may be reflected in changes of transcription and thus synthesis of proteins, this may ultimately render several signaling cascades dysfunctional. If the repair mechanisms are not adequately employed before mitosis, the mutations may be carried into daughter generations. Depending on the level of DNA damage, cells may become irreversibly dormant; senescent or be led into cellular death or turn malignant (Collado *et al*., 2005, Braig *et al*., 2005). Nanoparticle can cause DNA damage through many processes including ROS generation, NP accumulation (E-Said *et al*., 2014) or even novel routes such as purine nucleotide transmission (Bhabra *et al*., 2009).

DNA damage such as lesions activate cell cycle check points (Branzei *et al*., 2008, Huang *et al*., 2006). There are several accounts of metal oxide nanoparticles inducing cell cycle arrest. Al_2O_3 particles cause G2/S phase arrest (Li *et al*., 2016). Cytotoxicity induced by ZnO NPs includes cell cycle arrest among other factors such as ROS generation, mitochondrial dysfunction, glucose metabolism perturbation and cellular apoptosis (Lai *et al*., 2015). Also, substantial reduction of cytokinesis-block proliferation index (CBPI) was found for ZnO nm, while TiO_2 NP exhibited no toxicity in the same assay (Corradi *et al*., 2012).

CuO NP exposure resulted in cell cycle arrest and downregulation of proliferating cell nuclear antigen (PCNA), cell division control 2 (CDC2), cyclin B1 (CCNB1), target protein for Xklp2 (TPX2), and aurora kinase A (AURKA) and B (AURKB) (Hanagata *et al*., 2011). Further, Cell death at sub lethal concentration was avoided through the induced expression of nuclear receptors NR4A1 and NR4A3 growth arrest and DNA damage-inducible 45 β and γ (GADD45B and GADD45G, respectively).

A 2D gel proteomics analysis describes TiO_2 NP exposure as affecting gene products involved in, gene expression, proteasome activity, mitochondrial function, trafficking, glucose metabolism and DNA damage response (Armand *et al*., 2016). Cell proliferation and

cell cycle progression is impeded by activating p53 pathway. An enhanced chaperone

expression hint at homeostasis re-arrangement. TiO_2 NPs induce an increase in micronucleus

frequency, attributed to ROS generation. This is also accompanied by an upregulation of

ATM, p53, and CdC-2 and downregulation of ATR, H2AX, and Cyclin B1 hinting at DNA

double strand breaks. This can be ultimately associated with cell cycle arrest in G2/M phase

(Kansara *et al*., 2015). TiO_2 NPs induced G2/M arrest along with proliferation inhibition and

disruption of mitochondrial membrane occurs at elevated doses of exposure until 200

microgram/ml (Wang *et al*., 2015).

One account of metal oxide NPs induced disruption of DNA repair pathway is the

genotoxicity induced by TiO_2. It is documented to impair DNA repair mechanisms such as

base excision repair (BER) and nucleotide excision repair (NER). Increased methylation of

DNA repair gene promoters and downregulation of NRF2 and BRCA1 is described further

(B-Clier *et al*., 2017). Oxidative stress raised by TiO_2 NP exposure can also act as a

transducer to activate genotoxic effects through activating HSP27 and SAPK/JNK (H-Roy *et

al*., 2016).

SiO_2 NPs were also shown to increase DNA strand breaks even in non-cytotoxic

concentrations of up to 300 microgram/ml (Maser *et al*., 2015). Both CuO and ZnO NPs

affected viability and caused DNA damage (Karlsson *et al*., 2008). TiO_2 both rutile and

anatase forms caused DNA damage, however viability remained unaffected. Fe_2O_3 NP

exposure neither resulted in DNA damage nor loss of cellular viability for the dose ranges

evaluated.

TiO_2 and CeO_2 though slightly cytotoxic were capable of inducing DNA damage

(Yamani *et al*., 2017). The same study showed ZnO affected cell survival and aided DNA

damage greatly. Intrinsic oxidant release is not proportional with DNA damage (Thongkam *et

al., 2016). It followed that despite ZnO being highly cytotoxic than TiO_2, both had DNA damaging potential. ZnO NPs cause DNA double strand breaks which increased with increasing ROS levels, although, Zn^{2+} could also cause these DNA damages without the involvement of ROS (Heim *et al*., 2015).

CuO particles are highly lethal causing more DNA damage than ZnO, TiO_2, Fe_2O_3 and Fe_3O_4 (Karlsson *et al*., 2008). Semisch A *et al*., 2014 claimed CuO caused a decrease in the colony forming units, induced DNA strand breaks. Cell death was in parts due to apoptosis, as evidenced by subdiploid DNA and translocation of the apoptosis inducing factor (AIF) into the cell nucleus. TiO_2 were abundantly internalized through endocytic pathway though they did not induce cytotoxic effects through ultrastructural lesions (Moschini *et al*., 2013).

TiO_2 is both cytotoxic and genotoxic at elevated doses of exposure (Stoccoro *et al*., 2017). Also, presence of citrate enhances this effect by causing epigenotoxic effect evidenced by reduction in LINE-1 methylation levels. Alinovi *et al*., 2017 suggested that TiO_2 exposure caused autophagy with down regulation of miRNA-21 and miRNA-30a.

CeO_2 NPs are slightly toxic and have no long-term effects on colony forming efficiencies. Though they are genotoxic like the cytotoxic ZnO NPs (Yamani *et al*., 2017).

Long-time exposure to TiO_2 NPs induces DNA damage and increased 53BP1 foci counts associated with intracellular NP accumulation (Armand *et al*., 2016). Though viability isn't that affected, chronic exposure beyond two months enables cells to cope the stress by decreasing proliferation, stabilization of accumulated NPs and sensitization to MMS (Methyl methane sulfonate).

Internalization as a mechanism for toxicity

TEM (Transmission Electron Microscopy) evidenced internalization of NPs was shown for CuO, ZnO, Sb_2O_3, Co_3O_4, Mn_3O_4, MgO, Al_2O_3, Fe_3O_4, SiO_2, TiO_2, WO_3 (Ivask *et al*., 2015), SiO_2 up to 400nm were also shown to be internalized by another study (Mohamed *et al*., 2011). Stringer *et al*., 1996 successfully demonstrated internalization of TiO_2 and Fe_2O_3. Internalization of Bi_2O_3 was studied by Abudayyak *et al*., 2017. CuO NP was discovered to be accumulated in both cytoplasmic and nuclear fractions (Akhtar *et al*., 2016). The first report of TiO_2 internalization was that of nuclear presence from Ahlinder *et al*., 2013.

Modulation of protein synthesis

Proteins are important biological macromolecules and the regulation of protein synthesis is a crucial cellular process for maintenance of homeostasis in an organism. Therefore, the impact of nanoparticles in living organisms at the protein level is a critical parameter that should necessitate attention from researchers. Unfortunately, there are very few reports that are available on the effect of metal oxide nanoparticles on translation regulation in eukaryotes. One report elucidates SiO_2 NP modulated expression of mitochondrial uncoupling proteins (UCP2), Calpain12 and HSP90 (O-Evans *et al*., 2013).

Reports also suggest that SiO_2 NPs elevated aquaporin concentrations transiently (Hao *et al*., 2016). Matrix metalloproteinases such as MMP1, MMP9 and MMP-10 were also activated by SiO_2 exposure (Horie *et al*., 2014). CoO and CeO_2 exposure encoded markers involved in immune processes (Verstraelen *et al*., 2014). V_2O_3 reduced protein levels while detrimentally affecting viability (W-Knirsch *et al*., 2007). CuO exposure also upregulated Hsp70 along with Rad51, MSH2 (Ahamed *et al*., 2010).

Metal oxide nanoparticle induced cell death

Cell death is the ultimate cellular response mounted as an irreversible consequence of unmanageable cellular stress. There are several well studied routes of death, these notably include; Autophagy, Apoptosis and Necrosis. Types of Autophagy include macro, micro and chaperone-mediated autophagy, all of which promote self-degeneration to maintain energy homeostasis in the cell (Glick *et al*., 2010). Apoptosis is an organized, ATP dependent cell death involving formation of apoptotic bodies while Necrosis involves cell swelling and membrane disruption, cytoplasm release and inflammation and is ATP-independent (Elmore 2007). Yet another type of cell death is recently defined; Necroptosis. An energy dependent and orchestrated version leading to cellular outburst (Vandenabeele *et al* 2010). Though there are no studies that have conclusively implied it, because of metal oxide nanoparticle exposure on A549 cells.

Some accounts of Me-Ox (metal oxide) nanoparticle mediated cell death is enumerated. CuO NPs have been shown to induce autophagic pathway (Sun *et al*., 2012). Mohamed *et al*., 2011 showed SiO_2 induced ATF2 nuclear translocation, which was dependent on phosphorylation of p39 and JNK1/2. SiO_2 NPs of about 30nm effect inflammatory processes inducing apoptotic pathway evidenced by up-regulation of ATM, TNFα and IL1b (Fede *et al*., 2014). Bi_2O_3 exposure resulted in Necrosis (Abudayyak *et al*., 2017). ZnO induces cell cycle arrest progressing into apoptosis (Lai *et al*., 2015). The apoptotic pathway mediated by ZnO exposure is cascaded through ROS generation and p53 upregulation. Bax/bcl2, Caspase 3 and 9 were also induced in a dose dependent manner (Akhtar *et al*., 2012). Autophagy was associated with CuO induced cell death (Cronholm *et al*., 2013) evidenced by an elevation of LC3-II autophagic biomarker (Sun *et al*., 2012). There was also an upregulation of p38 and p53 (Wang *et al*., 2012).

Other accounts of cellular damage:

Loss of Membrane integrity, organelle damage and regression in proliferative and migrative capability are some of the other instances of metal oxide nanoparticle induced stress. Though not well studied, some results are discussed herein. ZnO affected cell proliferation, viability, membrane integrity, colony formation (Kim *et al*., 2010). Zn^{2+} caused deglycosylation of Lamp1 and Lamp2 (Qin *et al*., 2017), glucose metabolism perturbation (Lai *et al*., 2015) along with mitochondrial and lysosomal damage. There was also an increase in caspase 1 activity and LDH release. Within 15 minutes of ZnO treatment, ion channel inhibition was documented by Yang X *et al*., 2012. SiO_2 caused LDH release evidencing membrane damage (Horie *et al*., 2014). Cr_2O_3 showed haemolytic activity (Hedberg *et al*., 2010). CuO also resulted in mitochondrial damage (Karlsson *et al*., 2009). CuO exposure also regulated pathways modulating hypertonic stress (Boyles *et al*., 2016). TiO_2 perturbed endoplasmic reticulum and induced p53 (Alinovi *et al*., 2017). Further, TiO_2 and CeO_2 affected colony forming efficiencies, though this was not a long-term consequence (Yamani *et al*., 2017). From the reports reviewed in this article, we could predict a trend in toxicity realized by various metal oxide nanoparticles on A549 cells.

Table 1 – Trend of metal oxide nanoparticle induced toxicity on A549 cells

Source Article	Trend (~ suggestive of comparable toxicity)
Kim I S *et al*., 2010	$ZnO > Al_2O_3, CeO_2, TiO_2$
Ivask A *et al*., 2015	$CuO > ZnO > Sb_2O_3 > Co_3O_4 > Mn_3O_4 > Al_2O_3$, Fe_3O_4, MgO, TiO_2, WO_3
Sun T *et al*., 2012	$CuO > SiO_2 > TiO_2 > Fe_2O_3$
Lai X *et al*., 2015	$ZnO > Fe_2O_3$
Titma *et al*., 2016	$CuO > ZnO, Co_3O_4 > Sb_2O_3, Mn_3O_4, TiO_2$
Alinovi R *et al*., 2017	$Co_3O_4 > TiO_2$
Ivask A *et al*., 2015	$CuO > ZnO > Co_3O_4 > Al_2O_3 \sim TiO_2 \sim Fe_2O_3$

As per **Table 1**, the trend in toxicity among the most studied and utilized, metal oxide nanoparticles on A549 cells could be summarized as:

$CuO > ZnO > Co_3O_4 \sim Sb_2O_3 > Mn_3O_4 > Al_2O_3 > TiO_2 > Fe_2O_3$.

During the phase of exposure, nanoparticles adsorb protein along the nasal septa, respiratory trachea and alveolus. Essentially protein adsorbed on to nanoparticle, called protein corona dictates cell-nanoparticle interactions (Saptarshi *et al*., 2013).

It was noted that, contribution to toxicity by metal ions were consistently insignificant to the overall level of toxic stress generated. This discourages metal ion release as a significant player in metal oxide nanoparticle induced toxicity on A549 cells.

Internalization of metal oxide nanoparticles was universally documented with all metal oxide nanoparticle exposure on A549 cells. Though the degree of uptake and dissolution thereafter, both might play a role in dictating the level of toxicity (Vandebriel *et al*., 2012).

The fourth well studied mechanism of nanoparticle toxicity as per Djurisic *et al*., 2015 is accumulation of nanoparticle on membrane surface, on which there aren't any reports thus far, so whether this mechanism contributes in realizing the stress is unclear.

There are reports of autophagic death, apoptosis and necrosis owing to metal oxide nanoparticle exposure across the spectrum of less lethal to most lethal nanoparticles. No pattern to predicting the route of cell death has been discovered yet. Cellular stress is a highly multi factorial process. Dose and time dependent results vary as per experimental designs, though the trend of toxicity remains constant (Loret *et al*., 2016). Cellular responses of A549 cells to metal oxide nanoparticle exposure include cytokine release, cytoskeletal re-organization inducing changes in morphology, DNA damage and modulation in protein expression. Loss of membrane integrity, organelle damage and impairment in both proliferation and cellular metabolism were also documented. However, these changes aren't common throughout the range of exposure from less lethal to highly lethal nanoparticles. As such further research is necessitated to explore these paradigms and predict any inherent patterns in designing better therapeutic solutions to stress recovery. This will also help in building ingenious and efficient management systems for a wide range of applications.

Many quantitative structure-activity relationship (QSAR) models have already been developed that can extrapolate experimental toxicity data of few candidates to accurately predict effects of most metal oxide nanoparticles based on their similar molecular descriptors (Leszczynski, 2010 and Puzyn *et al*., 2011). Puzyn *et al*., 2011 investigated toxicity conferred

27

by metal nano-oxides on *E.coli* and developed a QSAR mathematical model to predict the

toxicity as a function of bond dissociation energy of the chemical species in the nanoparticles. Though there are no parameters discovered to explain the mechanism of metal oxide nanoparticle induced stress in alveolar type II cells. Also, because mechanisms in play with this kind of toxicity has not yet been characterized.

GAPS IN EXISTING RESEARCH

With the broad literature survey, several gaps in research were identified in the study of metal oxide nanoparticle induced stress in A549 cells. Some of them were put forward as the PhD thesis objectives. These were the documentation of:

1.   Changes in cellular morphology through regulation of Small GTPases.

2.   Effect of metal oxide nanoparticles on protein synthesis machinery.

3.   Effect of metal oxide nanoparticles on cell cycle regulation.

4.   Discovery of descriptors to metal oxide nanoparticle induced stress

Changes in cellular morphology as a function of Small GTPase modulation on metal oxide nanoparticle toxicity has not been documented. Nanoparticle exposure could be examined for specific patterns of gene expression. Particularly Rac1, RhoA and Cdc42 modulation in response to stress may give insights to changes in morphology, as their expression is well studied to cause signatory changes to the cell structure.

There are no reports available about involvement of metal oxide nanoparticles in the regulation of protein synthesis. A common cellular response to stress; translational regulation of protein synthesis including inhibition of protein synthesis may provide ample opportunities for the cell to conserve resources and trigger efforts of cellular repair and revival.

There are several reports on how nanoparticles interact with cells and what kind of stress results out of this interaction (ROS). But what follows this interaction; the cellular

response to tackle this stress is poorly understood including signal cascades leading to alteration in chaperone expression, possibility of EMT transitions and Cell cycle modulation.

Further, the mechanism of metal oxide nanoparticle induced stress in type II alveolar cells has not yet been well characterized. Following these gaps, I have also tried to address; discovery of descriptors to this stress. An attempt of quantification of any relevant descriptors discovered could be developed into predictive tools such as a quantitative structure activity relationship-based models.

CHAPTER 1

Differences and Similarities in cellular responses of A549 cells to ZnO and TiO₂ nanoparticle exposure

1.1 Introduction:

A thorough understanding of the biological mechanisms of toxicity enables testing available whilst also designing novel therapeutic agents in future to alleviate effects of nano-toxicity towards stress recovery. To understand these differences in cellular responses of A549 cells between less lethal and highly lethal metal oxide nanoparticles, we have chosen two candidate metal oxide nanoparticles of different toxicities to alveolar A549 cells. These are ZnO and TiO_2, ZnO being more lethal than TiO_2 (Ivask A *et al*., 2015, Titma *et al*., 2016).

Well characterized and commercial NPs were chosen for this study; Sigma Aldrich ZnO (a heterogenous mixture of 35nm to 100nm) with molecular weight of 81.3814 $gmol^{-1}$ and TiO_2 (Hombikat make- 18nm) with molecular weight of 79.88 $gmol^{-1}$ to model the commercially used NPs and industrially discharged UFPs of similar size ranges.

Assays were planned and executed towards establishing and analysing the differences in cellular responses to ZnO and TiO_2 treatment. Viability was foremost monitored; total and mitochondrial dysfunction related, by trypan blue dye exclusion method using a neubauer's hemocytometer (Narayana *et al* 2002) and resazurin reduction assay respectively (Dukie *et al*., 2005, Santimano *et al* 2013). Changes in cell and nuclear morphology as a dose and time dependent function of nanoparticle exposure was also documented.

Changes in the cellular morphology reflect the stability of the cell since they play an important role in many cellular processes such as migration, differentiation, apoptosis, necrosis and senescence. Thus, characterizing the morphological state of cells is vital to diagnosis of stress. It may even be developed into a signatory pattern for different kinds of stress.

A prominent and accepted method of characterizing the morphological state is through studying the expression of Small GTPases that regulate cytoskeletal organization (Guo *et al*., 2009), primarily its Rho family members; Rac, Rho and cdc42 (Stankiewicz and Linseman, 2014). These proteins cycle between an inactive (GDP-bound) and an active (GTP-bound) conformation in which they interact with specific effector proteins (Royal *et al*., 2000, **Figure 1**). Activation of Rho promotes the formation of stress fibers and focal adhesion complexes (Ridley and Hall, 1992), Rac promotes the polymerization of actin at the cell membrane, producing lamellipodia and membrane ruffles (Ridley *et al*, 1992) and cdc42 promotes the formation of filopodia and microspikes at the cell periphery (Kozma *et al*., 1996, Nobes and Hall, 1995, **Figure 2**). Thus, expression of Rho family of Small GTPases such as Rac1, RhoA and cdc42 were evaluated both at mRNA and protein level to assess any differences in morphology attributed by changes in their expression.

Figure 1 – GTP / GDP cycling towards switching of activity with small GTPases
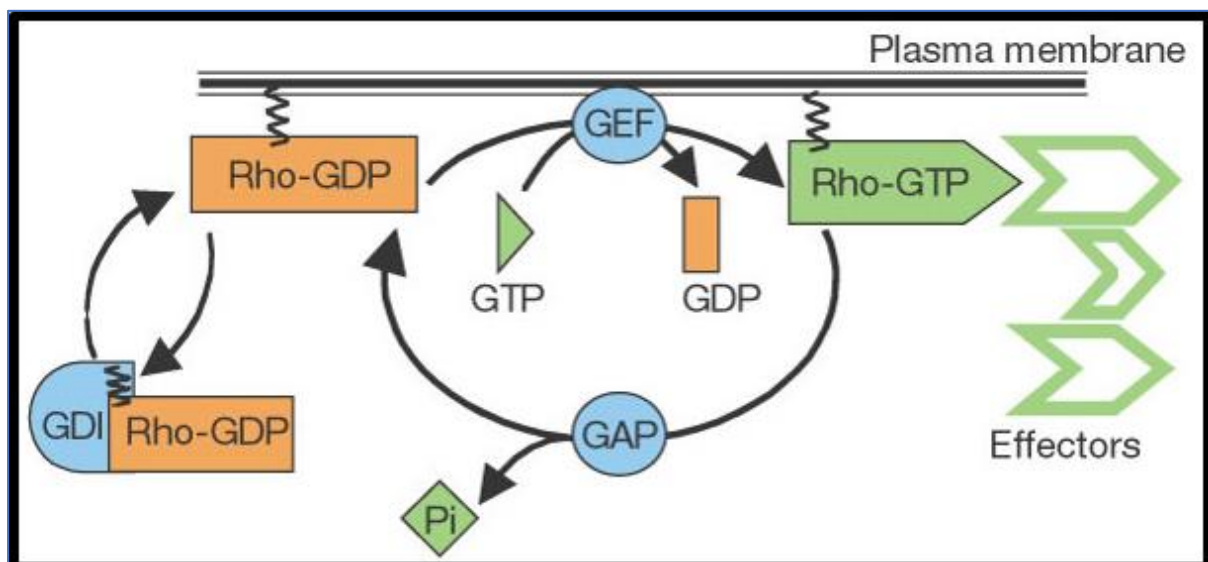
Referred from Etienne-Manneville *et al*., 2002; Depicted herein, a candidate of the small GTPase family; Rho GTPases. There are 20 Rho family proteins described in mammals. Like

other small GTPases, they cycle between an active and inactive form. The active form is
bound to Guanosine triphosphate (GTP) while the inactive form is bound to Guanosine
diphosphate (GDP). About 60 GEFs (Guanine nucleotide exchange factors) enable exchange
of GDP with GTP. Further 70 GAPs (GTPase activating proteins) drive hydrolysis of GTP to
GDP.

Figure 2 – Over activation of Rho GTPase members induces changes to actin and adhesion
complexes
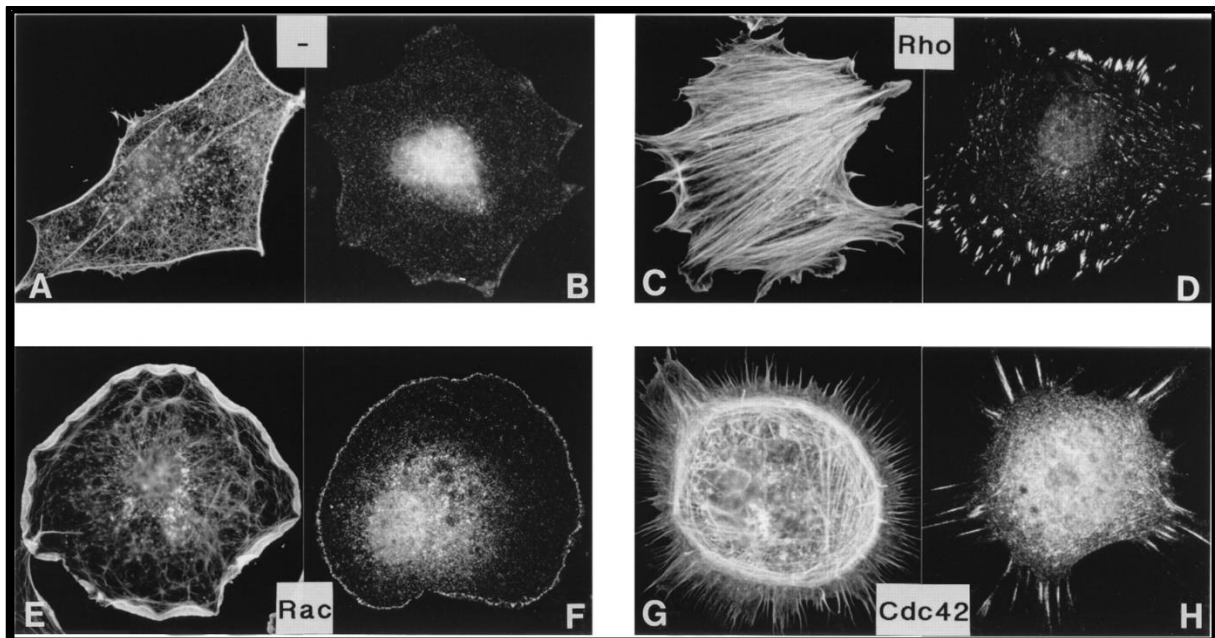
Referred from Hall 1998; Cytoskeletal re-organization are modulated by Cdc42, Rac and
Rho. Swiss 3T3 fibroblasts are serum deprived and each of the prominent Rho family
members are over activated to assess their effect individually. (A) stained for actin filaments
and (B) stained for adhesion complexes containing vinculin in quiescent control cells. (C) and
(D) document increase in stress fibres and focal adhesion complexes in response to over
activation of Rho. Rac injected, expresses lamellipodia (E) and associated adhesion

complexes (F). Improving activation for cdc42 enhances filopodia (G) and associated

adhesion complexes (H). Scale: 1 cm = 25 μm.

Protein damage is often a significant manifestation of stress including cases of nano-toxicity (Martin and Sarkar, 2017), although there aren't many scientific reports available in this field. Thus, it was crucial to examine how MeOx NPs affect protein expression, particularly the protein synthesis machinery related to stress response. Therefore, expression of eIF2α and its phosphorylated form along with chaperone Hsp70 was evaluated.

The eukaryotic initiation factor (eIF2) is a well-known translation factor, and its phosphorylated form is associated with global inhibition of protein synthesis, one of the first events to occur during, 'Integrated Stress responses'. eIF2 is a multimeric protein consisting of 3 subunits; α, β and γ. Their sequences are greatly conserved across several species indicating possible roles crucial to cellular viability (Kimball *et al*., 1999). The eIF2α phosphorylation at ser51 is also a highly sustained and adaptive response that can cause down regulation of translation initiation under several types of stresses and regulate gene expression. It also routes in unfolded protein responses through PERK; PKR like endoplasmic reticulum kinase (Sidrauski *et al*., 2013). Human eIF2α accepts phosphate groups from kinases PKR (Double stranded RNA activated protein kinase); activated in response to viral infection (Schmedt *et al*., 1995) and interferons in mammalian cells (Meurs *et al*., 1990). Also, the expression of HRI (Heme regulated inhibitor of translation); activated in response to heme deprivation, heavy metals (Chen and London, 1995, Sarkar *et al*., 2005) and GCN2 in response to nutrient deprivation (Hinnebusch, 1994) results in phosphorylation of eIF2α at residue 51-serine. Phosphorylation of eIF2α was hence studied as a dose and time dependent function of MeOx NP toxicity to quantify the level of, 'Integrated stress response' (**Figure 3**).

Figure 3 – Cross talk between ISR and UPR
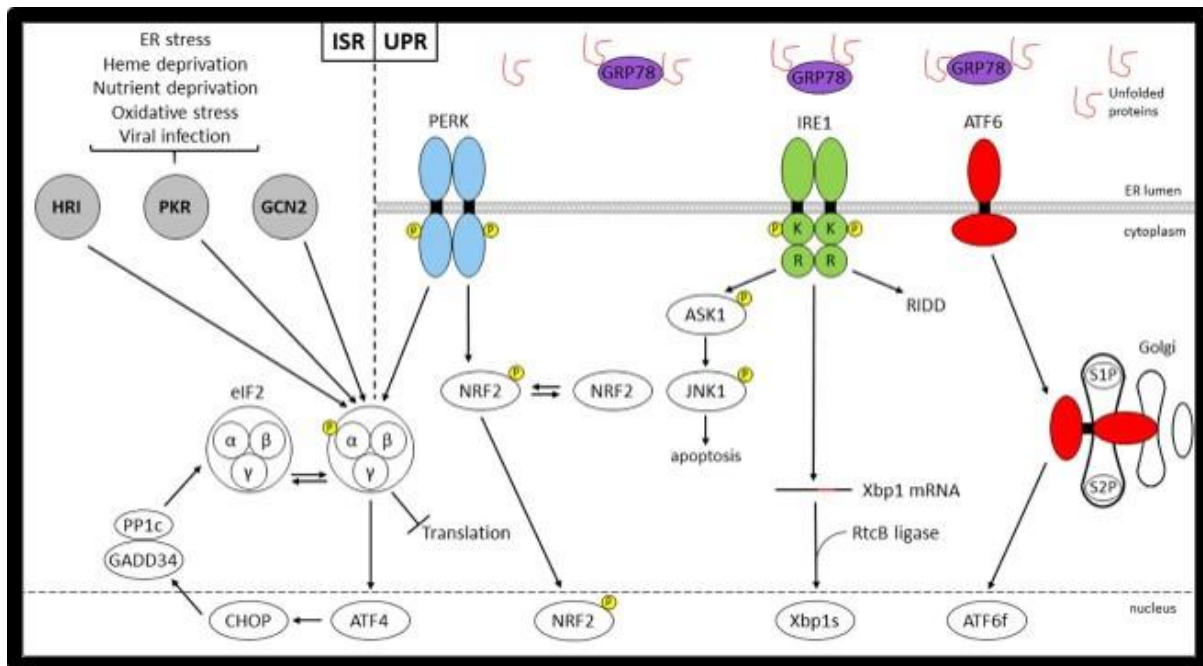
Referred from McMahon *et al*., 2017; Sensors within the unfolded protein response cascade are present along the endoplasmic reticulum (ER) membrane. These are inositol-requiring enzyme1 (IRE1; green), activating transcription factor 6 (ATF6; red) and protein kinase R-like ER kinase (PERK; blue). Their respective cytoplasmic domains activate transcription factors and regulate gene expression. These are XBP1s (X-box-binding protein-1s), NRF2 (nuclear factor, erythroid 2-like 2 transcription factor), CHOP (C/EBP homologous protein), ATF4 and ATF6. The Integrated stress response (ISR) merges with the UPR cascade at the PERK sensor (Protein kinase R like endoplasmic reticulum kinase). Like its counterpart HRI (Heme regulated eIF2α kinase), PKR (Protein kinase R) and GCN2 (General control non-repressible 2 protein kinase); PERK phosphorylates ser 51 in eIF2α causing inhibition of global protein synthesis.

As ER stress increases with increased accumulation of unfolded proteins, transcription factors ATF6, XBP1, ATF4 and ATF 5 are sequentially activated. This is triggered by GRP78/Bip (78KDa glucose regulated protein or binding Immunoglobulin

protein) dissociation from the ER domains of ATF6, IRE-1 and PERK respectively, activating them in the process (McMahon *et al*., 2017). GRP78 or Hsp70 is a stress related chaperone which is crucial for activation of all ER transmembrane signaling molecules (Wang *et al*., 2009) and may also be expressed while eIF2α stays phosphorylated through activation (Kepp *et al*., 2015). Thus, studying the expression of Hsp 70 enables analysis of the degree of unfolded protein response triggered to MeOx NP toxicity. To better understand such cellular responses, Hsp70 expression is evaluated at the protein level, for both ZnO and TiO_2 exposure on A549 cells.

Finally, expression of NFκB1 transcript is checked as a cellular response to metal oxide nanoparticle exposure. The NFκB protein is a transcription factor that is activated by several stress conditions to translocate into the nucleus and regulate specific gene expression. They relay signaling cascades to appropriately respond to foreign particles, radiation, cytokine release and chemical radicals in the form of growth, differentiation and cell death (Morgan and Liu, 2011). NFκB proteins are thus crucial to inflammatory and immunity processes (Hayden and Ghosh, 2008, Vallabhapurapu *et al*., 2009).

1.2 Methods:

1.2.1   Materials

Common laboratory reagents were acquired from Himedia (India) and Sigma, Aldrich (USA), antibodies were procured from Cell Signaling (USA), Biolegend (USA) and Abcam (USA). Human A549 cells were obtained from National Centre for Cell Sciences, India. Characterized nanoparticles were obtained through Sigma, Aldrich (USA). Plastic ware used for cell culture were secured from 'Corning'.

1.2.2   Cell Culture

A549 cells were cultured *in vitro* and maintained in DMEM supplemented with 10% FBS (37°C with 5% CO_2). For all experiments, cells were charged with nanoparticles at 80% confluence, unless otherwise mentioned.

1.2.3   Charging of Nanoparticles

ZnO and TiO_2 NPs were dispensed in a stock concentration of 1 mg/ml (12.2mM ZnO and 12.5mM TiO_2). The doses of charge chosen were; control (0 µg/ml = 0 mM), 12.5 µg/ml (~0.15mM), 25 µg/ml (~ 0.31 mM), 50 µg/ml (~ 0.62 mM), 100 µg/ml (~ 1.24 mM) and 200 µg/ml (~ 2.48 mM) for ZnO and TiO_2 NPs. Doses were chosen based on our viability assays (Santimano *et al*., 2013) along a range commonly observed at industrial sites (Rogaczewska and Matczak, 1984). Our dose range of investigations allows evaluation of crucial biological differences in cellular responses to sub-lethal concentrations of nanoparticles. Stocks were prepared in DMEM aseptically and charged for experiments in the chosen doses after

thorough vortex to avoid aggregation and to ensure exposure to nano-scale particles. Serum was added separately to ensure a consistent 10% concentration throughout various experiments.

1.2.4 Study of Cellular Viability

A549 cells were exposed to different concentration of NPs (0.15, 0.31, 0.62, 1.24 and 2.48mM) for 24h, 48h and 72h. Cell growth and proliferation was monitored by determining the cell number using neubauers-hemocytometer following trypan blue dye exclusion test (Strober 2015).

1.2.5 Mitochondrial activity Assay

Viability was investigated using resazurin as per Santimano *et al*., 2013. 2.5×10^4 cells were added per well in a 24 well plate. This was done to ensure resolution along the range of doses tested. Post 24 hours of seeding, fresh media was added, maintaining 10% serum to better dispense nanoparticles away from aggregation. Nanoparticles were added after thorough vortex from the least concentrated stock to maintain a minimum aggregation at charging, this method was developed by us for proper dispersion of NPs at the time of charging to mimic the dispersion typical of aerosolized NPs. The design is detailed in Table 2. Resazurin was added in a working concentration of 440μM. After 4 hours of incubation at 37°C, positive difference (absolute value) in absorbance at wavelength of 580 nm and 615 nm for each well compared to control (+) were documented and percentage conversion of resazurin to resorufin was calculated and described as a degree of toxicity. The observation correlating to absence of reduction was procured by calculating OD_{580}–OD_{615} of (-) control. Dose which realized to 50% cellular death was assigned LD_{50}.

1.2.6 Cell Morphology Documentation

Cells charged with nanoparticles were incubated for time periods of 24 and 48 hours respectively. Dose points of metal oxide nanoparticles evaluated were; 0.15, 0.31, 0.62, 1.24 and 2.48- mM. Cells of the monolayer were washed with sterile phosphate buffered saline and fixed with 3.7% formaldehyde for 2 minutes. This was followed by permeabilization with 100% ice cold methanol and staining with Hoechst (Hoechst 33342, thermos fischer) for 15 minutes. Fluorescent pictures of nuclei were captured by an inverted microscope to aid visualization of nucleus. A DAPI filer was used that allowed for illumination of light around 340-380nm and emission around 465nm.

1.2.7 Small GTPase expression study at mRNA level

Cellular RNA was secluded by TRIzol reagent (Invitrogen, Carlsbad, CA, USA), as per the brochure instructions. The extracted cellular RNA was reverse transcribed into cDNA utilizing the Bioline cDNA synthesis kit. Specific targets on cDNA were amplified using polymerase chain reaction. The primer sequences utilized for polymerase chain reaction were as follows: cdc42- 5'-gcccgtgacctgaaggctgtca-3' (sense); 5'-tgcttttagtatgatgccgacacca-3' (anti-sense), Rac1- 5'-ggagaatatatccctactgtc-3' (sense); 5'-cttcttctccttcagtttct-3' (anti-sense), RhoA- 5'-cccagataccgatgttatac-3'(sense); 5'-aacctctctcactccatctt-3' (anti-sense) and GAPDH- 5'-agaacatcatccctgcctctac-3' (sense); 5'-ctgttgaagtcagaggagacca-3' (anti-sense). The conditions for polymerase chain reactions set were as described: initial denaturation- 2 min at 97°C and 35 cycles. Cycling parameters comprised denaturation of 1 min at 94°C. This was proceeded by annealing at 57°C for 1min 30 seconds for GAPDH, 68°C for CDC42, 50°C for Rac1 and 53°C for RhoA. Extension was levied for 1 min at 70 °C, with an ultimate extension time of 5 minutes at 70 °C. Amplified targets were separated on 1.2% agarose gel

electrophoresis. BioRad documentation followed and analysis was carried out by Image J. The intensity of each target amplicon was normalized to expression of the internal control; GAPDH.

1.2.8 Small GTPase expression study at protein level

After cell lysate (40 µg) was resolved by 12% SDS-PAGE the western blot was carried out as per Sarkar *et al*., 2007. In brief, the PVDF membranes were washed with tris-buffered saline followed by blocking with 5% non-fat dried milk or 3% BSA as was suited. The membranes were incubated at 4˚C overnight with primary target specific antibodies for cdc42 (Cell Signaling- 1:500), Rac1 (Cell Signaling- 1:750), RhoA (Cell Signaling- 1:750) and β-Actin (Sigma- 1:2000). The membranes were then incubated with secondary antibodies coupled to horseradish peroxidase for optimised time periods at room temperature. The membranes were washed in combinations of TBS and TBST at room temperature. Immunoreactivities were detected by ECL reagents (Amersham GE Healthcare). Expression of target proteins was normalized to β- Actin.

1.2.9 Analysis of phosphorylation status of eIF2α and Hsp70

Protocol followed was as section 1.2.8. Primary antibodies used were β-Actin (Sigma- 1:2000), Hsp70 (Sigma Aldrich- 1:4000), eIF2α (Cell Signaling- 1:2000) and Phospho-eIF2α (Cell Signaling- 1:1000).

1.2.10 Studying the expression of NFκB1 transcript

Protocol followed was as section 1.2.7. The primers used for NFκB1 amplification were 5'-tctgttttgcacctagc-3' (sense); 5'-ccaggtcatagagaggc-3' (anti-sense). Annealing temperature was optimized to be 51ºC.

1.3 Results

All expression studies have basal level or control expression of target assigned at 100%. Expression analysis was performed by ImageJ, NIH. Where ever required, pictures were post processed for background reduction and contrast enhancement using PhotoScape, MOOII TECH, Korea. Standard deviation from 3 independent experiments have been annotated. All gel images photographed document the best representative in a set of 3 independent experiments. P values are calculated, to assess statistical validity by regression data analysis, Microsoft. P value ratings are set as; significant (*) for $0.01 \leq p < 0.05$, very significant (**) for $0.001 \leq p < 0.01$ and extremely significant (***) for $p < 0.001$.

1.3.1   The Trypan blue dye exclusion test

The viability varied as a dose and time dependent manner (**Figure. 4**). ZnO exposed cells documented a percentage viability of 73, 48, 38, 17 and 5 for respective doses (in mM) of 0.15, 0.31, 0.62, 1.24 and 2.48 at 24 hours of incubation. At 48 hours, the viability percentages dropped to 26, 21, 13, 10 and 0 respectively. Cells recovered slightly at 72 hours until an exposure dose of 0.62mM, while at higher doses the cell death increased. Viability data at 72 hours for doses (in mM); 0.15, 0.31, 0.62, 1.24 and 2.48 were 62, 36, 24, 0.2 and 0% respectively.

A similar pattern of viability response is seen in cells exposed to TiO_2 but with less cell death. At 24 hours of incubation, for doses (in mM) 0.15, 0.31, 0.62, 1.24 and 2.48 the viability percentages were 99.6, 92, 64, 24 and 7. The cell death dropped with further incubation up to 48 hours with percentage viability documented at 57, 26.2, 16, 14.3 and 8 correspondingly. Again, cell recovery was seen with further incubation at 72 hours for doses

up till 0.62mM. Viability percentages at 72 hours registered at 63, 53, 46, 15 and 6 for the evaluated set of doses.

Figure 4 - Viability assay by trypan blue dye exclusion method
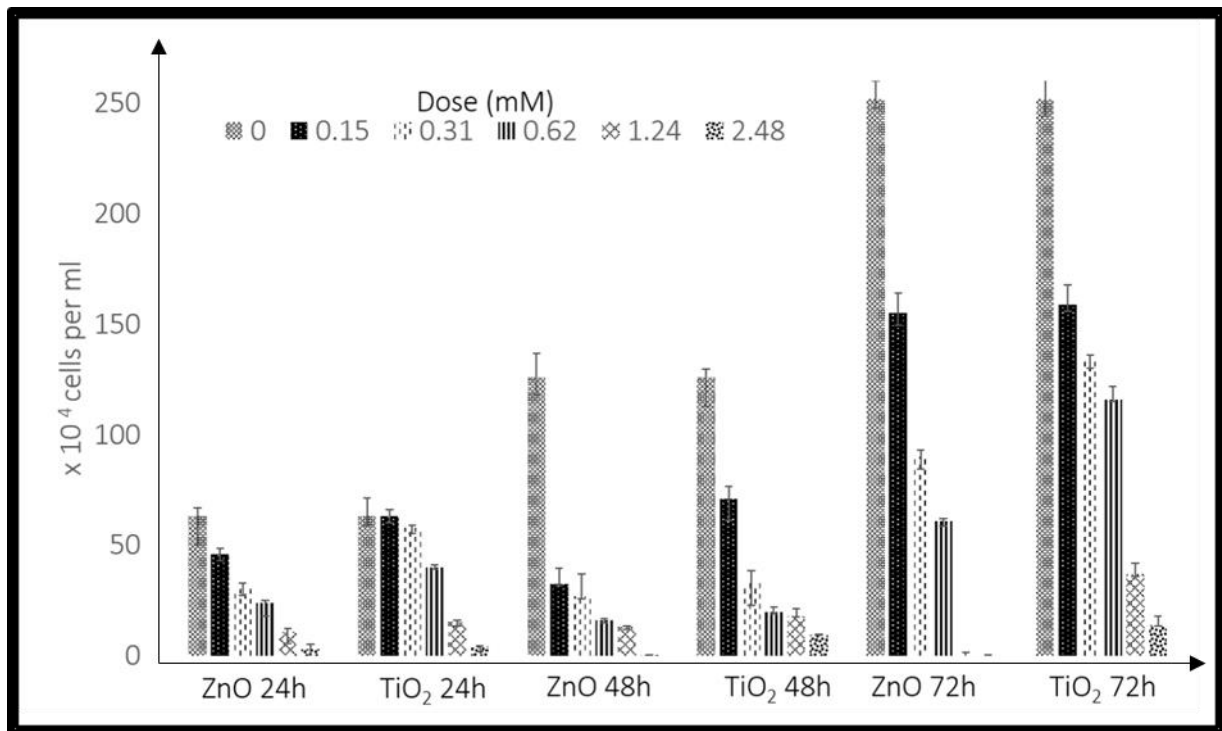
Unstained cells counted by Neubauer's haemocytometer and plotted as a function of dose and incubation time to TiO$_2$ and ZnO NP treatment. P values are as follows; ZnO 24h- 0.002953 (**), TiO$_2$ 24h- 0.000267 (***), ZnO 48h- 0.05 (*), TiO$_2$ 48h- 0.023576 (*), ZnO 72h- 0.013468 (*) and TiO$_2$ 72h- 0.002275 (**).

1.3.2 Resazurin Reduction assay was performed at 24 hours to assay for mitochondrial damage.

The resazurin reduction percentage (**Fig. 5 A**) for ZnO at doses (in mM) 0, 0.15, 0.31, 0.62, 1.24, 2.48, 4.96, 9.92, 19.84, 39.68 and 79.36 (I to XI) were 79.7, 79.1, 73.2, 71.8, 67.8,

60.2, 43.9, 6, 1.9 and 0 respectively. Corresponding values for TiO_2 exposure were 87.3, 87.3, 85.5, 82.1, 74.4, 73.8, 70.7, 67.4, 55.3 and 8.5. LD_{50} for ZnO exposure was 2.26 mM while for TiO_2 was 44.15 mM. Resazurin plate as in **Fig. 5 B**, shows increasing doses (I to XI and negative control) of ZnO resulting in less resorufin production as compared to TiO_2.

Figure 5 A - Assessment of mitochondrial dysfunction
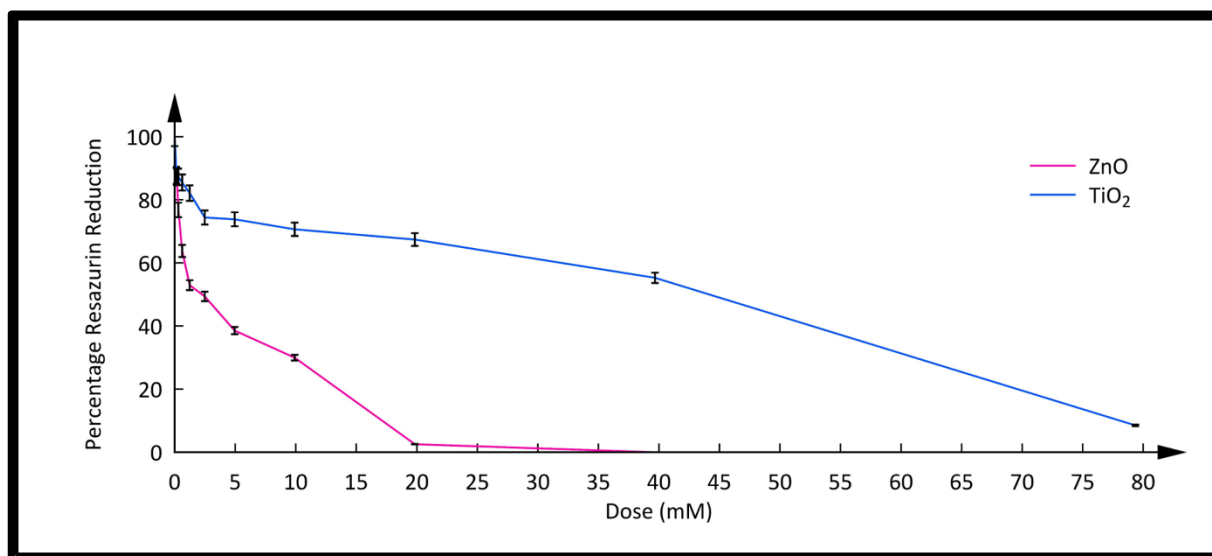
Percentage resazurin reduction is plotted against dose of exposure for TiO_2 and ZnO NP treatment. Resazurin reduction value of the untreated control is considered as a positive control with 100% reduction. P values are as follows; ZnO 24h- 0.002026 (**), TiO_2 24h- 0.0000022 (***)

Figure 5B - Plate picture for resazurin reduction assay
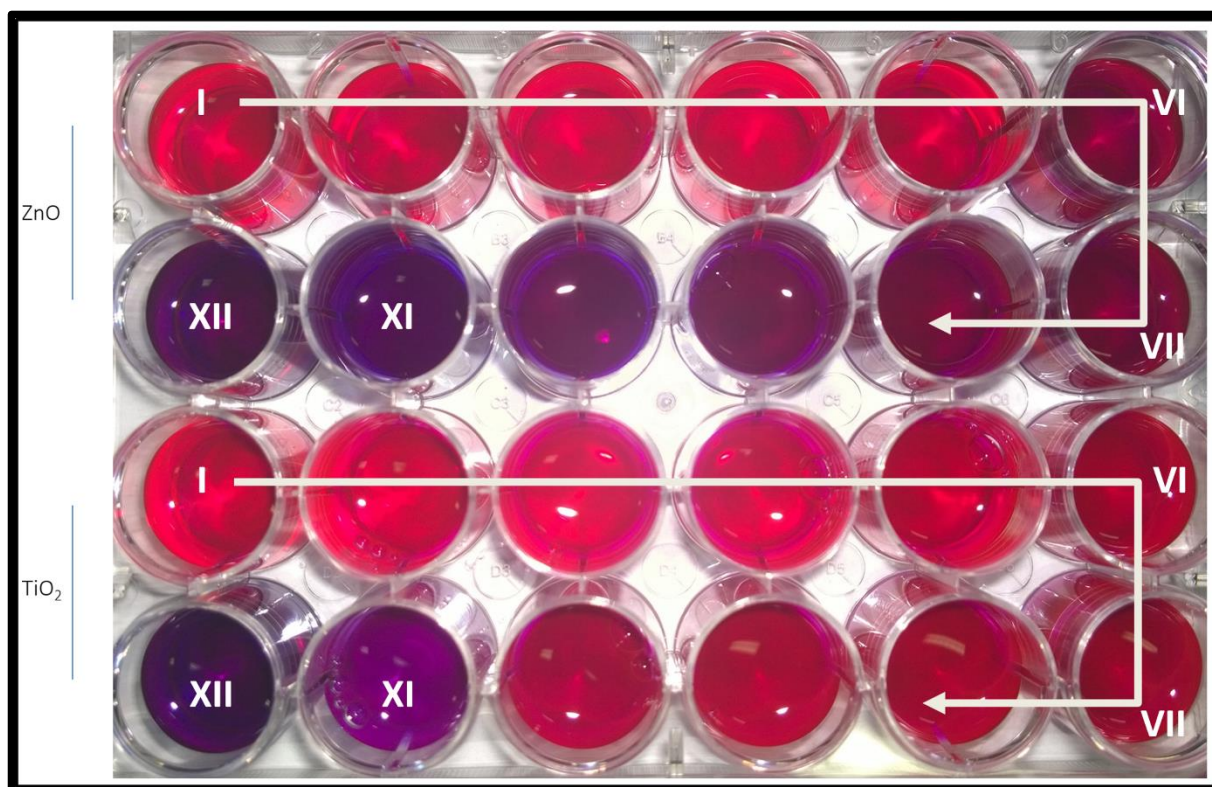
Resazurin reduction in experimental wells are photographed for various doses from 0 - 79.36 mM of MeOx NP exposure and negative control (No NPs and No cells seeded; 0% reduction) and are designated I-XII. With increase in dose, percentage reduction of resazurin (purple) to resorufin (pink) drops drastically for ZnO as compared to TiO_2 NPs.

1.3.3   Morphological Documentation

Photographing of Hoechst stained cells was carried out utilizing an inverted microscope. Following nanoparticle exposure at various dose and time intervals, the cell morphology was documented and analysed (**Fig. 6 A**). Hoechst staining showed enlargement of nucleus (such as in i', n', o', p', q' and u' shown by orange arrows) and necrotic like cells more than apoptotic like cells with increasing exposure to ZnO NPs. In comparison, response to TiO_2 NPs showed a reduction in cell number only after exposure to 50 µg/ml (0.62 mM)

TiO$_2$. Necrotic like cells (indicated by arrows; d, e, f, k, l, r and x) were seen starting from 200µg/ml (2.48 mM) for TiO$_2$ NP exposure and from 50µg/ml (0.62 mM) for ZnO. Few apoptotic like bodies were documented in cells exposed to ZnO NPs (represented by yellow arrows in h', j', e' and f'). Nuclei characterized by increased fluorescence were commonly seen in cells exposed to ZnO NPs starting from 1.24mM (as depicted by red arrows in k' and l'). Spherical morphology was seen in some TiO$_2$ exposed cells (blue arrows in t and u). Filopodial spikes were seen more in response to TiO$_2$ treatment than to ZnO (highlighted by blue diamond arrows in c, e and g for ZnO treated samples and n, o, p, q, s, t, u, v, w and x in TiO$_2$ exposed cells).

Fig. 6 B demonstrates the differences in morphological changes of a single cell following ZnO and TiO$_2$ exposure at 24 hours. The panel for ZnO is published in Santimano *et al*., 2013. Morphological alterations for ZnO from 24 hours to 72 hours follows a dose dependent pattern. At 0.15mM of exposure, stress fibres are visible in a cell enlarged as compared to the control (**Fig. 6 B a**), upon 0.31mM (**Fig. 6 B b**) of treatment cells appear more flattened. Further stress up till 0.62 mM (**Fig. 6 B c**) is presented with spicules and vacuole like granules that seem to fill the cytoplasmic periphery. In the case of morphological response to TiO$_2$ NPs, **Fig. 6 B d-f**, we find increased number of elongated cell protoplasm as indicated by the arrows. These extensions are most likely filopodial spikes.

Figure 6 A - Dose and time dependent morphological documentation of MeOx NP treatment
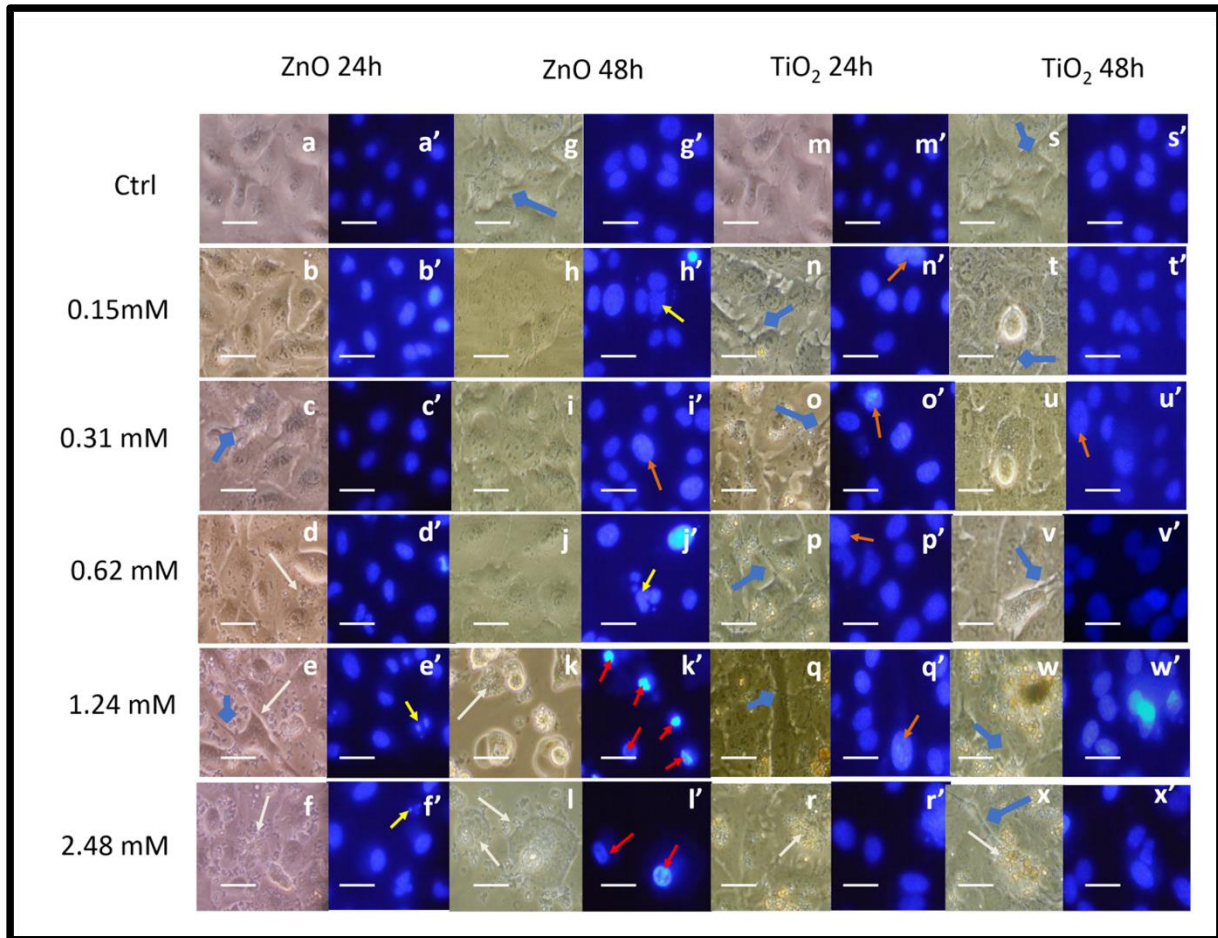
Inverted microscope pictures (a,b etc.) are laid adjacent to fluorescent hoechst pictures (a', b' etc.) of the same field. With increase in dose, pronounced cell death and loss of monolayer is evident for ZnO while, increased cell extensions for TiO_2 NP treatment. Scale bar: 40µm. Arrows indicate specific morphological changes as discussed in the result section 1.3.3.

Figure 6 B - Dose dependent morphological documentation of a single cell to MeOx NP treatment
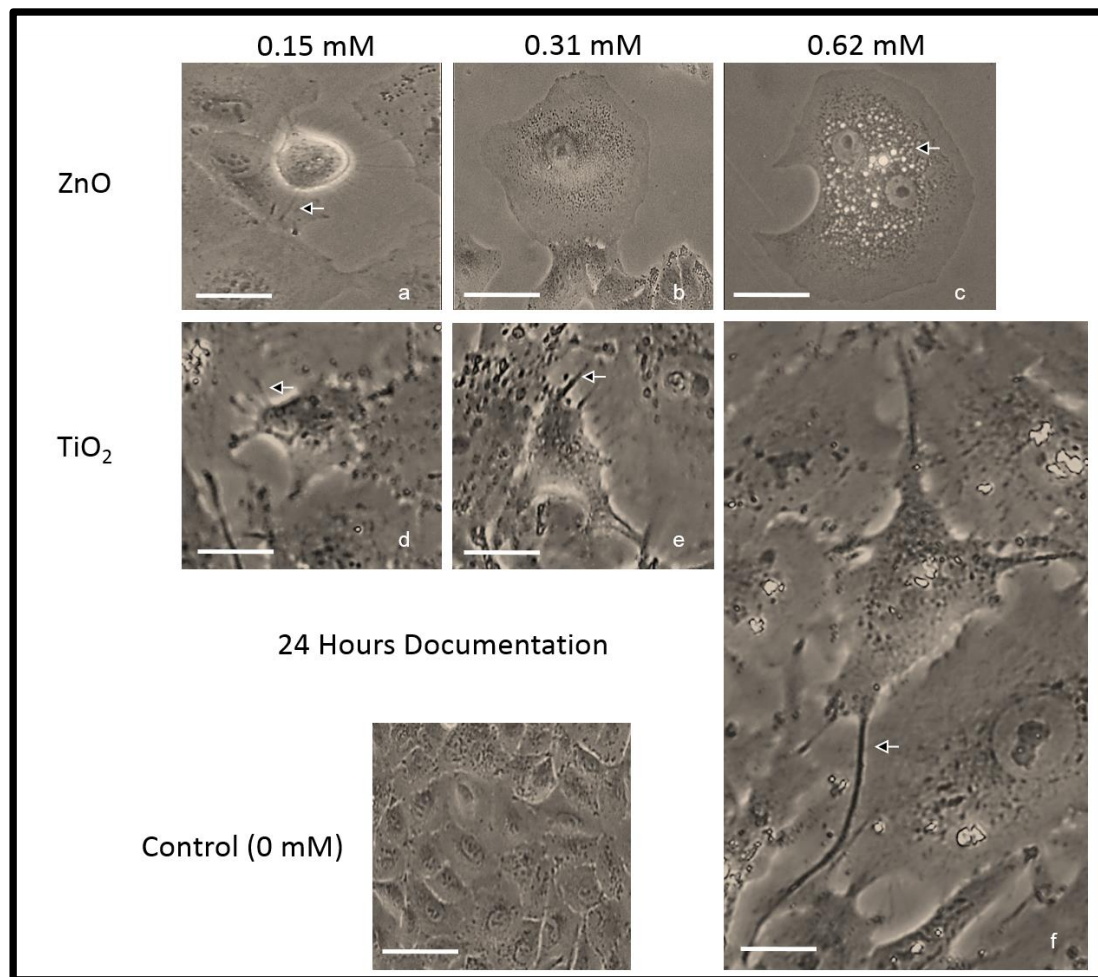
Changes in cell structure to MeOx NP treatment, for 24 hours at dose points of 0.15-0.62 mM is photographed using an inverted microscope and compared to the untreated control. Scale bar: 20 µm. Arrows indicate specific morphological changes as discussed in the result section 1.3.3.

1.3.4 RT PCR analysis of Small GTPase expression.

RT PCR profile is documented for Rho family GTPases (**Fig. 7 A**); Rac1, RhoA and cdc42 in response to ZnO and TiO_2 exposure Doses A, B and C correspond to 0.15mM, 0.31mM and 0.62mM. cdc42 increases at 0 up to a dose of 0.62-mM at 24 hours and decreases from 0.15 to 0.62-mM at 48 hours for both TiO_2 and ZnO exposure. Our experimental evaluation records an average of 10-20% more expression of cdc42 with TiO_2 NPs exposure as compared to ZnO.

Rac1 increases at exposure from 0.15 to 0.62-mM for both 24 hours and 48 hours to ZnO and TiO_2 exposure. At 48 hours, Rac1 shows 30-40% more expression at the mRNA level in TiO_2 treated cells against ZnO NPs.

RhoA also increases as per exposing intensity and time of exposure in response to both ZnO and TiO_2. Although at 0.62mM for 48 hours it begins to reduce for ZnO. RhoA expression to TiO_2 stays elevated around 60% more than control from doses 0.15 – 0.62mM. Densitometric analysis of the same was carried out by ImageJ, NIH and represented in **Fig. 7 B**.

Figure 7 A - Small GTPase expression at mRNA level by RT PCR.
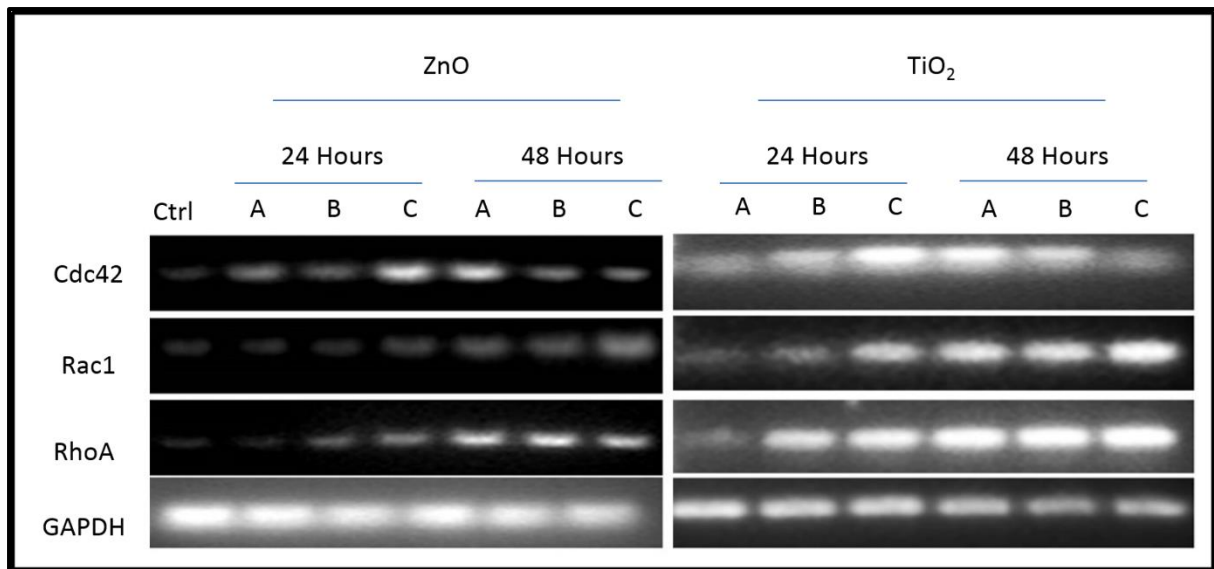
24 hours expression at mRNA level of Small GTPase members; cdc42, Rac1 and RhoA in a dose dependent manner are recorded by photographing with a Gel Documentation set up. Doses: A-0.15, B-0.31 and C- 0.62 mM.

Figure 7 B - Statistical analysis of Small GTPase expression at mRNA level by ImageJ, NIH.
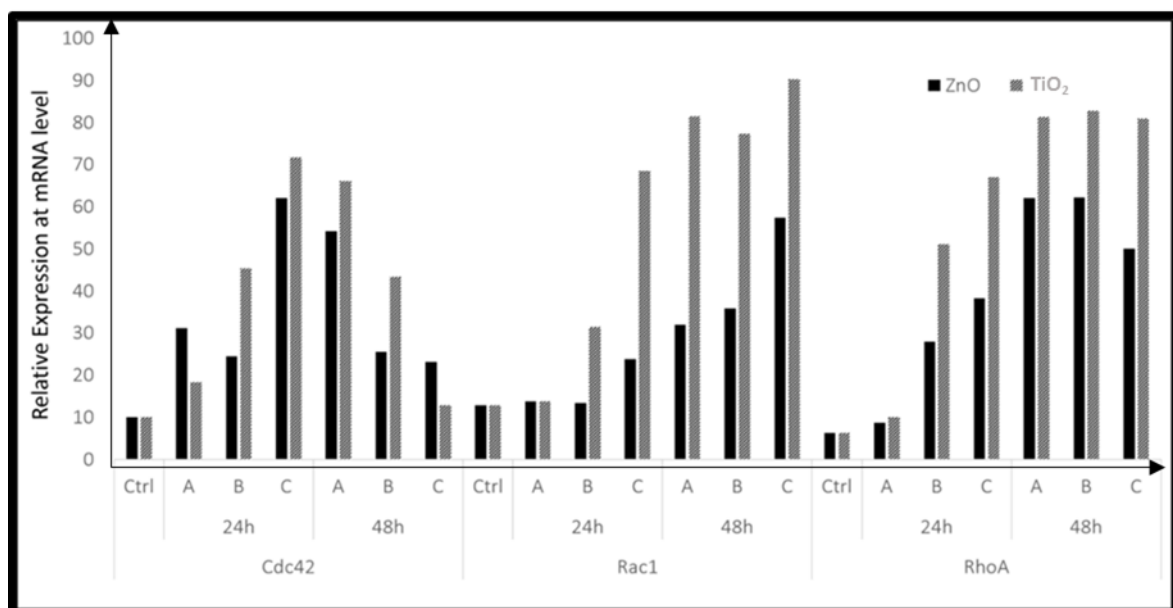
Expression profile is plotted for cdc42, Rac1 and RhoA, relative to the internal control GAPDH in response to MeOx NP treatment. P values are ZnO 24h; Rac1- 0.03 (*), Cdc42- 0.0025 (**), RhoA- 0.026 (*), ZnO48h; Rac1- 0.0045 (**), Cdc42- 0.04 (*), RhoA- 0.0032 (**), TiO$_2$ 24h; Rac1- 0.0085 (**), Cdc42- 0.0241 (*), RhoA- 0.02 (*), TiO$_2$ 48h; Rac1- 0.0031 (**), Cdc42- 0.025 (*), RhoA- 0.0018 (**).

1.3.5 Western Blot analysis of Small GTPase expression.

Small GTPase expression at the protein level was investigated and revealed the following details (**Fig. 8 A**). cdc42 increases up to the evaluated dose of 0.62mM for TiO$_2$ while it down regulates for ZnO at 24h. At the highest dose evaluated; 0.62 mM, cdc42 expression increased 60% of control in TiO$_2$ exposed cells, while decreased 40% to ZnO treatment.

Rac1 remains increased in expression from 0.15 to 0.62-mM in response TiO$_2$ while, ZnO exposed cells see upregulation till 0.31mM and the expression is downregulated thereafter at 0.62mM. Highest expression was noted at 0.62mM for TiO$_2$ with 100% more than control, while the peak for ZnO was observed at 0.31mM at 50% more than untreated samples.

RhoA on the other hand does not show any drastic increase in expression pattern, although the up regulation is seen more pronounced in TiO$_2$ exposure than ZnO. Highest expression of RhoA was seen at 0.31mM in cases of both ZnO and TiO$_2$ treatment, again TiO$_2$ dictated 10% more expression than ZnO treated samples. Densitometric analysis calculated by ImageJ, NIH, is presented in **Fig. 8 B**.

Figure 8 A - Small GTPase expression at protein level by western blot analysis.
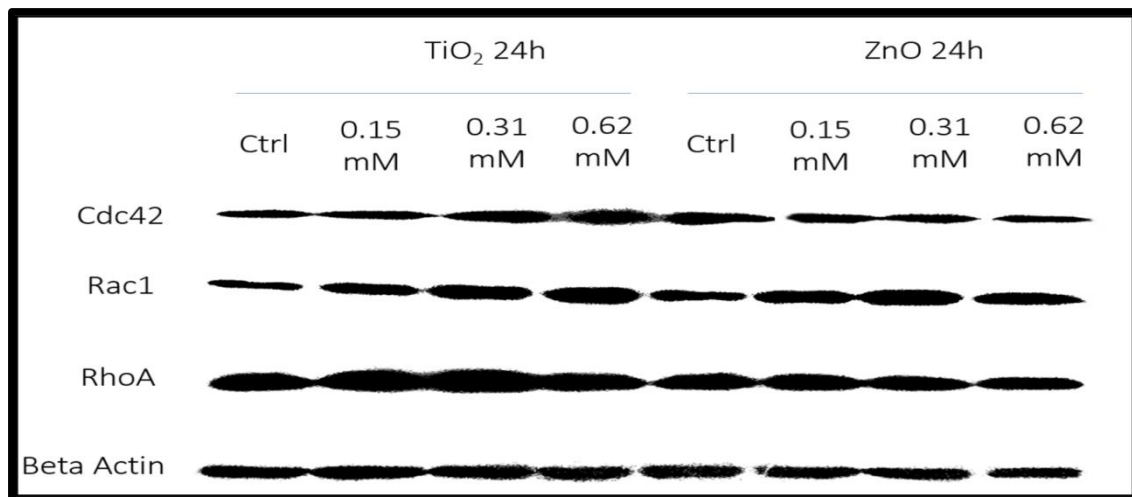
24 hours expression pattern at the protein level, of Small GTPase members; cdc42, Rac1 and

RhoA is recorded in a dose dependent manner.

Figure 8 B - Statistical Analysis of Small GTPase expression at protein level by ImageJ,
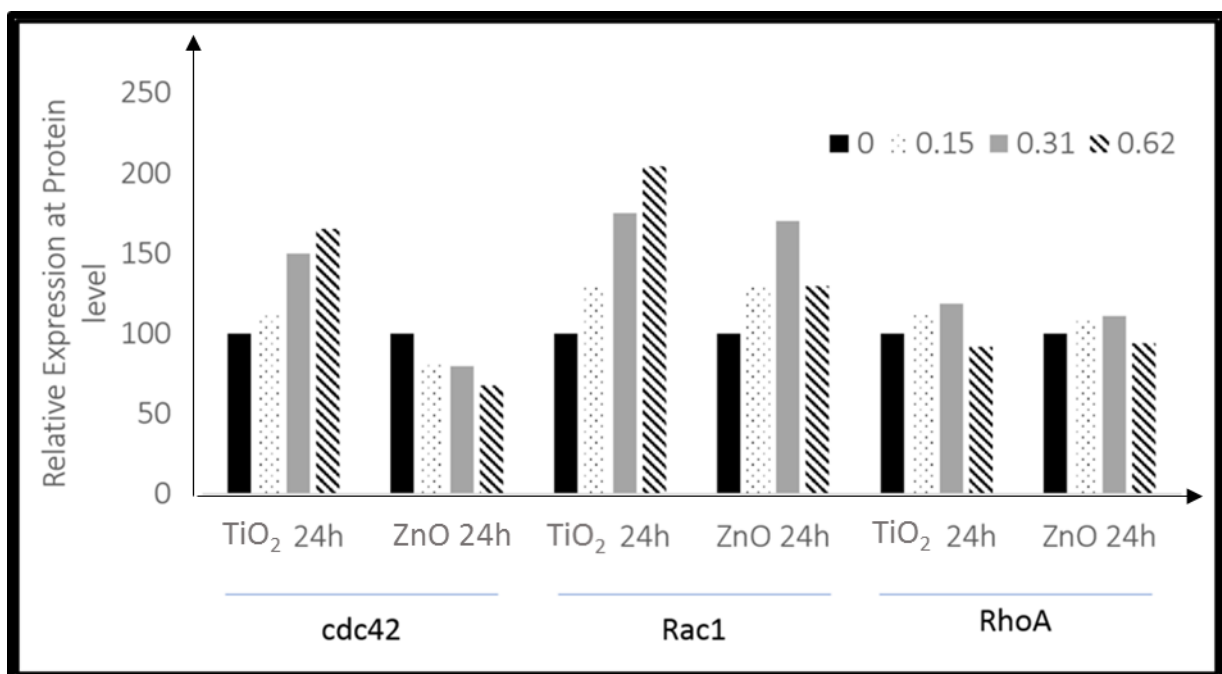
NIH.

Expression profile is plotted for cdc42, Rac1 and RhoA, relative to the internal control β-

Actin in response to MeOx NP treatment. P values are, ZnO 24h; cdc42- 0.003 (**), Rac1-

0.0034 (**), RhoA- 0.037 (*), TiO$_2$ 24h; cdc42- 0.0048 (**), Rac1- 0.0007 (***), RhoA-0.028 (*).

1.3.6 Western Blot analysis of phosphorylation status of eIF2α.

Phosphorylation status of eIF2α was documented to study global inhibition of protein synthesis as a stress response to MeOx NP toxicity by western blot (**Fig. 9 A**). Phospho-eIF2α expression increased up to the evaluated 0.62mM for both ZnO and TiO$_2$ expression at 24 hours. With further incubation, up till 48 hours however, p-eIF2α levels dropped in case of ZnO exposure but stayed elevated in response to TiO$_2$ exposure. Densitometric analysis by ImageJ, NIH is given in **Fig. 9 B**.

Figure 9 A - Evaluation of the phosphorylation status of eIF2α by western blot analysis
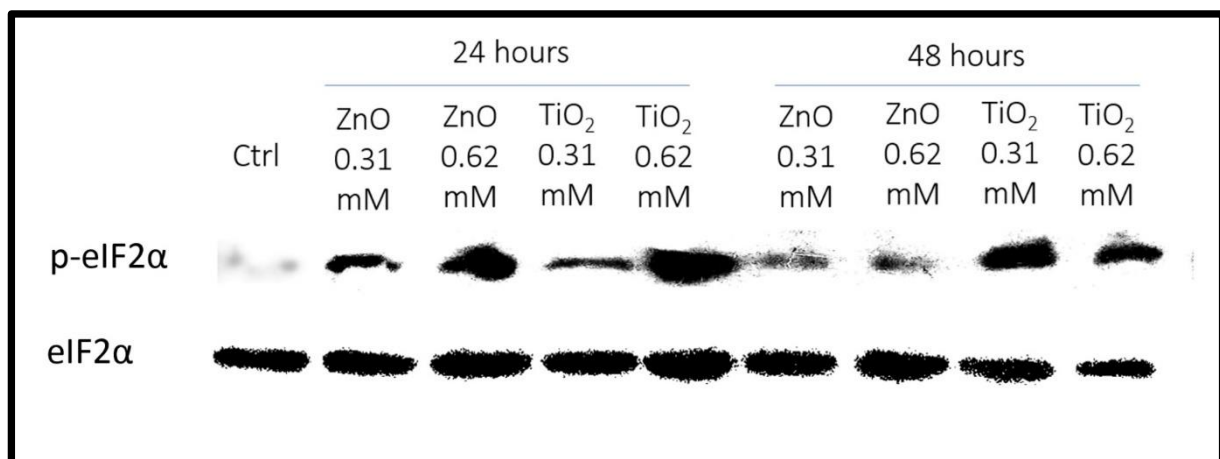
Dose and time dependent analysis of the phosphorylation status of eIF2α was carried out as documented.

Figure 9 B - Statistical Analysis of the phosphorylation of eIF2α by ImageJ, NIH
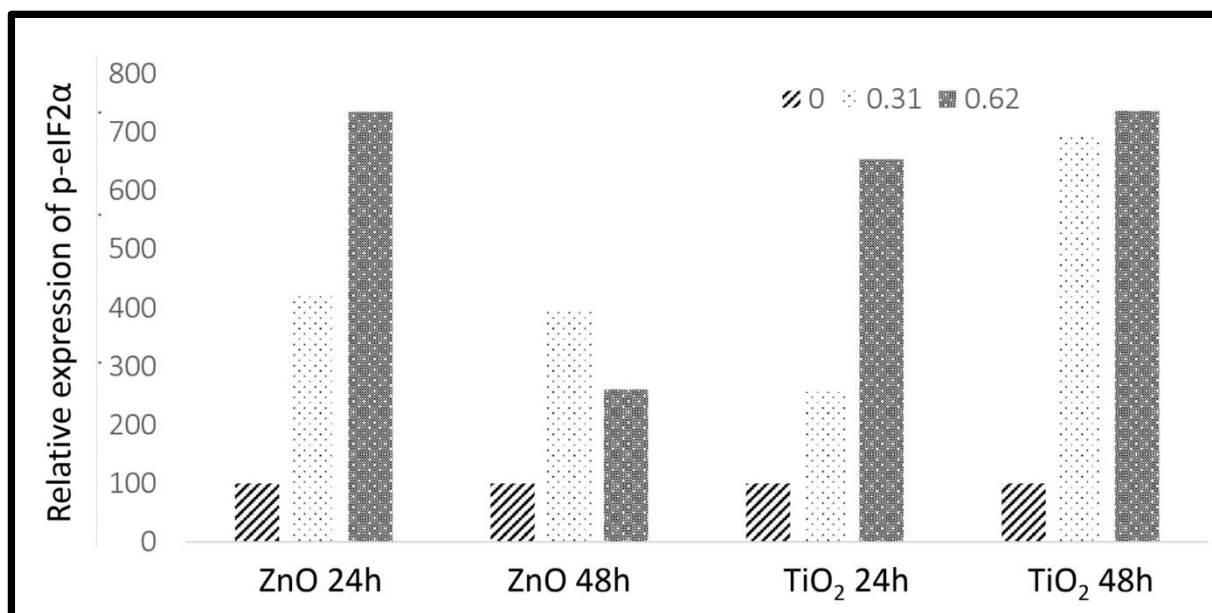
Expression profile of p-eIF2α is plotted, after normalizing with the internal control; the total eIF2α following MeOx NP treatment. P values are, ZnO 24h- 0.0032 (**), ZnO 48h- 0.021 (*), TiO$_2$ 24h- 0.0054 (**), TiO$_2$ 48h- 0.0028 (**).

1.3.7 Protein level analysis of Hsp70 expression in response to MeOx nano-toxicity.

Chaperone Hsp70 expression was documented to nanoparticle exposure at 24 hours and 48 hours as a dose dependent function (**Figure 10 A**). With TiO$_2$ exposure at 24 hours, Hsp70 expression upregulated with increase in dose up till the documented dose of 0.62mM at 3 times the control expression. Further incubation of 48 hours also showed an increase in Hsp70 expression with increase in dose, though maxima reached among the documented doses was at 0.62mM with 1.96 times control expression.

However, ZnO treatment for 24 hours reached maxima at 2.44% of control at 0.15mM. There after further increase in dose, observed a decrease in Hsp70 expression. Increased incubation of 48 hours documented downregulation of Hsp70 with expression

percentage at 100, 73, 64 and 50.5 for doses 0, 0.15, 0.31 and 0.62mM respectively. Densitometric analysis by ImageJ, NIH is plotted in **Figure 10 B**.

Figure 10 A - Analysis of the Hsp70 expression at the protein level by western blot analysis.
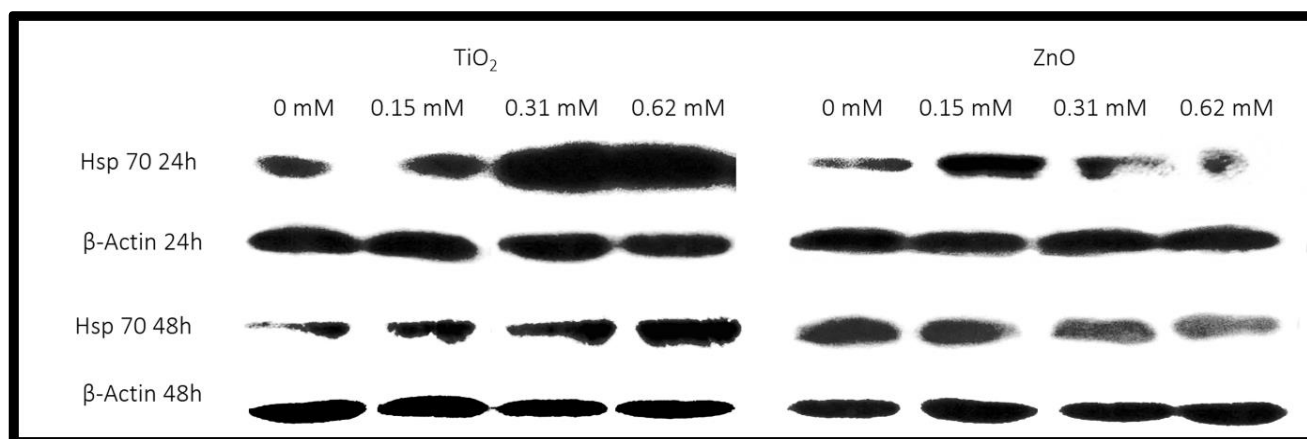
Dose and Time dependent expression of Hsp 70 was recorded as shown.

Figure 10 B - Statistical Analysis of Hsp70 expression by ImageJ, NIH.
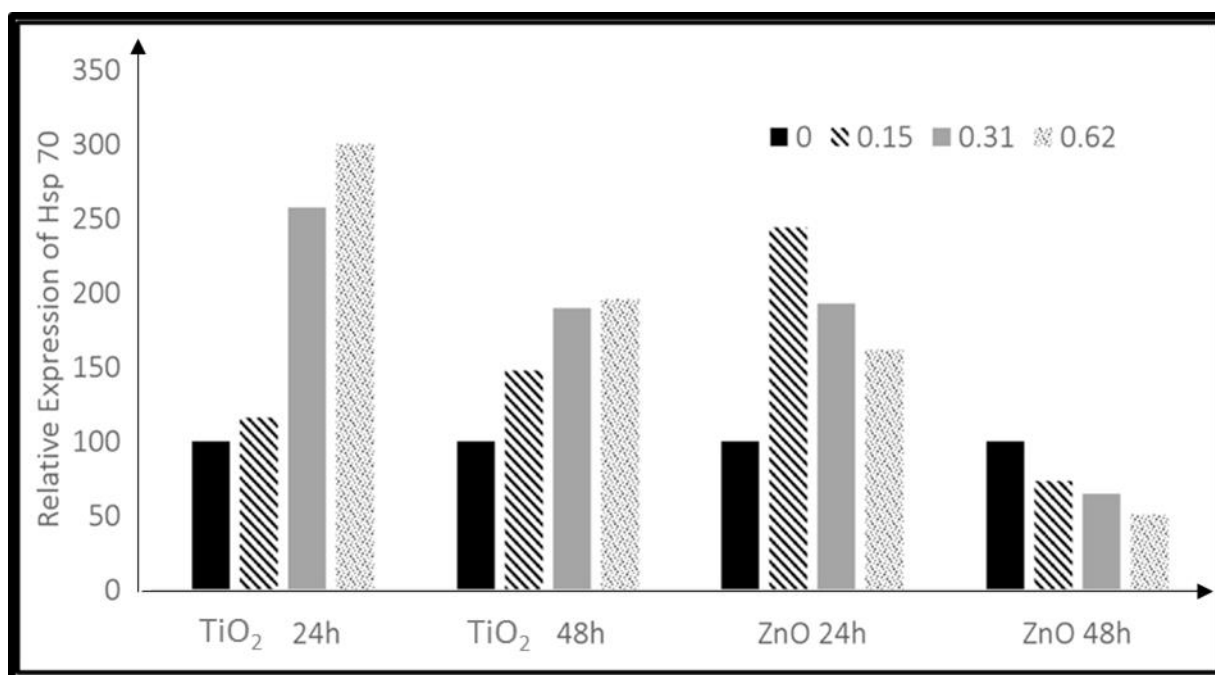
Dose and time dependent expression of Hsp70 is plotted, after normalizing with the internal control; β-Actin in response to MeOx treatment. P values are TiO$_2$ 24h- 0.037 (*), TiO$_2$ 48h- 0.016 (*), ZnO 24h- 0.0288 (*), ZnO 48h- 0.039 (*)

1.3.8   mRNA level analysis of NFκB1 as a response to MeOx nano-toxicity

NFκB1 transcript expression was documented at 24h as a dose dependent function of ZnO and TiO$_2$ nanoparticle exposure (**Fig. 11 A**). **Figure 11 B** gives the densitometric analysis of this evaluation. Average NFκB1 transcript expression increases on exposure to ZnO nanoparticles and peaks at 0.31mM with an expression to GAPDH of 152.15%, when the basal level expression is considered as 100% expression. Thereafter with further increase in exposing dose, tested up till a dose of 2.48mM, the expression drops to 127.51%, but stays above the basal control expression.

In case of TiO$_2$ treatment, average expression of NFκB1 transcript drops to 91% at 0.15mM. At 0.31mM, it raises slightly to 93.12mM. With further increase in dose to 0.62mM, the expression sharply peaks at 159.73%. With successive exposure to higher doses, the amount of NFκB1 transcript drops to 130.34% at 1.24mM and 111.11% at 2.48mM.

Figure 11A- Analysis of NFκB1 expression at mRNA level by RT PCR
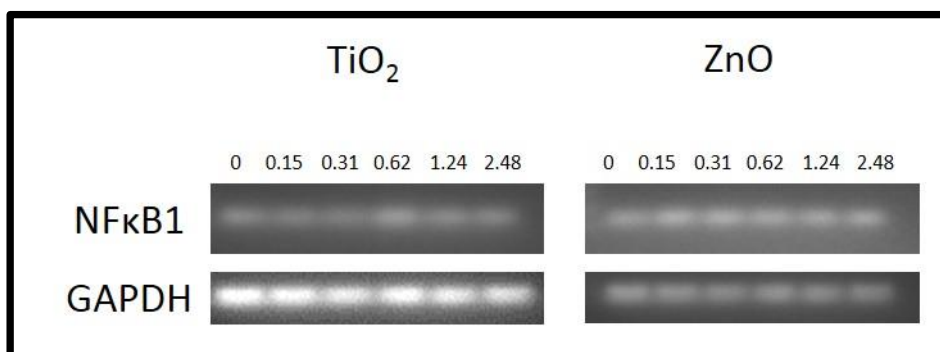
24h documentation of NFκB1 transcript expression to ZnO and TiO$_2$ nanoparticle exposure.

All doses are in units mM.

Figure 11B- Densitometric analysis of NFκB1 transcript expression
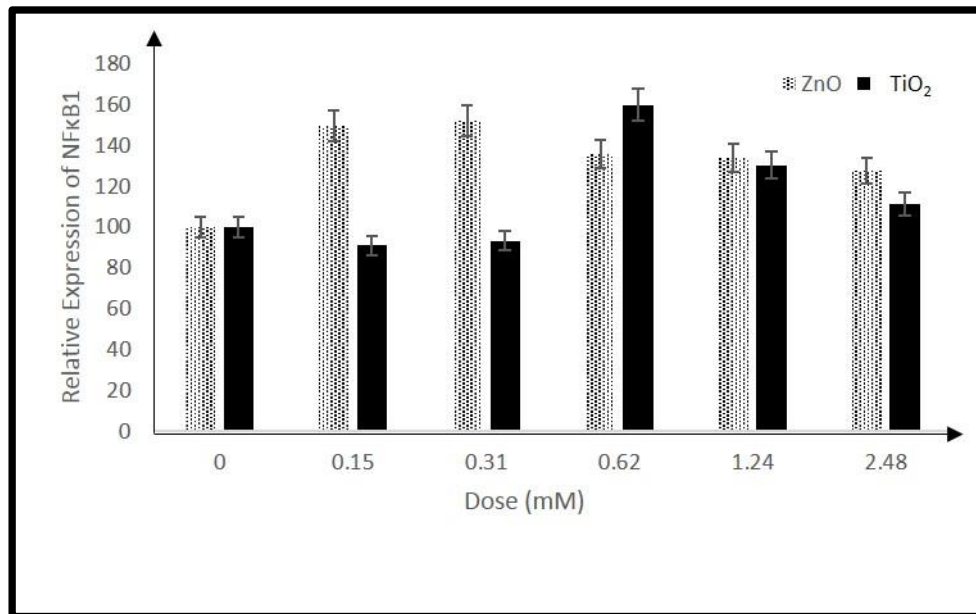
Dose dependent expression of NFκB1 is plotted, after normalizing with the internal control;

GAPDH in response to MeOx treatment. P values are TiO$_2$ 24h- 0.0025 (**) and ZnO 24h-

0.00034 (***)

1.4 Discussion

We selected two candidate nanoparticles of varying toxicities; ZnO and TiO_2, to draw out any differences in cellular responses of A549 cells to their exposure.

A similar total viability response was observed of decrease in viability with increase of exposing dose. However, as expected ZnO was more lethal than TiO_2. With increased incubation periods, viability improves in case of both TiO_2 and ZnO exposure, especially at 72 hours. This might be because cells in question are alveolar type II cells (A549 cells) which are known to display higher tolerance to stress (Ravindran *et al*., 2017).

Resazurin reduction assay was performed to understand the metabolic activity and mitochondrial health of cells exposed to metal oxide nanoparticles. ZnO did confer higher lethality over TiO_2, with LD_{50} value of 2.26mM as against 44.15mM for the latter. Also, resazurin reduction values were significantly higher than total viability values, for respective doses evaluated, suggesting mitochondrial dysfunction may not be the only cause of death.

Morphological documentation reveals less budding typical of apoptosis and more cells with ruptured plasma membrane with increase in exposure, especially for ZnO treatment. This allied with analysis from trypan blue dye exclusion test and resazurin reduction assay suggest a majorly necrotic mode of death.

We had explored the phosphorylation status of eIF2α to understand if this well-studied stress response is also an occurrence in nanoparticle mediated toxicity. A continued phosphorylation of eIF2α, particularly at 48 hours in response to TiO_2 as compared to ZnO nanoparticles was observed. Global inhibition of protein synthesis is a consequence of phosphorylation of eIF2α and it marks the onset of integrated stress responses. This could be an adaptive response by providing the cell with an opportunity to limit deleterious effects of noxious agents and help conserve resources.

Further, expression studies for Hsp70 revealed TiO_2 treatment enables its upregulation more than ZnO NPs. Since Hsp70 is known to aid stress recovery (Sheikh and Fornace, 1999) and TiO_2 exposure results in a significant tolerance over ZnO NPs, it could be deduced that TiO_2 subjection realizes more of the unfolded protein response. Over expression of the heat shock protein, Hsp70, is known to reverse misfolded proteins including cytoplasmic aggregations such as the stress granules (Kedersha and Anderson, 2002). This in tandem with our morphological documentation studies; ZnO NP treatment does result in granular accumulation (**Fig 6 B c**) within cells not seen in TiO_2 treated cells.

Another crucial assessment from the Hsp70 expression analysis is that though ZnO shows markedly less Hsp70 upregulation than TiO_2, however it stays elevated up till 0.15mM for 24 hours. Thereafter, with increased incubation to 48 hours, Hsp70 expression gets downregulated. TiO_2 exposure is documented for Hsp70 upregulation for 24 and 48 hours up till the evaluated dose point of 0.62mM. This presents that both ZnO and TiO_2 NP exposure have some amount of protein misfolding as a cellular response. As amplification of Hsp70 precedes repair of misfolded protein conformers (Mayer and Bukao, 2005). Hsp70 is capable of binding to the hydrophobic domain of their misfolded substrate and aid repair by stabilizing against aggregating denaturation (Evans *et al*, 2010). There are many forms of protein misfolding such as improper degradation, localization errors, dominant negative mutations and gain of toxic function (Valastyan and Lindquist 2014). Irrespective of the route, misfolded proteins often exacerbate the generation of reactive oxygen species (ROS) and reactive nitrogen species (RNS) resulting in oxidative stress (Gregersen and Bross 2010). Oxidative stress has already been documented in nano toxicity induced by ZnO and TiO_2 (Dubey *et al*., 2015). Our studies are in tandem with this research and indicate that oxidative stress could well be a significant contributing factor to the mechanism of toxicity induced by MeOx NPs.

The phosphorylation of eIF2α is also a translational regulation event (Baird *et al*., 2014), which may account for the differences in expression profiles of small GTPases between the mRNA and the protein level.

mRNA level expression of small GTPase for both ZnO (Santimano *et al*., 2013) and TiO$_2$ exposure follow a similar pattern; upregulation of RhoA and Rac1 while a spiked expression for cdc42. This pattern varies however between ZnO and TiO$_2$ exposure at the protein level. With cdc42 upregulating up to 60% more than control at 0.62mM in case of TiO$_2$ and downregulating to 40% of control expression at the same dose for ZnO. This can directly be co-related to the increased filopodial phenotypic expression to TiO$_2$ not observed with ZnO exposure. Moreover, models of study *in vitro*, present a zone of stress in toxicity studies (Soldatow *et al*., 2013). It is thus probable that expression of more filopodial extensions in response to TiO$_2$ treatment may help cells become more migratory in nature and escape the zone of stress. Thereby, making them tolerant to higher doses of nanoparticle exposure.

Analysis of NFκB1 transcript expression for both ZnO and TiO$_2$ nanoparticle exposure, reveals presence of inflammatory cellular response evidenced by a transient upregulation of NFκB1 (Lawrence 2009). ZnO exposure upregulates NFκB1 at a lower dose exposure as compared to TiO$_2$ treatment, suggesting a higher degree of cellular stress particularly ER stress (Tam *et al.*, 2012), in case of ZnO nanoparticle subjection.

Chapter 2

Degree of migration between ZnO and TiO$_2$ NP treated cells.

2.1 Introduction

Cellular migration broadly connotes to movement of cell from one location to another in two-dimensional space. Cellular migration is one of the cellular responses in A549 cells to TiO_2 over ZnO NP exposure. It is executed by a polarized cell morphology that enables protrusion over a trailing end. Potency for integrin associated attachment to basal lamina is also vital. Together the contraction and release of cytoskeletal structures enable cell movement (Petrie *et al*., 2009).

Triggers for migration activate crucial cell surface receptors and induce morphological changes. Cellular movement necessitates the orchestrated set of events highlighted by restructuring of the actin cytoskeleton, thereby, enabling tightening of cell cortex, re-assembly of focal adhesion points, ultimately forming a leading edge. Novel focal contacts further contract the cell cortex driving the cell forward in the direction of migration. The cycle continues until cell reaches the chemokine source and the high local concentration ceases the gradient, also arresting the movement with it (DeFea, 2013).

Cell migration (**Figure 1**) is ordained by a series of signal transduction pathways that include small GTPases, cytoskeleton-modifying proteins, kinases, lipid second messengers and motor proteins. Cells achieve movement when different signaling cascades are consistently presented in specific locations within the cell while maintaining potency of response to extra cellular triggers (Welf and Haugh, 2012). Both epithelial and mesenchymal cells can migrate, although what external cues trigger specific cellular changes to channel directional movement is still under considerable research. However, mesenchymal phenotype has increased migratory and invasive capabilities, combined with a greater resistance to cell death (Kalluri and Weinberg, 2009). Epithelial to mesenchymal transition (EMT) thus greatly

enables migration and invasiveness, though migration alone does not necessitate EMT

(Schaeffer *et al.*, 2014).

Figure 1 – Understanding cell motility
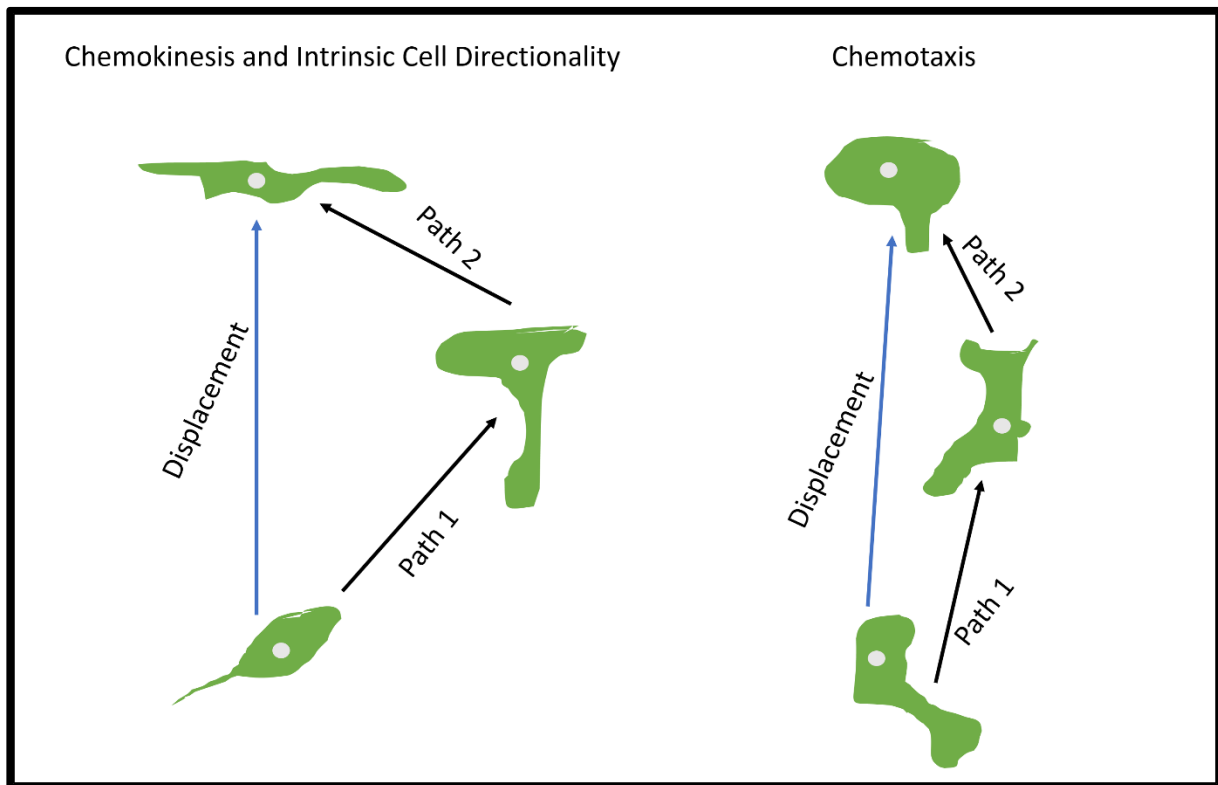
Recreated along Petrie *et al*., 2009; Motility of a cell can be random such as in chemokinesis. The path of movement need not be the shortest path to final spatial displacement. The cell takes arbitrary path until arriving at the most favourable state. Chemotaxis, an example of directed migration exhibit movement closest to the shortest path of favourable displacement in response to a stimulus.

Cellular responses of A549 cells in exposure to MeOx NPs were tested for their
migrative and invasive capabilities with wound healing and transwell invasion assays. Our
previous research concluded a marked change in morphology with pronounced filopodial
spikes in response to TiO_2 NP exposure. Thus, MeOx NP treated samples were also tested for
Epithelial to Mesenchymal transition by characterizing the expression pattern of an allied set
of markers; E Cadherin, N Cadherin, EGFR and Clathrin. Filopodial extensions preceded by
loss of cell adhesion often occur at the onset of cell migration during EMT (Berndt *et al.*,
2008). Downregulation of E Cadherin along an upregulation in N Cadherin is the hallmark of
EMT (Zhang *et al.*, 2013). E Cadherin and EGFR also regulate cell adhesion.

Figure 2 – Interplay between E Cadherin and EGFR governs cell adhesion
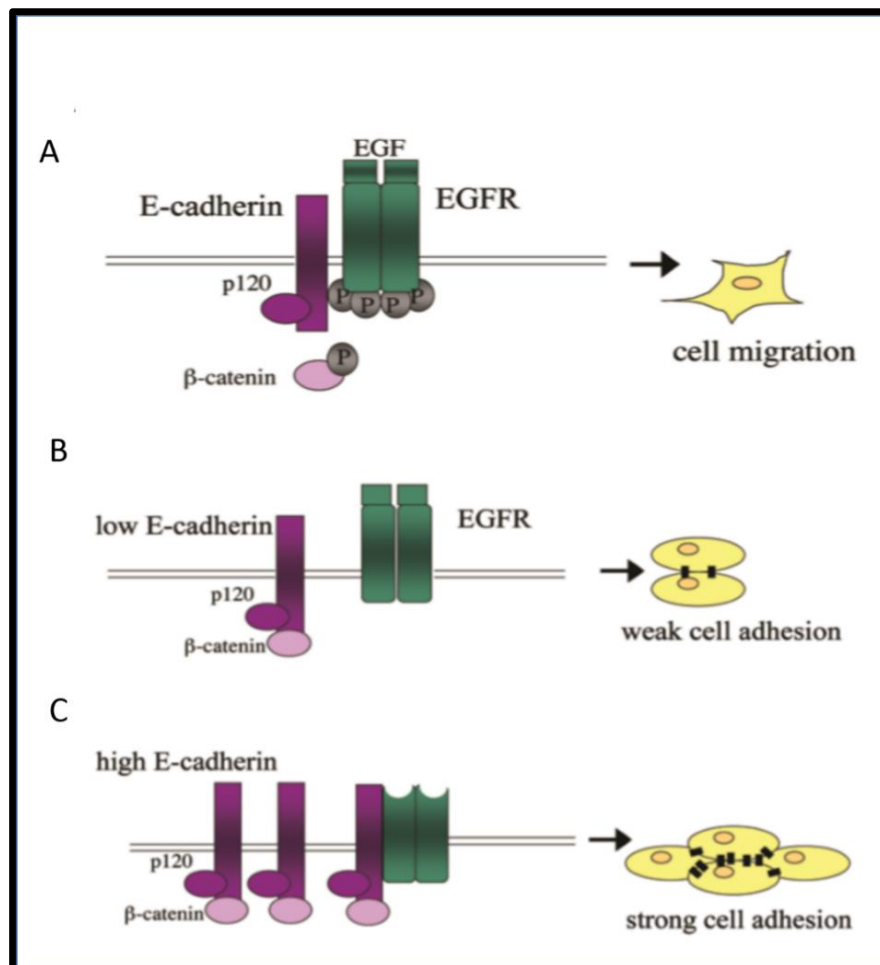
Referred from Andl *et al*., 2004; A- Migration; EGFR activation triggers disruption of adherens junctions causing increased cellular migration. B- weak cell adhesion; is documented for decreasing expression of E-cadherin which permits some EGFR activity. C-strong cell adhesion; is the case for high E-cadherin expression. EGFR is immobilized and adheren junctions remain intact.

The internalization of epidermal growth factor receptor (EGFR) is largely mediated by clathrin coated vesicles (Sigismund *et al*., 2008). Though there are conflicting reports of whether this internalization deflates or prolongs the EGFR signaling (Tomas *et al*., 2014). Thus, we have also examined the expression pattern of clathrin in this signaling context.

2.2 Methods

Materials

Common laboratory reagents were acquired from Himedia (India) and Sigma-Aldrich (USA) and antibodies were procured from Cell Signaling (USA), Biolegend (USA) and Abcam (USA). Human A549 cells were obtained from National Centre for Cell Sciences, India. Characterized nanoparticles were secured through Sigma, Aldrich (USA).

2.2.1   Cell Culture

A549 cells cultured *in vitro* were maintained in DMEM supplemented with 10% FBS (37ºC with 5% CO_2). For all experiments, cells were charged with nanoparticles at 80% confluence, unless otherwise mentioned.

2.2.2 Charging of Nanoparticles

ZnO and TiO_2 NPs were dispensed in a stock concentration of 1 mg/ml (12.2mM ZnO and 12.5mM TiO_2). The doses of charge chosen were; control (0 µg/ml = 0 mM), 12.5 µg/ml (~0.15mM), 25 µg/ml (~ 0.31 mM), 50 µg/ml (~ 0.62 mM), 100 µg/ml (~ 1.24 mM) and 200 µg/ml (~ 2.48 mM) for ZnO and TiO_2 NPs. Doses were chosen based on our viability assays (Santimano *et al*., 2013) along a range commonly observed at industrial sites (Rogaczewska and Matczak, 1984). Our dose range of investigations allows evaluation of crucial biological differences in cellular responses to sub-lethal concentrations of nanoparticles. Stocks were prepared in DMEM aseptically and charged for experiments in the chosen doses after vortexing thoroughly to avoid aggregation and to ensure exposure to nano-scale particles.

Serum was added separately to ensure a consistent 10% concentration throughout various experiments.

2.2.3 Wound Healing Assay to demonstrate changes in proliferation potential on exposure to nanoparticles.

A wound was created in the monolayer by a 200µl tip. The original wound was photographed. Samples were treated while maintaining a control. Doses evaluated are 0.15, 0.31, 0.62, 1.24 and 2.48-mM respectively for ZnO and TiO_2 NPs. Post 24h and 48h incubation with nanoparticles, the wound was washed with PBS and re-photographed. ImageJ was used to quantify the gaps in each of the pictures and percentage proliferation of the treated samples were calculated relative to the control.

2.2.4 Transwell Invasion Assay to investigate Migration Potential of cells in response to nanoparticle exposure

Matrigel and 24 transwell chambers were secured from Corning Life Sciences. Transwell chambers were prepared for the experiment by coating them with 50µl of 30µg/ml of matrigel. Commercial matrigel stock was diluted with DMEM as required. Coated chambers were incubated at 37°C for 24h. 100µl of 24h nanoparticle treated cells, containing 2×10^5 cells/ml ware suspended in DMEM with 2% serum and added onto the upper chamber. 700µl of DMEM with 20% serum was added onto the lower chamber. Nanoparticle doses evaluated include 0.15, 0.31, 0.62, 1.24 and 2.48-mM of ZnO and TiO_2 NPs. Upper chamber was placed over the lower chamber and incubated at 37°C for 8 hours. A positive control was exacted by further reducing the serum concentration in the upper chamber to 0.5%, this increases the concentration difference across the membrane and expedites the rate

of migration. A negative control was exacted by resuspending untreated control cells in

phosphate buffered saline, this restrains migration owing to lack of nutrition. Post incubation, media from upper chamber is removed and the chamber is washed twice in PBS. Cells were fixed by adding formaldehyde (3.7% in PBS) both in upper and lower chamber for 2 minutes. Formaldehyde is removed, and the chambers were washed twice in PBS. Cells were then permeabilized with 100% ice cold methanol for 20 minutes. Methanol was removed from chambers and they were washed twice with PBS. Staining was done by incubating chambers with 2% fresh crystal violet for 20 minutes. Non-migrated cells were gently scraped using cotton swabs and removed. Migrated cells were photographed and counted using ImageJ.

2.2.5 Expression study at mRNA level to assess epithelial to mesenchymal (EMT) transition

cDNA was synthesized, and gel electrophoresis carried as described in section 2.6. The primer sequences utilized for polymerase chain reaction were; N Cadherin- 5'-gatgtttacagtgcagtctt-3' (sense); 5'-actgactcctcagttaaggt-3' (anti-sense), E Cadherin- 5-aggagctgacacaccccctgt-3' (sense); 5'-catcgtccgcgtctgtggct-3' (anti-sense), Clathrin- 5'-gaccgggctcatattgctca-3' (sense); 5'-tctgacggatgttggcagac-3' (anti-sense), EGFR- 5'-caagtgtaagaagtgcgaagg-3' (sense); 5'-cagaggaggagtatgtgtgaagg-3' (anti-sense) and GAPDH-5'-agaacatcatccctgcctctac-3' (sense); 5'-ctgttgaagtcagaggagacca-3' (anti-sense). The parameters for PCR are as described; start up denaturation for 2 min at 95°C proceeded by 35 cycles. Cycling conditions included denaturation for 30s at 95°C. This was proceeded by annealing for 30 s at 57°C for GAPDH, 53°C for N Cadherin, 55°C for E Cadherin, 57°C for EGFR and 57°C for Clathrin. Extension parameters were 30s at 72 °C, with an ultimate extension of 7 min at 72°C.

2.2.6 Western Blot Analysis to study EMT

After cell lysate (40 µg) was resolved by 10% SDS-PAGE the western blot was carried out as per Sarkar *et al*., 2007. In brief, the PVDF membranes were washed with tris-buffered saline followed by blocking with 5% non-fat dried milk or 3% BSA as was suited. The membranes were incubated at 4˚C overnight with primary target specific antibodies for EGFR (Cell Signaling- 1:500), E Cadherin (Biolegend- 1:100), N Cadherin (Biolegend- 1:100) and β-Actin (Cell Signaling- 1:2000). The membranes were then incubated with secondary antibodies coupled to horseradish peroxidase for optimised time periods at room temperature. The membranes were washed in combinations of TBS and TBST at room temperature. Immunoreactivities were detected by ECL reagents (Amersham GE Healthcare). Expression of target proteins was normalized to β- Actin.

2.3 Results

All expression studies have basal level or control expression of target assigned at 100%. Expression analysis was performed by ImageJ, NIH. Where ever required, pictures were post processed for background reduction and contrast enhancement using PhotoScape, MOOII TECH, Korea.

2.3.1 Wound Healing Assay to assess Proliferation capacity in response to nanoparticle exposure

The control healing potential of the original wound in an untreated sample, was recorded at 53.89 % in 24 hours, while 58% for 48 hours. ZnO exposed cells showed wound healing only at 0.15mM of exposure, with 13.7% for 24 hours (**Figure. 3 A**) and 31.68% for 48 hours (**Figure. 3 B**). With further increase in dose for ZnO exposure, there was increased cell death with no distinct wound boundary visible. The proliferation capacities in response to TiO_2 exposure for 24 hours were 22.66%, 15.28%, 18.39%, 16.69% and 11. 46% for doses 0.15, 0.31, 0.62, 1.24 and 2.48mM respectively. The subsequent proliferation values increased upon incubation at 48 hours up till the dose of 1.24mM. They were 36.21%, 27.16%, 29.56% and 19.38% for doses 0.15, 0.31, 0.62 and 1.24 mM. At 2.48mM of dose of TiO_2 exposed to 48 hours, the proliferation rate dropped to 1.84%. Statistical analysis is provided in **Figure. 3 C and Figure. 3 D.**

Figure 3 - Wound healing assay to evaluate Proliferation capacity
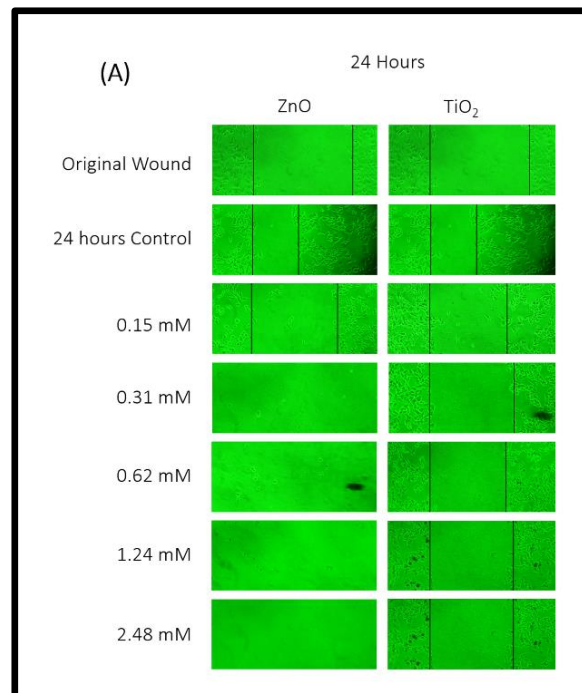
A- Dose dependent documentation by Inverted microscopy at 24 hours is presented. ZnO and

TiO$_2$ NP
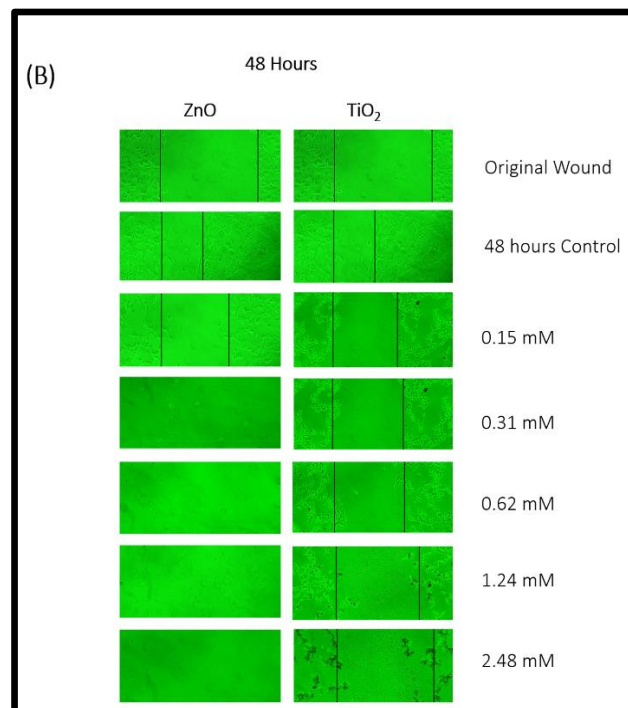
B- Wound Healing Assay recorded for 48 hours.
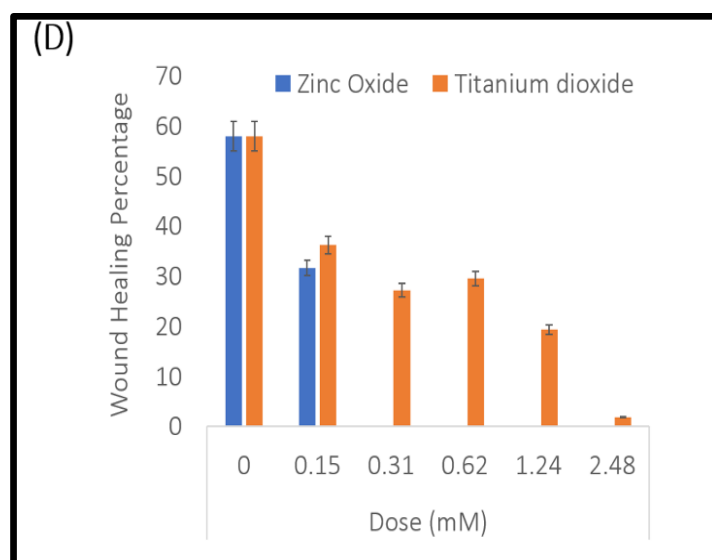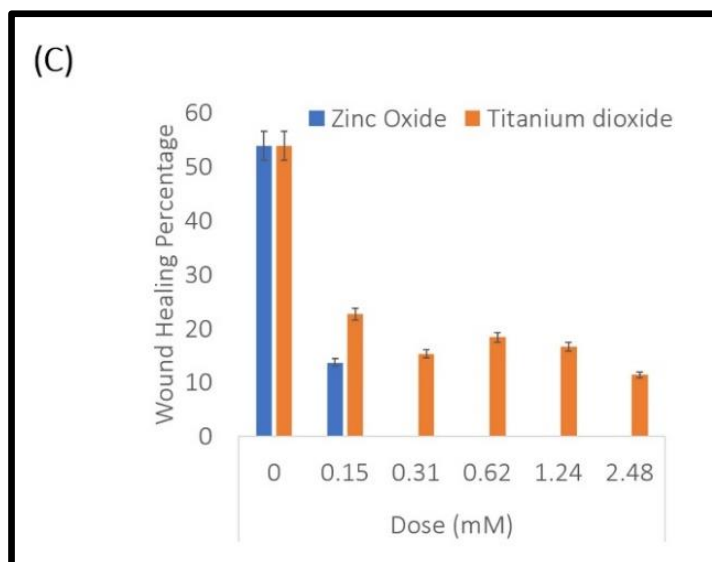
C- Statistical analysis of wound healing assay for 24 hours data. D- Statistical analysis of wound healing assay for 48 hours data. Results are summarized in section 3.10. P values calculated are; ZnO 24h- 0.14636 (ns- to be noted; data was not available beyond 0.31mM in this experimental set up), TiO_2 24h- 0.0178037 (*), ZnO 48h- 0.09484 (ns- to be noted; data was not available beyond 0.31mM in this experimental set up) and TiO_2 48h- 0.0013234 (**).

2.3.2 Transswell Invasion Assay to evaluate migration potential in response to nanoparticle exposure.

ZnO exposed cells showed a decline in the number of cells migrating with increase in dose of exposure till 0.62mM at 24 and 48 hours. Upon further increase in dose, no migrated cells were observed. However, TiO_2 treated cells, showed an increase in migration with a maximum at 0.62mM for 24hours and 0.15mM for 48 hours (**Figure. 4**). The number of migrated cells is plotted against dose of exposure for TiO_2 and ZnO exposure in Fig. 5.

Figure 4 - Transwell invasion assay to evaluate migration potential in response to MeOx NP treatment
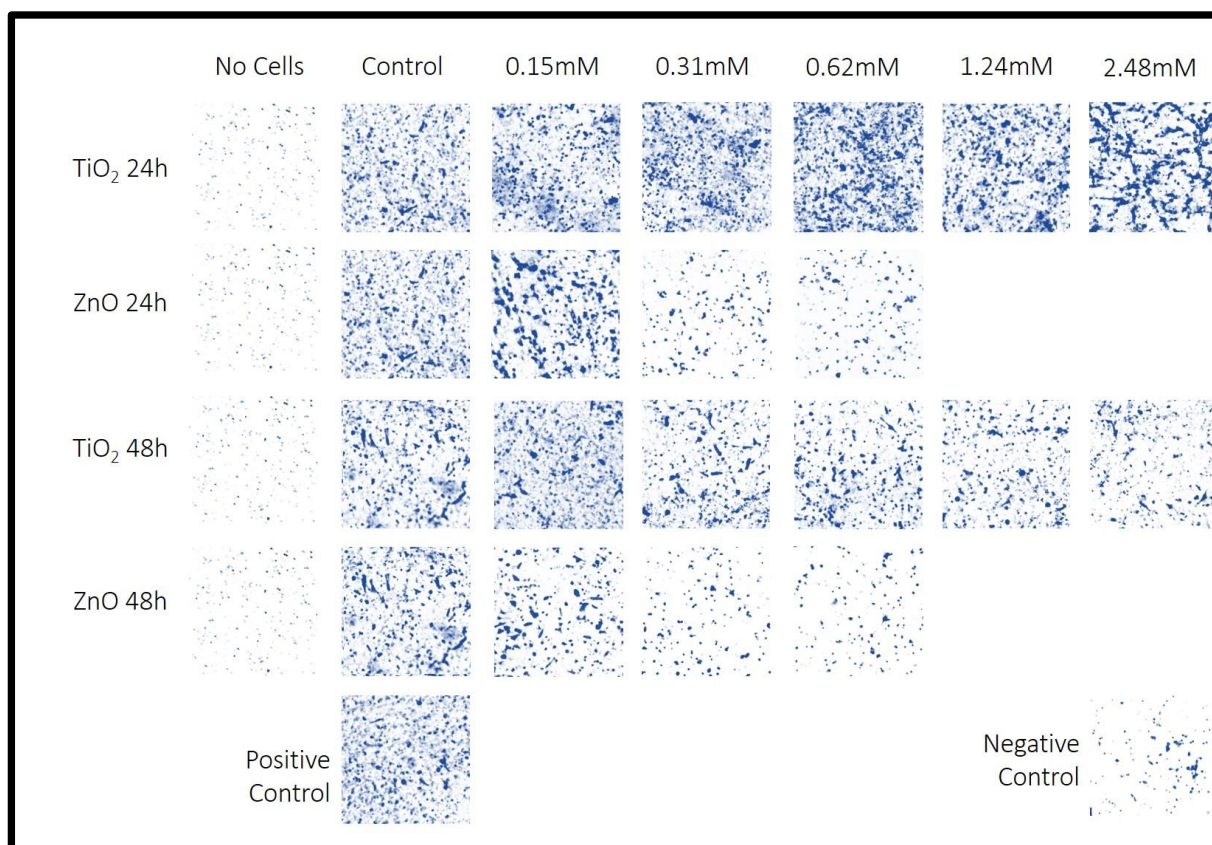
Dose and time dependent documentation of migrated cells against control (untreated membrane) is studied. A positive control and a negative control is also set in the experiment to validate results effectively.

Figure 5 - Statistical analysis of migration potential
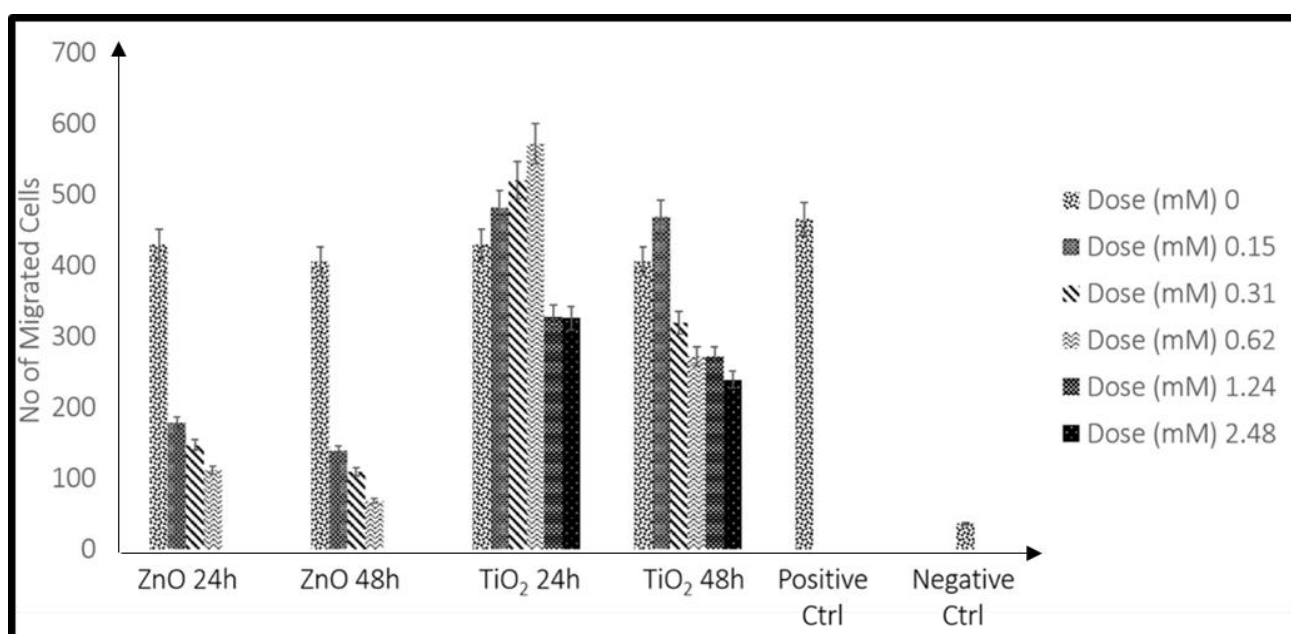
Number of migrated cells are counted using ImageJ, NIH. Migration capacities are plotted as number of migrated cells in a time and dose dependent manner. Number of migrated cells for the positive and negative control is also calculated. P values are; ZnO 24h- 0.05000 (*), ZnO 48h- 0.0505 (*), TiO$_2$ 24h- 0.0004067 (***) and TiO$_2$ 48h- 0.00047933 (***).

2.3.3 RT PCR analysis for studying Epithelial to mesenchymal transition.

Relative expression at mRNA level of targets E Cadherin, N Cadherin, EGFR and Clathrin were evaluated in response to exposure with ZnO and TiO$_2$ nanoparticles (**Figure. 6**). Doses evaluated were 0mM (Control), 0.15mM (A), 0.31mM (B), 0.62mM (C) and

1.24mM (D). GAPDH expression was used as the internal control. E Cadherin upregulated in response to ZnO exposure along with EGFR. EGFR showed a significant upregulation, at 100% expression more than basal level for 1.24mM of exposure. However, in response to TiO_2, both E Cadherin and EGFR showed a marked downregulation. N Cadherin upregulated in response to both ZnO and TiO_2, though it was more pronounced in response to TiO_2. Clathrin, upregulated up till 0.31mM in response to ZnO NPs, while it stayed elevated till 0.62mM with TiO_2 exposure with 75% of control. A further dose treatment at 1.24mM was documented by a depreciation in expression to 25% more than control level. Densitometric analysis by ImageJ, NIH is given in **Figure. 7**.

Figure 6 - Evaluation of EMT by mRNA level expression of E Cadherin, N Cadherin, EGFR and Clathrin
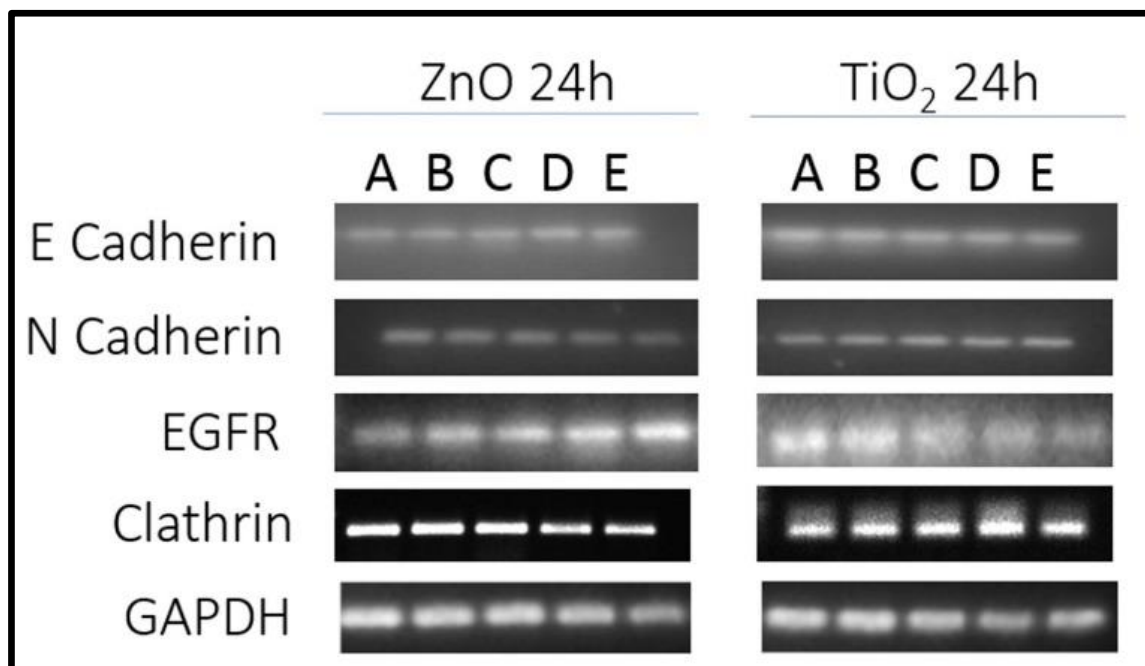
24 Hours expression pattern of E Cadherin, N Cadherin, EGFR and Clathrin at the mRNA level was documented in a dose dependent manner. Doses; A- 0, B- 0.15, C-0.31, D-0.62 and E-1.24 mM.

Figure 7 - Statistical Analysis mRNA level expression of E Cadherin, N Cadherin, EGFR and Clathrin.
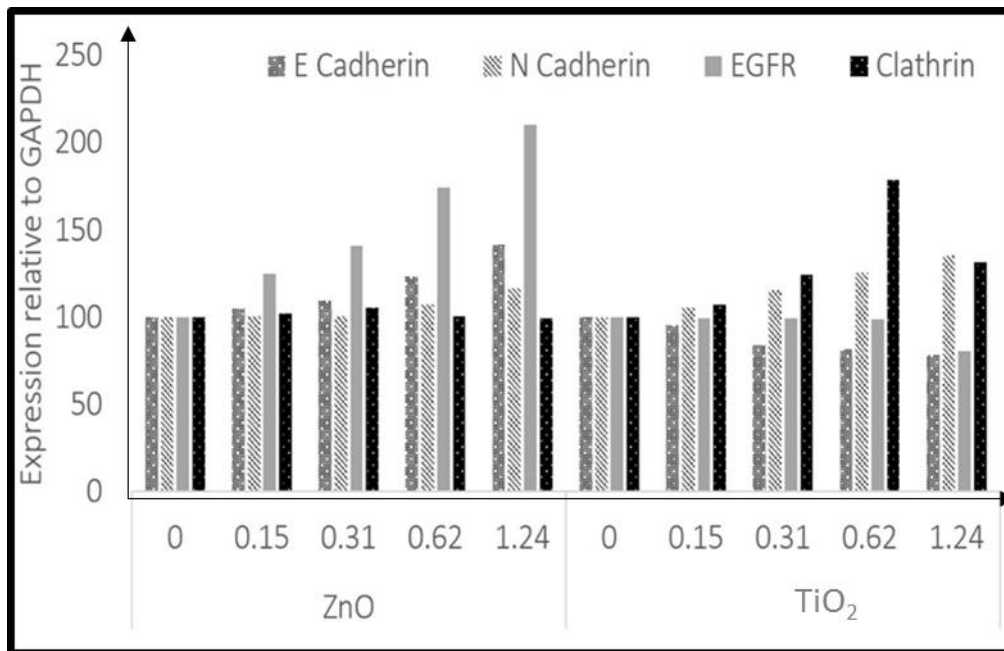
Dose dependent expression profile is plotted for E Cadherin, N Cadherin, EGFR and Clathrin, relative to the internal control GAPDH in response to MeOx NP treatment. P values for ZnO treatment are; E Cadherin- 0.000001773 (***), N Cadherin- 2.75E-06 (***), EGFR- 0.000404547 (***) and Clathrin- 9.05E-06 (***). TiO$_2$ exposure resulted in P values of; E Cadherin- 0.0001219 (***), N Cadherin- 3.816E-05 (***), EGFR- 4.1E-05 (***) and Clathrin- 0.010 (**).

2.3.4   Western Blot Analysis for studying Epithelial to mesenchymal transition.

Expression at protein level for EGFR, E Cadherin and N Cadherin were evaluated and normalized to expression of β-Actin as the internal control (**Figure. 8**). The expression was in tandem with RT PCR results. EGFR and E Cadherin downregulated in response to TiO$_2$ NPs while they upregulated with ZnO exposure. ZnO treatment rendered 60% increase in E Cadherin expression and 70% increase in EGFR expression at 0.62mM among all dose points

evaluated. TiO_2 exposure resulted in a downregulation of E Cadherin to 40% of control, while EGFR to just 20% of basal expression.

N Cadherin upregulated in response to both ZnO and TiO_2 exposure, though for the latter, the expression was more pronounced, with about 20% more than the basal expression. Densitometric analysis was represented in **Figure. 9**.

Figure 8 - Evaluation of EMT through protein level expression of E Cadherin, N Cadherin and EGFR by western blot analysis
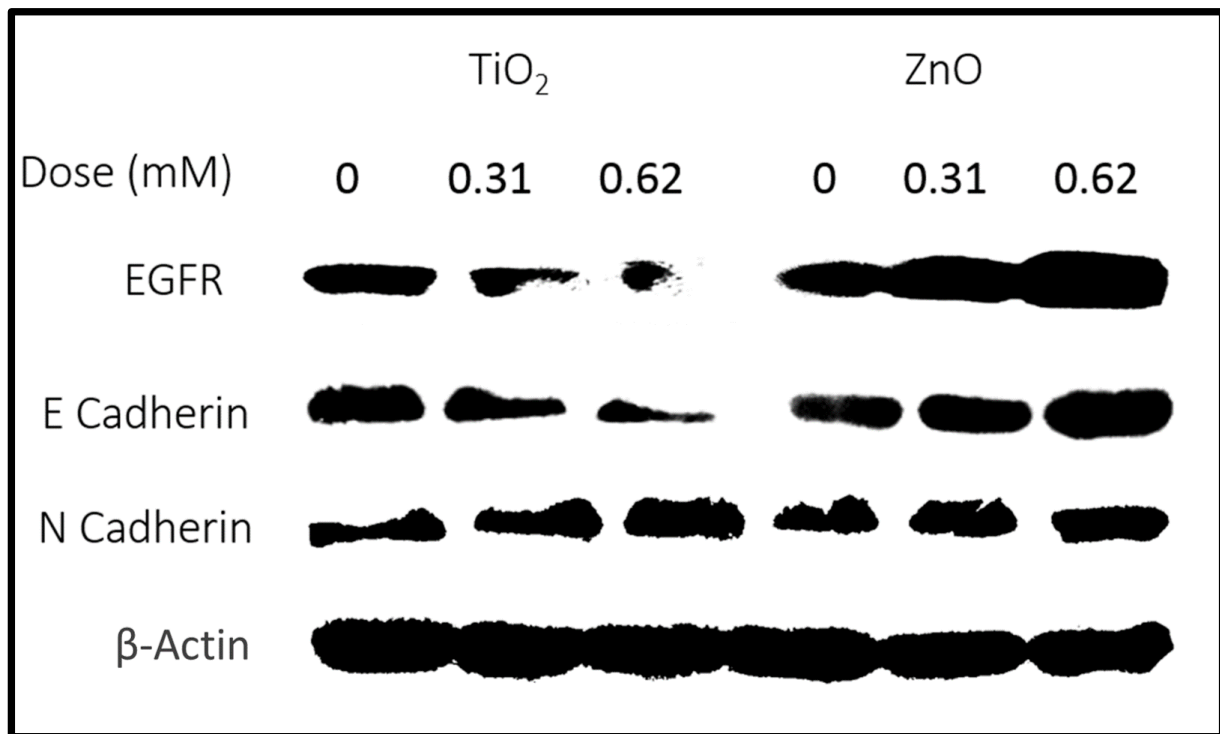
Dose dependent expression of E Cadherin, N Cadherin and EGFR is documented to MeOx NP treatment.

Figure 9 - Statistical Analysis of EMT markers E Cadherin, N Cadherin along with EGFR at protein level by ImageJ, NIH.
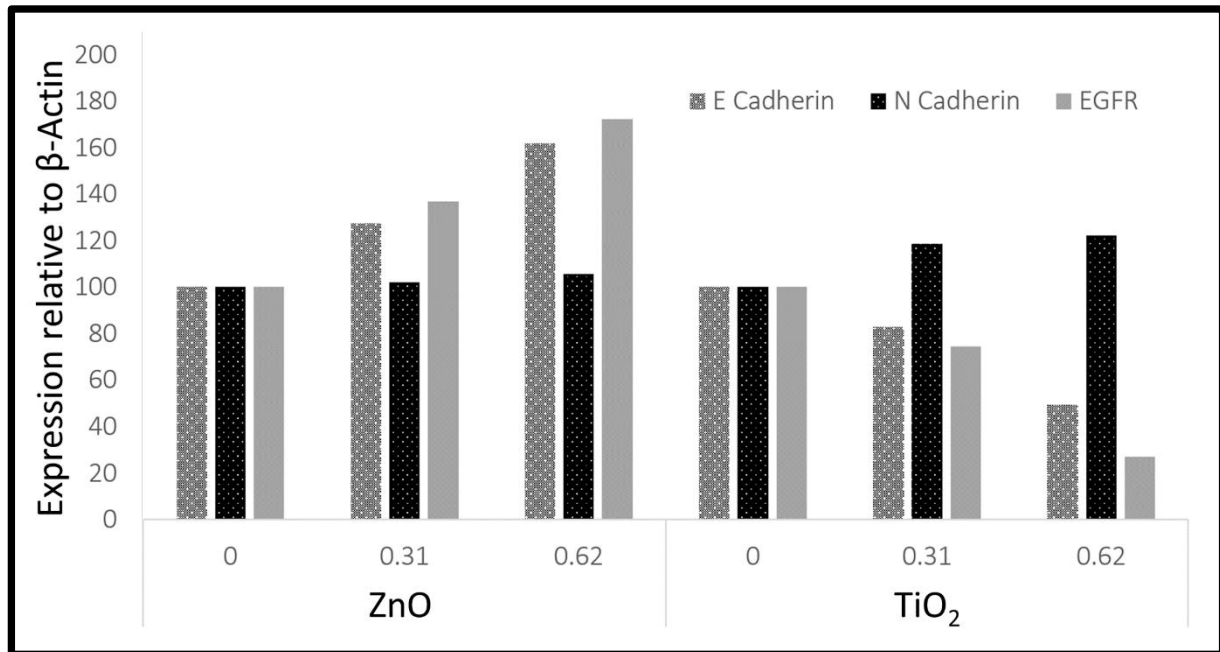
Dose dependent expression of E Cadherin, N Cadherin and EGFR is plotted, after normalizing with the internal control; β-Actin in response to MeOx treatment. P Values for ZnO treatment are; E Cadherin- 0.017406 (*), N Cadherin- 0.00404711 (**) and EGFR- 0.0027940 (**). TiO$_2$ exposure resulted in p values of; E Cadherin- 0.037336 (*), N Cadherin- 0.0350571 (*) and EGFR- 0.04914 (*).

2.4 Discussion

Increased proliferative and migrative capacity of TiO_2 NP treated cells over ZnO was documented through wound healing and transwell invasion assays. This is the first report of this kind. Wound healing assay shows a marked preservation in proliferation capacity with TiO_2 NP treatment as compared to ZnO. Though for all doses evaluated for both ZnO and TiO_2 exposure, mitotic capacities lagged with the untreated control, suggesting, MeOx NP treatment does negatively affect cellular proliferation, irrespective of lethality. Mitotic capacity is the mean mitotic index at any temporal point characterized by an increase in cell proliferation and thus an increased cell density (Grover *et al*., 2015).

We also have discovered E Cadherin downregulation in response to TiO_2 exposure along with N Cadherin upregulation. This is not evident with ZnO. This is supplemented with the allied EGFR expression that follows trend with E Cadherin (Gavard and Gutkind, 2008). Clathrin is crucial to EGFR internalization. Particularly the clathrin-assembly lymphoid myeloid leukemia protein; CALM along with Grb2 are significant in this process (Huang *et al*., 2004). Further it was observed in Hela cells, Clathrin mediated endocytosis (CME) prolongs EGFR activated signaling cascades including processes such as DNA synthesis. In stark contrast clathrin independent endocytosis of EGFR committed the receptor for degradation, substantiating the role of CME in enhanced EGF induced signaling rather than degradation with Hela cells (Sigismund *et al*., 2008).

In our study, we found that, at mRNA level, clathrin expression does stay elevated up till a dose of 0.62mM at 78.34% more than control under TiO_2 exposure. Whereas, clathrin peaks at 0.31mM with just 5% more than control to ZnO treatment. Thereafter, with further dose exposure, clathrin expression downregulates. These results suggest, with MeOx exposure on A549 cells, clathrin upregulation and its mediated internalization of EGFR, result in

degradation of EGFR. Our studies fare an example of how biological responses can differ based on the type of cell in the study.

Cell death varies as a function of dose and time for metal oxide nanoparticle toxicity (Martin and Sarkar, 2017). However, our data sufficiently proves, A549 cells can withstand a greater dose of exposure from TiO$_2$ NPs as compared to ZnO. This is due to the epithelial to mesenchymal transition that occurs at the molecular level along with cdc42 expression that renders filopodial extensions. Our data also shows an enhanced migration capability to TiO$_2$ exposed cells. These cells may thus, migrate away from the zone of stress, enabling them to tolerate higher TiO$_2$ exposure as compared to ZnO.

In toxicity assessments particularly, that of the *in vitro* set up, a zone of stress represents the layers of variant shear stress in a culture vessel (Zhang *et al*., 2014). We postulate that adherent cultures exhibit high stress on cells close to the basal membrane, with marked nutrient deprivation and increased steric hindrance through crowding of the cells. The density dependent depletion in cell growth and proliferation is widely documented for confluent cultures (McClain and Edelman, 1980). It is possible that epithelial to mesenchymal transition allows cells to float away from the lamina into a region more conducive for survival. Moreover, the regulated release of cytokines and chemokines by stressed cells also less affect the cells away from the high zone of stress at the basal lamina (Zhang *et al*., 2014).

Epithelial cells enable tissue specific functions while mesenchymal cells involve in accessory roles. The importance of trans-differentiation through processes such as epithelial to mesenchymal transition (EMT) and mesenchymal to epithelial transition (MET) is crucial for maintaining the integrity of life. These processes are avidly observed during tissue repair, biological responses to pathological stresses and inflammation. EMT involves the gradual transition of polarized epithelial cells with normal interactions to the basal membrane to

mesenchymal phenotype. This is characterized by multiple biochemical changes, invasiveness, enhanced migratory potential, production of extracellular matrix components and finally the degradation of the underlying basement membrane (Kalluri and Weinberg, 2009).

Figure 10 – Epithelial to Mesenchymal Transition

Epithelial phenotype | Intermediate phenotypes as cells transition | Mesenchymal phenotype

Epithelial cells

Mesenchymal cells

E-cadherin
Cytokeratin
ZO-1
Laminin-1
Entactin

Syndecan
MUC1
Desmoplakin
α1 (IV) collagen
miR200 family

Progressive loss of epithelial markers and gain of mesenchymal markers

FTS binding protein FAP
FSP-1
N-cadherin
Vimentin
Fibronectin
β-catenin
OB-cadherin
α5β1 integrin
Syndecan-1
miR10b

Snail
Slug
ETS
SIP1
α-SMA
Twist
Goosecoid
LEF-1
FOXC2
miR21

Referred from Kalluri and Weinberg, 2009; The progressive set of changes in Epithelial to Mesenchymal transition is depicted.

Epithelial to mesenchymal transition (**Figure 10**) as a cellular response to metal oxide nanoparticle mediated stress has never been documented before. Our study is the first of its kind to discover and sufficiently prove this phenomenon with consistent and validated experimental results.

Further epithelial to mesenchymal transition, is also known to phosphorylate eIF2α through protein kinase RNA-like ER kinase (PERK) activating the unfolded protein response (UPR) in response to endoplasmic stress (Feng *et al*., 2014). We have earlier substantially proved that TiO_2 NP treated cells do have an increased duration for which eIF2α remains phosphorylated as compared to ZnO exposure. This may well be related to the onset of

epithelial to mesenchymal transition observed in TiO_2 NP treated cells, not observed with

ZnO exposure.

Our novel findings predict LD_{50} value for TiO_2 nanoparticle treatment on A549 cells is almost 20 times more than that with ZnO. Crucial cellular responses to TiO_2 nanoparticle treatment include extended duration of eIF2α phosphorylation, epithelial to mesenchymal transition and enhanced expression of Hsp70. These results could be successfully developed in the future to design relief strategies to alleviate metal oxide nanoparticle mediated stress (**Figure 11**).

Figure 11 – Key molecular changes discovered between ZnO and TiO_2 NP treated cells
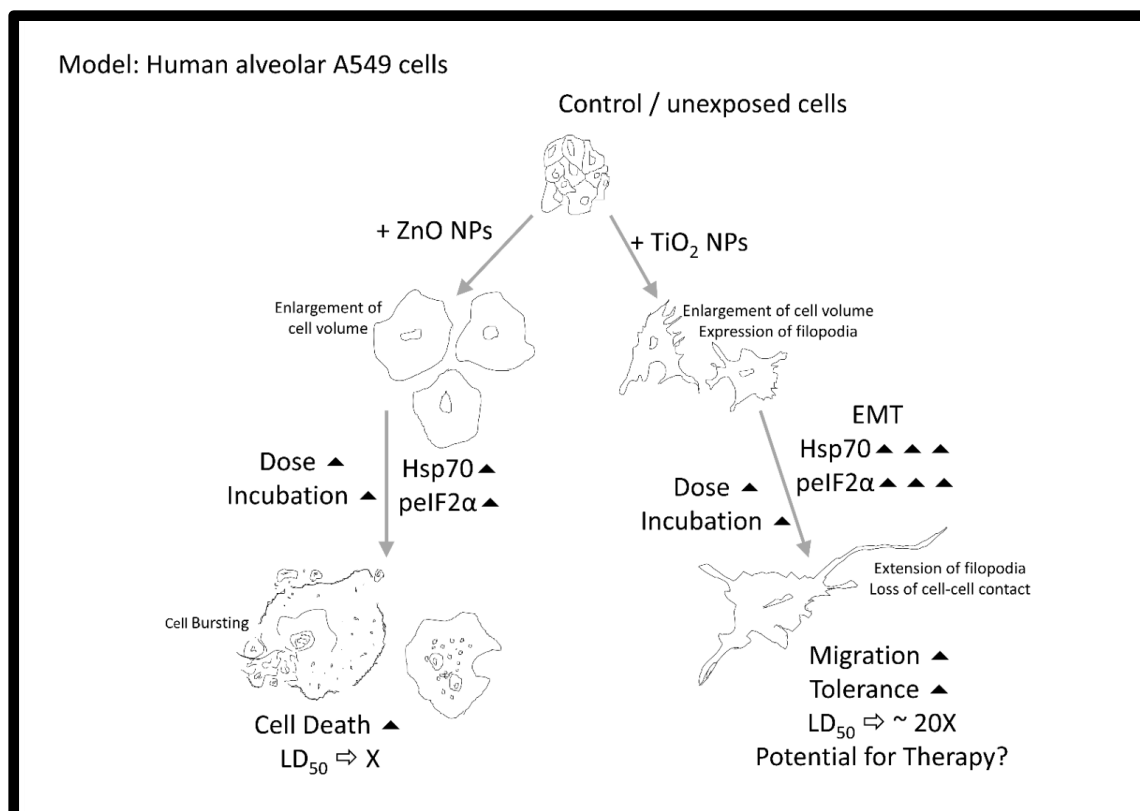
Potential for therapeutic molecular designs to alleviate metal oxide nanoparticle toxicity; EMT, enhanced expression of Hsp70 allied with increased duration in phosphorylation of eIF2α.

Chapter 3

Quantitative Structure – Activity based model to predict the toxicity of metal oxide nanoparticles on A549 cells.

3.1 Introduction

Nano-toxicity manifests vastly differently than stress conferred from bulk and macro materials, often resulting in increased genotoxic stress characterized by chromosomal damage (Semisch and Hartwing, 2014). It differs from one system to another and varies in the modes of their deliverance. Recognizing this need to understand mechanisms of nanoparticle-based toxicity and documentation of nanoparticle entry portals into biological systems; studies on molecular models of toxicity have progressed in earnest.

Several attempts have already been made to predict nanoparticle conferred toxicity. But there remains a large paucity in available data sets over reliability and reproducibility as very few studies on nanoparticle toxicity converge with concordant results (Tsuji *et al*., 2006, Triboulet *et al*., 2015). Success in this field is often dependent on the predictive potential of a toxicity model simply because actual estimation of every single engineered nanomaterial ever synthesized is tedious and time consuming. Thus, toxicity models being developed were designed to predict lethal doses based on extrapolation or interpolation of existing experimental data sets. They use effective computational methods to recognize patterns and predict toxicity as a dose dependent function (Gajewicz *et al*., 2014) Precision in such efforts is largely dependent on the presence of quantitative experimental data sets of acceptable accuracy. Because of experimental limitations this may not always be feasible, as such these models may serve true to accurately predicting toxicity for a similar system only given over-sampling techniques are used. Monte Carlo based modelling through various software such as CORAL (http://www.insilico.eu/coral) that employ over sampling (Toropova and Toropova, 2015), have already been used in developing optimal descriptors to response functions such as mutagenic potential, photocatalytic decolourisation rate, cellular viability (Toropov *et al*., 2015, Toropov and Toropova, 2015), catalytic activities for water oxidation (Shahbazy *et al*.,

2014) etc. Never the less, there is a continued need for a common consensus of understanding in building standard protocols and systems to better assess nanoparticle mediated toxicity.

Through our study, we have built a Nano-QSAR (Quantitative Structure Activity Relationship) model to predict the toxicity conferred by metal oxide nanoparticles on alveolar type 2 cells. Our model is the first of its kind in assessing the toxicity potential of metal oxide nanomaterials on alveolar type 2 cells.

Alveolar cells are highly susceptible to aerosolized nanoparticles that pose enormous risks of pulmonary stress. Metal oxide nanoparticles are a subclass of nanomaterials that find one of the highest instances of exposure as aerosolized matter and through various reports are known to impair function of type 2 pneumocytes (Ivask *et al*., 2015, Urner *et al*., 2014 and Andujar *et al*., 2014).

Many quantitative structure-activity relationship (QSAR) models have already been developed that can extrapolate experimental toxicity data of few candidates to accurately predicting effects of most metal oxide nanoparticles based on their similar molecular descriptors (Leszczynski, 2010, Puzyn *et al*., 2011). We have sought to investigate if indeed toxicity conferred by metal nano-oxides on human alveolar type II cells by using A549 cell line as a model follows a function of molar enthalpy change of formation of gaseous cation as shown with *E.coli* in the original study (Puzyn *et al*., 2011). There after we have explored if any additional mechanisms may also be involved. Most commonly encountered mechanisms include ROS generation, metal ion release, nanomaterial accumulation on membrane surface and internalization of nanomaterials (Djurisic *et al*., 2015).

3.2 Methods

Common laboratory reagents were acquired from Abcam and Sigma-Aldrich (USA) and Human A549 cells were obtained from National Centre for Cell Science, India. Chemicals for nanoparticle synthesis were obtained by Merck, India.

3.2.1 Synthesis and Characterization of Nanoparticles

Six metal oxides (e.g. Cr_2O_3, $\alpha\text{-}Fe_2O_3$, Co_3O_4, NiO, CuO and ZrO_2) were synthesized by using an aqueous EDTA precursor-based method (Hazra *et al*., 2012 and Hazra *et al*., 2015). The detailed experimental conditions are listed in table 1. In a typical synthesis, metal nitrates and EDTA were used as starting materials. Aqueous solutions of metal nitrate and EDTA were mixed in stoichiometric amount (**Table 1**) and then evaporated to dryness over a hot plate to obtain precursor powders. The precursor powders were then calcined at different calcination temperatures to obtain metal oxide nanoparticles.

Table 1: Synthesis conditions for metal oxide nanoparticles

Composition	Meta nitrate: EDTA ratio	Calcination temperature (time)
Cr_2O_3	1:1	550°C (2h 30 min)
$\alpha\text{-}Fe_2O_3$	1:1	450°C (2h 30 min)
Co_3O_4	1:1	450°C (2h 30 min)
NiO	1:1	450°C (2h 30 min)
CuO	1:1	450°C (2h 30 min)
ZrO_2	1:1	550°C (2h 30 min)

To synthesize Al_2O_3, $Al(NO_3)_3 . 9H_2O$ and Oxalic acid was used in 1:3 ratio and precursor were calcined at 800°C for 2h 30 min. ZnO and TiO_2 Nanoparticles were procured through Sigma Aldrich USA. Average particle size of TiO_2 NPs (Hombikat make) were 18nm and ZnO were 35nm.

Synthesized nanoparticles were characterized by using room temperature wide angle X-ray diffractometer and dynamic light scattering technique. X-ray diffraction (XRD) pattern of the synthesized nano powder at room temperature was recorded using an X-Ray diffractometer (Mini Flex II, Rigaku, Japan). The working parameters used were 40 kV and 30 mA, to use a copper radiation with Cu Kα(λ) = 0.15405 nm. The scanning scope of 2θ was set to 10-70º and the scanning speed to 2° per min. To obtain a diffraction, a thick (2mm) sample was layered. Multiple measurements were taken to aid accuracy. Particle size of the synthesized material was determined by dynamic light scattering (DLS) technique utilizing a particle size analyser (Delsa Nano S, Beckman Coulter, USA). XRD patterns of the metal oxides confirmed the formation of pure single-phase materials (**Figure 1**). Purity of metal oxides was checked by comparing the pattern of diffraction with the database of powder diffraction patterns maintained by, 'International centre for Diffraction data', (ICDD). It is important to note that, presence of any impurity phase was not detected. From DLS study (**Figure 2 A and B**) it was observed that, the average particle size of the synthesized materials lies within the range of 10-40 nm (**Table 2**). The highest dimension particle for each synthesized nanoparticle is reported below with its percentage in the total population of particles: -

Al_2O_3- 19nm (45.81%), Co_3O_4- 8.9nm (49.1%), Cr_2O_3- 2.9nm (39.76%), CuO- 10.72nm (47.1%), Fe_2O_3- 7.74nm (50.19%), NiO- 7.39nm (46.68%) and ZrO_2- 8.5nm (44.84%).

Figure 1: X-ray Diffraction (XRD) data for synthesized metal oxide nanoparticles

Co₃O₄
ICDD Card Number: 42-1467

(111), (220), (311), (222), (400), (422), (511), (440)

Intensity (cps) vs 2θ (Degree)

Al₂O₃
ICDD Card No: 37-1642

Intensity (cps) vs 2θ (Degree)
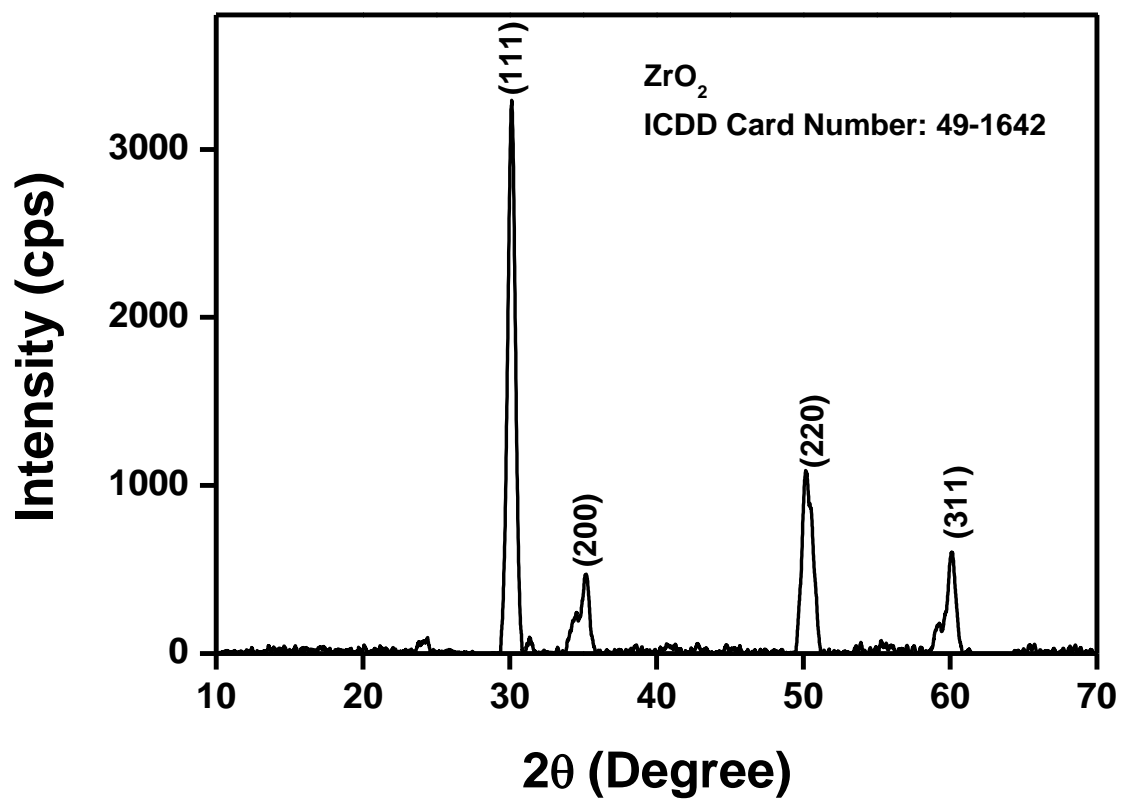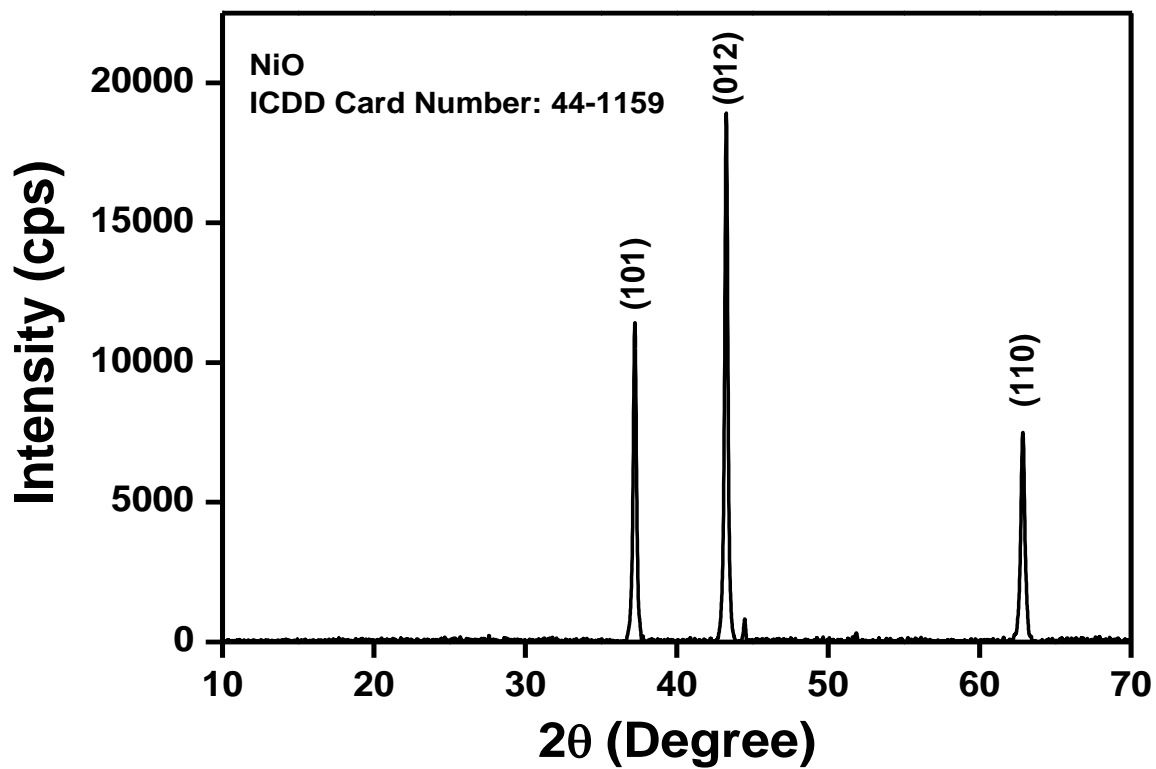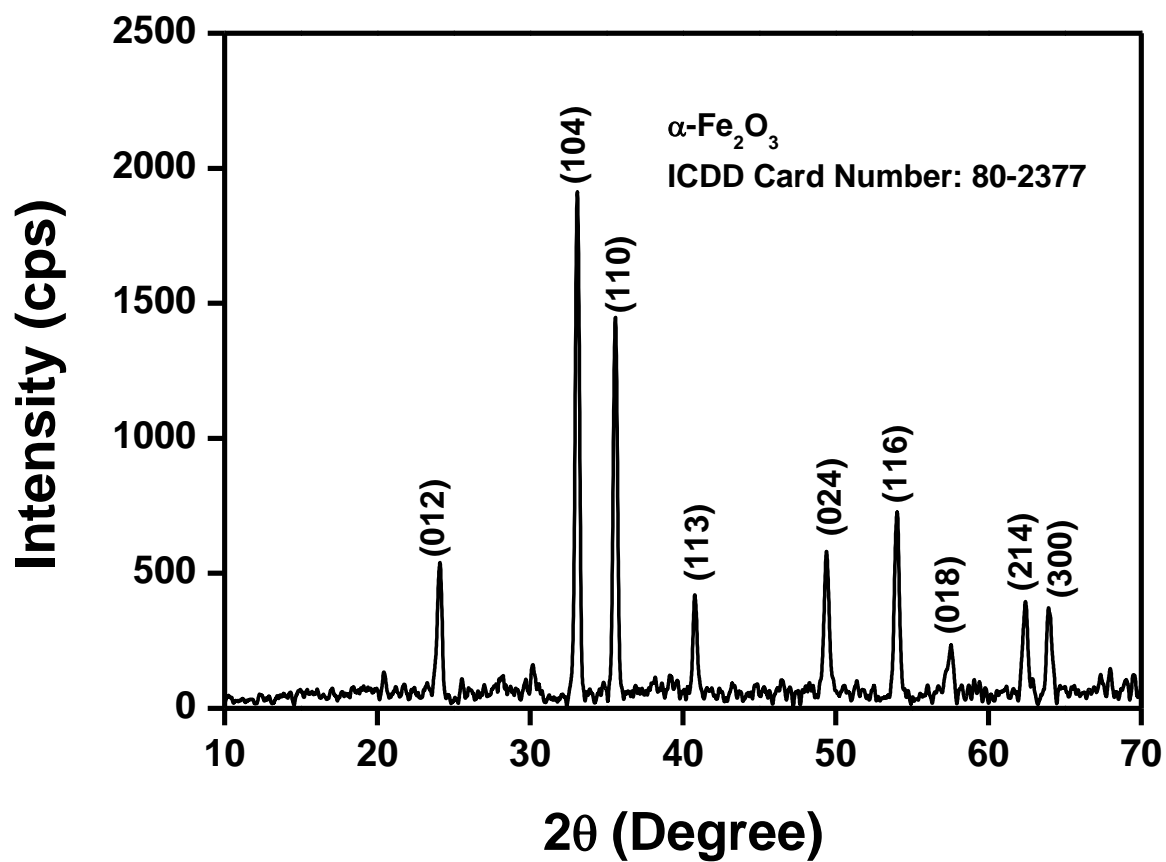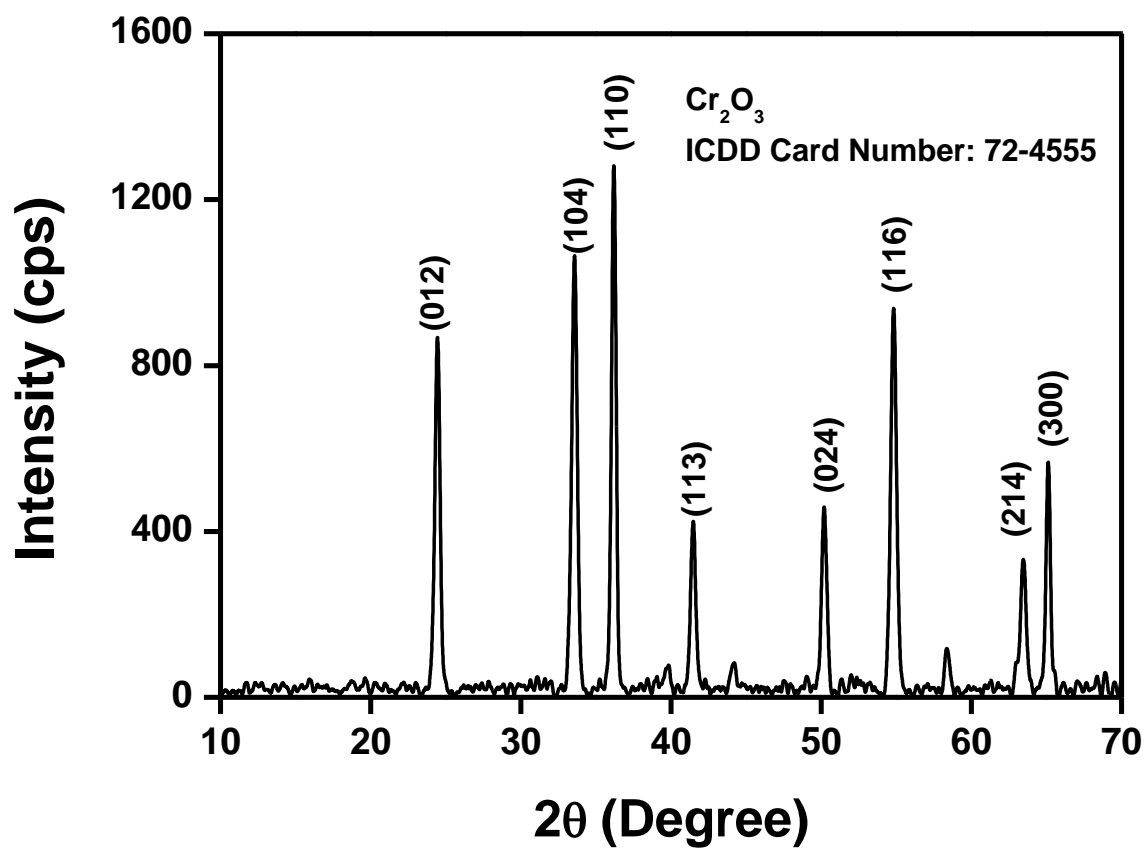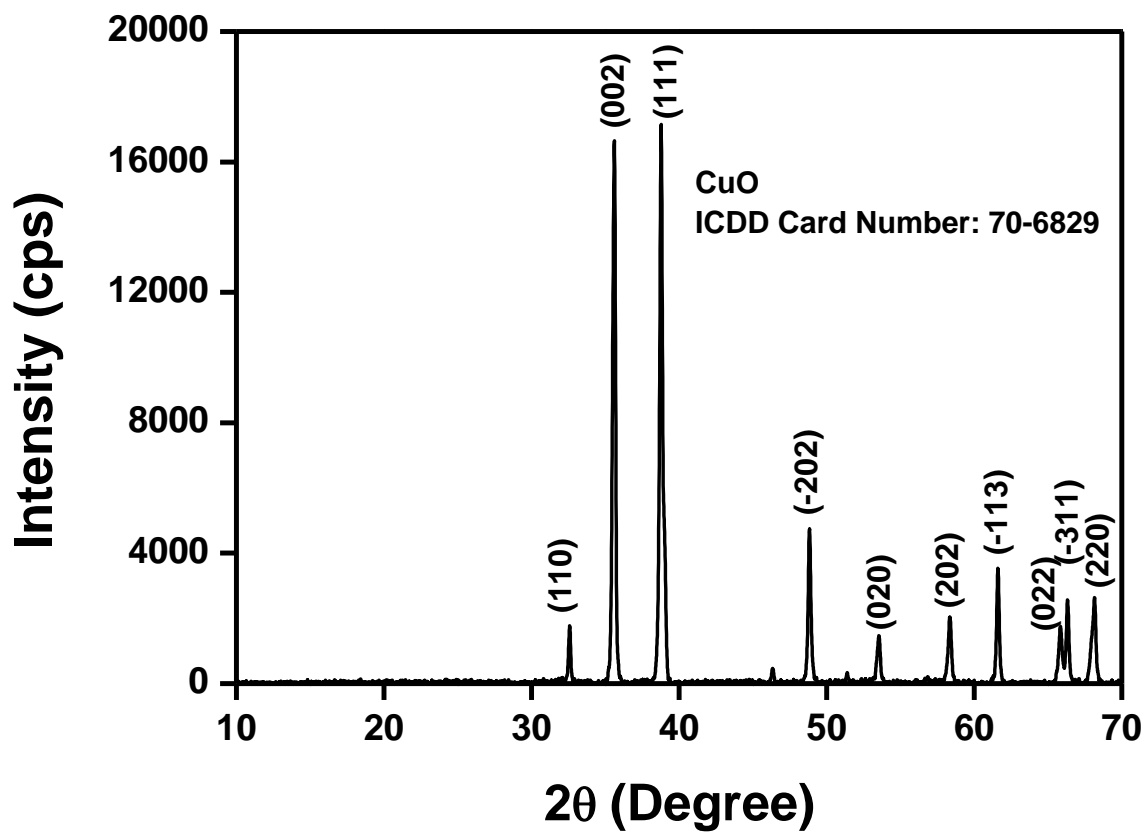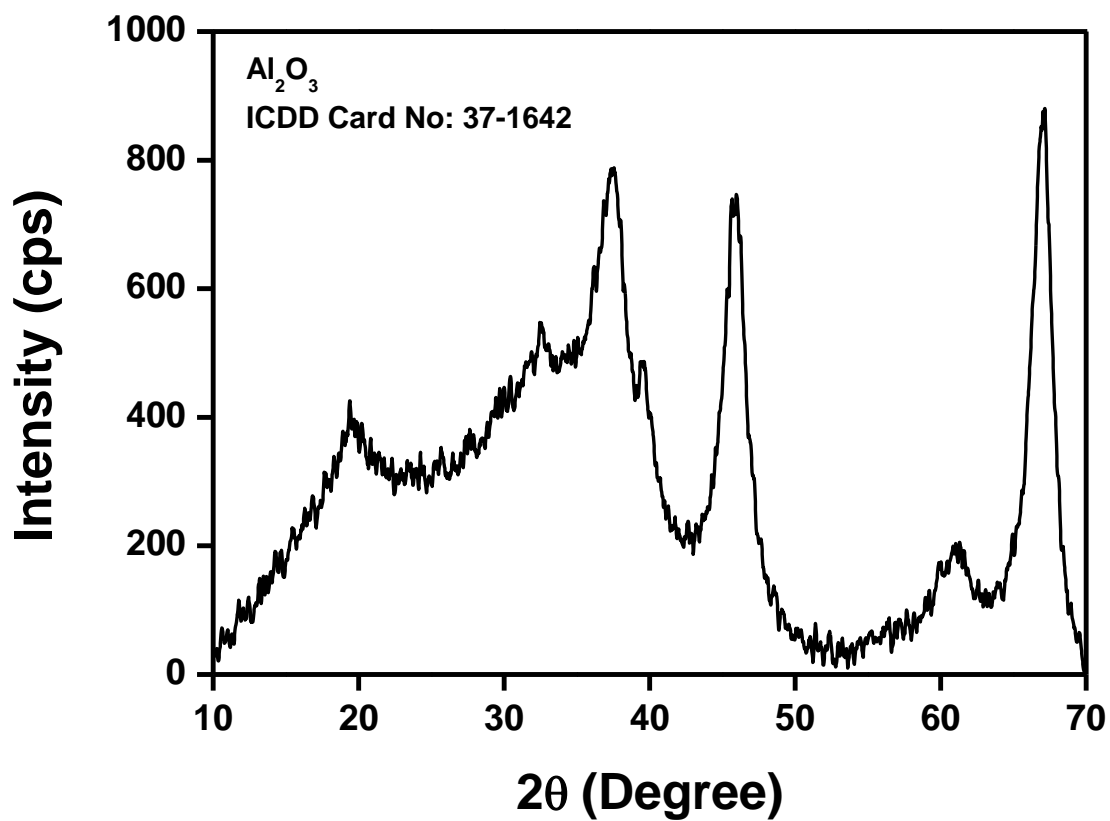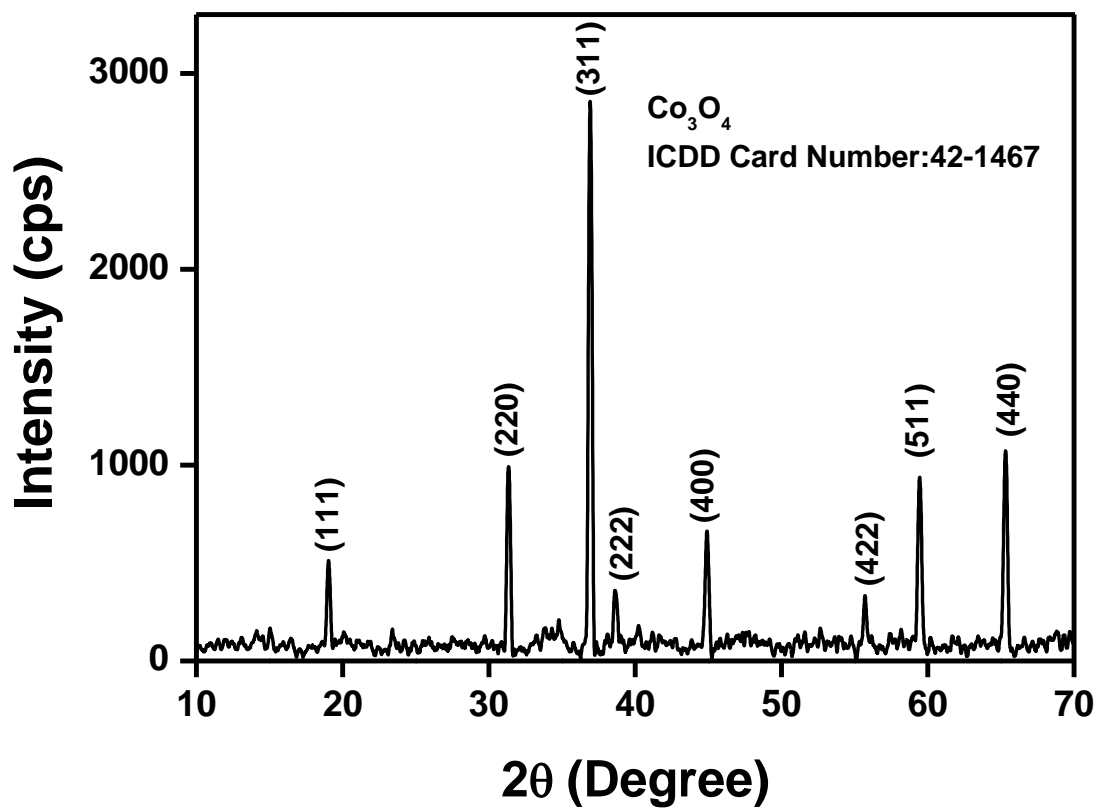
All metal oxide nanoparticles synthesized were tested to be pure and crystalline. The crystal

phase of the metal oxide nanoparticles was found to be monoclinic for ZrO_2, CuO, Al_2O_3,

cubic for Co_3O_4, Cr_2O_3, NiO and hexagonal (rhombohedral) for αFe_2O_3.

Figure 2 (a) – Dynamic Lights Scattering (DLS) Data for synthesized nanoparticles
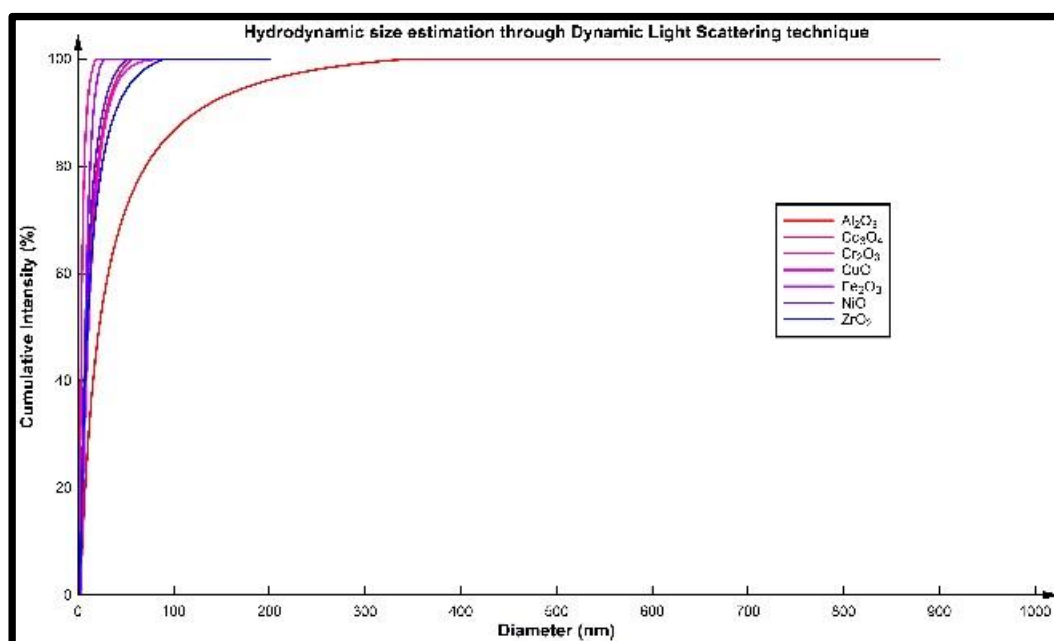
2 (b)- Average particle size of all metal oxide nanoparticles synthesized were under 100 nm.
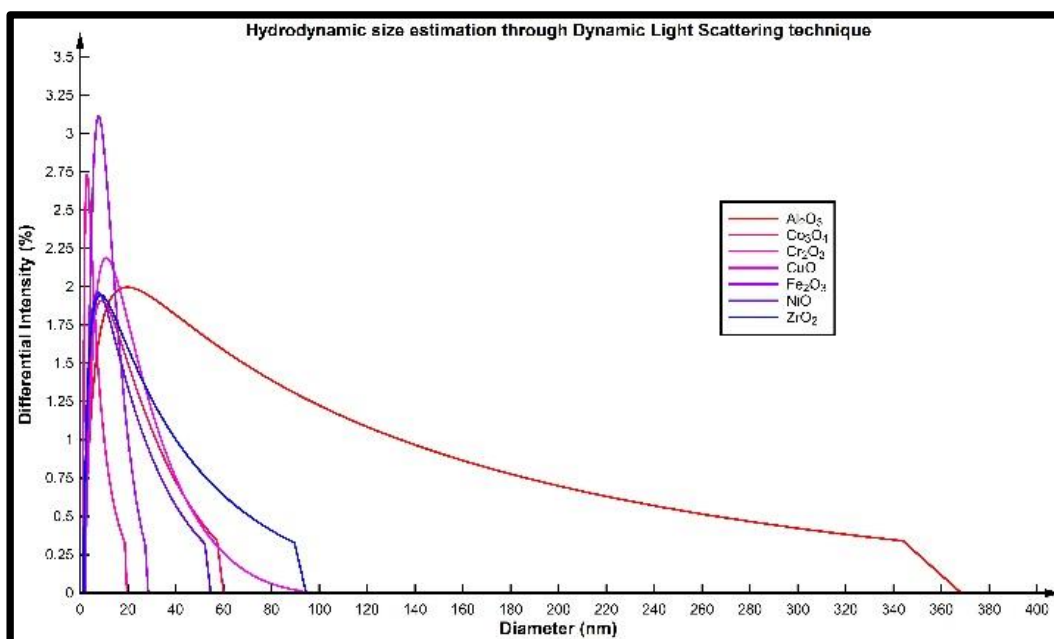
Table 2 - Average particle size and distribution range for synthesized nanoparticle size

Composition	Average Particle size (nm)	Distribution (nm)
Cr_2O_3	8.9	1.2-18.7
$\alpha\text{-}Fe_2O_3$	9.2	2.5-27.2
Co_3O_4	10.9	1.7-57.2
NiO	10.7	1.6-52.1
CuO	11.9	1.6-100
ZrO_2	14.6	1.6-89.6
Al_2O_3	35.8	2.1-343.9

Figure 3 - Scanning electron microscopy (SEM) analysis
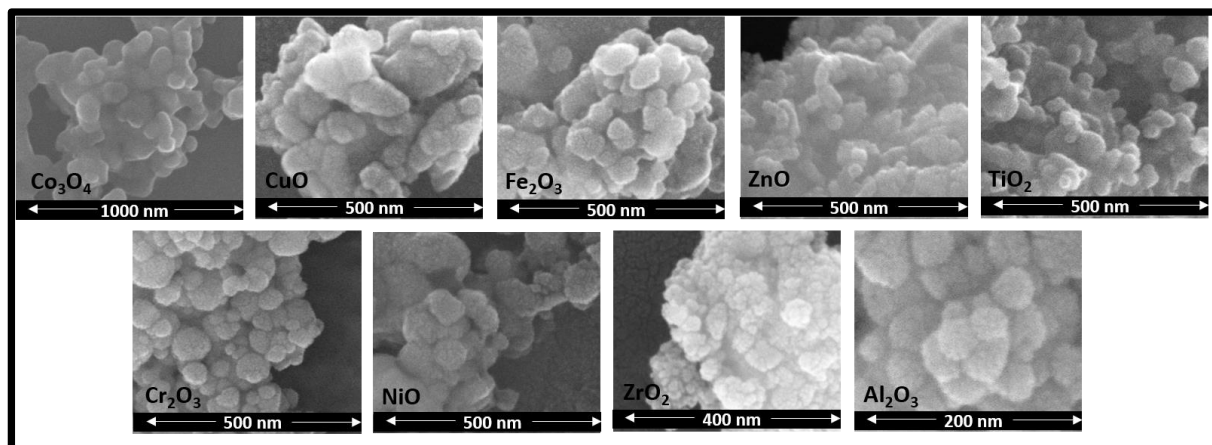
SEM analysis was undertaken as part of characterization to assess morphology and average diameter of the particle. This was done employing the FEI FE-SEM, Apreo LoVac model. Average Particle size (nm); (1). CuO 41.17, (2). Al_2O_3 49.29, (3). Cr_2O_3 29.8825, (4). ZrO_2 20.477, (5). Fe_2O_3 46.762, (6). TiO_2 32.1267, (7). ZnO 29.735, (8). NiO 70.415/10.7, (9). Co_3O_4 70.415. All particles had spherical structure.

SEM analysis has been documented with **Figure 3** and zeta potential measurements were additionally measured for further characterization (**Table 3**).

Table 3 – Zeta Potential measurements for various dispersions of metal oxide nanoparticles

Zeta Potential Measurements for Dose ->	Medium of Dispersion: 10 mM NaCl, pH7. Zeta potential: 3.25					Media of Dispersion: DMEM, pH 7. Zeta Potential: -7.18
NPs	0.1 mM	1 mM	5 mM	20 mM	40 mM	5 mM
CuO	-3.05	1.24	-5.42	-44.71	-129.74	-18.42
Cr_2O_3	6.82	-72	-11.02	-25.28	-33	-27.84
ZnO	-1.75	-9.02	0.39	-63.81	47.29	-27.45
NiO	18.06	3.78	386.88	-42.54	37.5	-30.51
ZrO_2	1.23	127.46	7.64	116.2	40.98	-43.56
Co_3O_4	2.43	0.21	24.96	22.6	11.92	-24.39
Al_2O_3	9.24	-0.01	41.36	49.55	53.49	-47.35
TiO_2	21.34	31.36	37.15	38.23	35.46	-21.09
Fe_2O_3	7.55	28.79	27.67	39.23	1426.06	-23.33

Zeta potential of metal oxide nanoparticles was measured using a particle analyser (Beckman Counter, Delsa Nano) in various doses with two mediums of dispersion; DMEM cell culture medium and 10mM NaCl solution. Zeta potential measures the magnitude of charge between particles in a dispersion. It is a crucial parameter that determines the stability of a formulation and can be used to regulate aggregation (Wei and Gao, 2010).

3.2.2 *In Vitro* Culture of A549 Cells

A549 cells were propagated *in vitro* and perpetuated at 37°C with 5% CO_2 in DMEM supplemented with 10% FBS, 1× antibiotic antimycotic solution and passaged at confluence.

3.2.3 Establishing the response curve by assessing mitochondrial function as a descriptor of cellular viability through Resazurin reduction assay

Resazurin assay was carried as per Chapter 1. Charging of nanoparticle were done as per **Table 4**. Percentage Resazurin reduction was used to develop the response variable (**Figure 4**) in terms of dose at 50% death (LD_{50}) for this study.

Table 4 - Design of Resazurin reduction assay for testing nanoparticle mediated mitochondrial dysfunction.

Dose (mM)	NP vol (µl)	Stock (mM)	DMEM (µl)	10% serum (µl)	Cells seeded
0 (Ctrl+)	0	0	1350	150	Yes
0.15	22.5	10	1327.5	150	Yes
0.31	46.5	10	1303.5	150	Yes
0.62	93	10	1257	150	Yes
1.24	186	10	1164	150	Yes
2.48	372	10	978	150	Yes
4.96	744	10	606	150	Yes
9.92	744	20	606	150	Yes
19.84	974	30	376	150	Yes
39.68	584.4	100	765.6	150	Yes
79.36	1168.8	100	181.2	150	Yes
Neg (-)	0	0	1350	150	No

This design developed by us, ensures equal serum concentration and nano-scale dispersion at the time of charging nanoparticles.

Figure 4: Response curve to assess toxicity
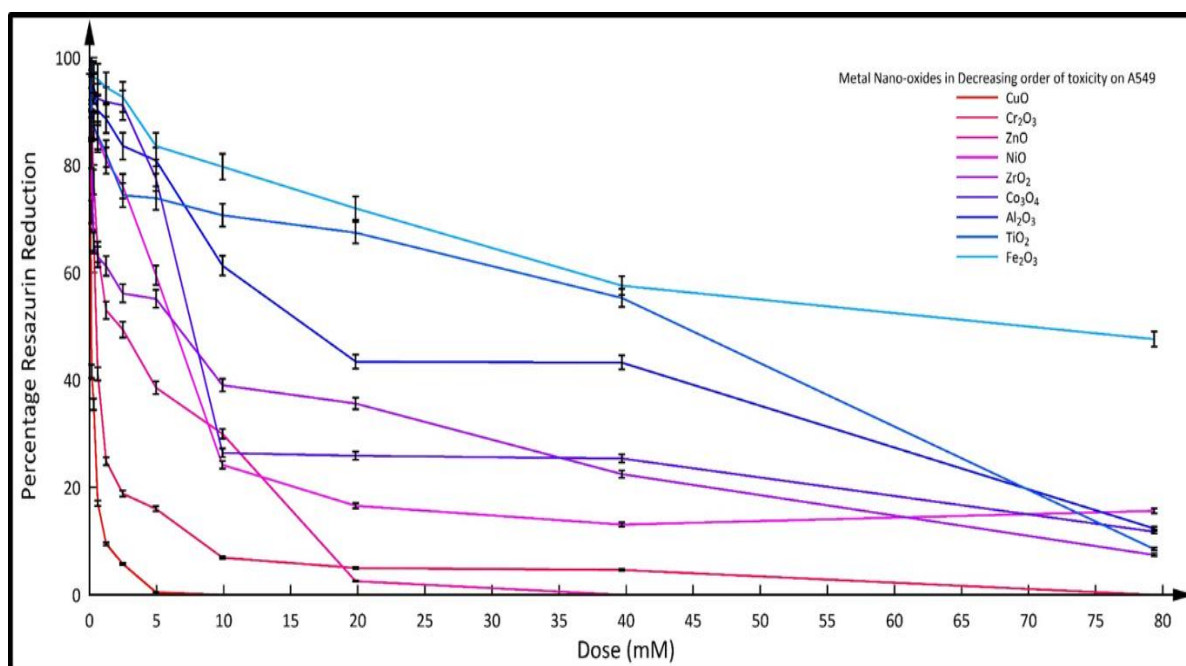
Toxicity is measured as Log ($1/LD_{50}$). P values are CuO 0.0034 (**), Cr_2O_3 0.0032 (**), ZnO 0.0028 (**), NiO 0.0019 (**), ZrO_2 0.0015 (**), Co_3O_4 0.0042 (**), Al_2O_3 0.00023 (***), TiO_2 0.0029 (**), Fe_2O_3 0.00056 (***)

3.2.4 Testing fitness of response curve to various descriptor

Response curve is represented as the average value of LD_{50} with standard deviation over three independently executed experiments with seeding density 2.5 x 10^4. Log ($1/LD_{50}$) is taken as the descriptor of toxicity and expressed as a function of enthalpy change for formation of one mole of gaseous cation with the same oxidation state as present in the metal oxide nanoparticles as per Puzyn *et al*. 2011. Coefficient of determination (R^2) is computed to

aid statistical quality of the fit. Several other parameters were also tested for their quality of

fitness to the response curve generated, including mulliken electronegativity, thermal conductivity, oxidation number, total metal electronegativity per oxygen (Table 5) and zeta potential measurements (Table 6).

Table 5 – The response curve for toxicity log(1/LD$_{50}$) plotted against various descriptors

log(1/LD50)	NPs	pH Enthalpy of formation of gaseous Cation (kcal mol-1)	Mulliken Elctronegativity (eV)	k, Thermal conductivity (W cm-1 K-1) at 300K	Oxidation Number	Total metal electronegativity per oxygen (eV)
3.891	CuO	706.25	4.25	4.01	2	1.9
3.293	Cr_2O_3	1268.7	4.36	0.937	3	1.107
2.577	ZnO	662.44	8.33	1.16	2	1.65
2.202	NiO	596.7	4.47	0.907	2	1.91
2.185	ZrO_2	1357.66	4.95	0.227	4	0.665
2.118	Co_3O_4	No Data	No Data	1	No Data	No Data
1.791	Al_2O_3	1187.83	3.44	2.37	3	1.073
1.355	TiO_2	1575.73	4.91	0.21	4	0.77
1.156	Fe_2O_3	1408.29	4.21	0.802	3	1.22
	Reference	Puzyn et al., 2011	Gajewicz et al., 2015	Ho et al., 1972	Yatsimirskii 1994, Walker CRC Press	Kar et al., 2014
	R^2 computed for Linear Fit (Dplot)	0.564	0.097	0.619	0.518	0.502

R^2 was computed as a fitness measure to assess if any of the descriptors describe the response curve generated

Table 6: The response curve is plotted against zeta potential values for various dispersions of nanoparticles

	Medium of Dispersion: 10 mM NaCl, pH7. Zeta potential: 3.25					Media of Dispersion: DMEM, pH 7. Zeta Potential: -7.18
Dose ->	0.1 mM	1 mM	5 mM	20 mM	40 mM	5 mM
R^2 (Dplot) computed for fitness with $\log(1/LD_{50})$	0.57	0.4	0.16	0.57	0.57	0.2

Zeta potential is discovered to be a poor descriptor of the response curve, with maximum correlation of about 57%. Zeta potential measurements from **Table 3**, are utilized to compute the R^2.

3.2.5 Investigating potency of protein corona as a descriptor for alveolar stress:

Two independent experiments were carried out to investigate the possible roles of the degree of protein corona adsorbed onto the nanoparticle surface in nanoparticle mediated toxicity. 10µl of nanoparticle charged spent media was loaded onto a 12% SDS-PAGE gel along with spent media from control (no NPs added) to check for any significant changes in the pattern, if any and silver stained as per Thierry Rabilloud *et al*., 1994, with 0.1% cold silver nitrate solution. Development was carried out with 2% Sodium Carbonate solution charged with formaldehyde and sensitized with sodium thiosulphate solution. Development at

appropriate intensity was arrested using 1% acetic acid solution. If added nanoparticles adsorb more protein onto their surface, then protein content remaining in the media depletes. Samples were deliberately loaded in the decreasing trend of response curve that was deduced in our study to ease the discovery of descriptors of toxicity (**Figure 4**)

Figure 5 – Assessment of spent media upon nanoparticle incubation
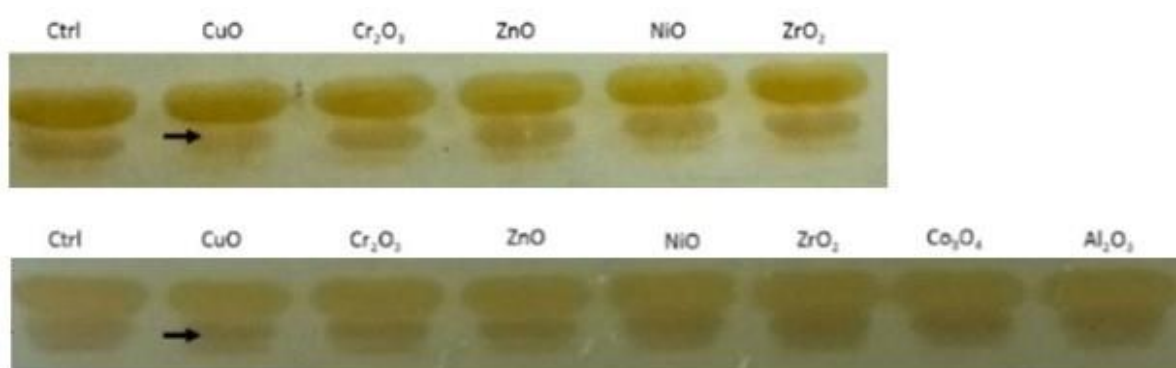
Bands around 70KDa, (serum) from two independent experiments are photographed and stacked here in.

5mM Nanoparticle dispersion is made using spent media (free of nanoparticle exposure) and incubated for 24 hours. Nanoparticles are pelleted, and absorbed protein is extracted using a tris-EDTA based buffer (20mM Tris.Cl pH 8.0, 1mM EDTA, 1mM PMSF, 10% Triton X 100). Protein eluted is quantified using Bradford's method. 40μg of protein is loaded onto each lane of a 10% SDS PAGE gel after denaturing with laemmli buffer (Lemmli, 1970) and electrophoretically run for resolution. Coomassie staining is applied for visualization of resolved protein bands (**Figure 5**).

Figure 6 - Corona protein loaded in the decreasing trend of toxicity
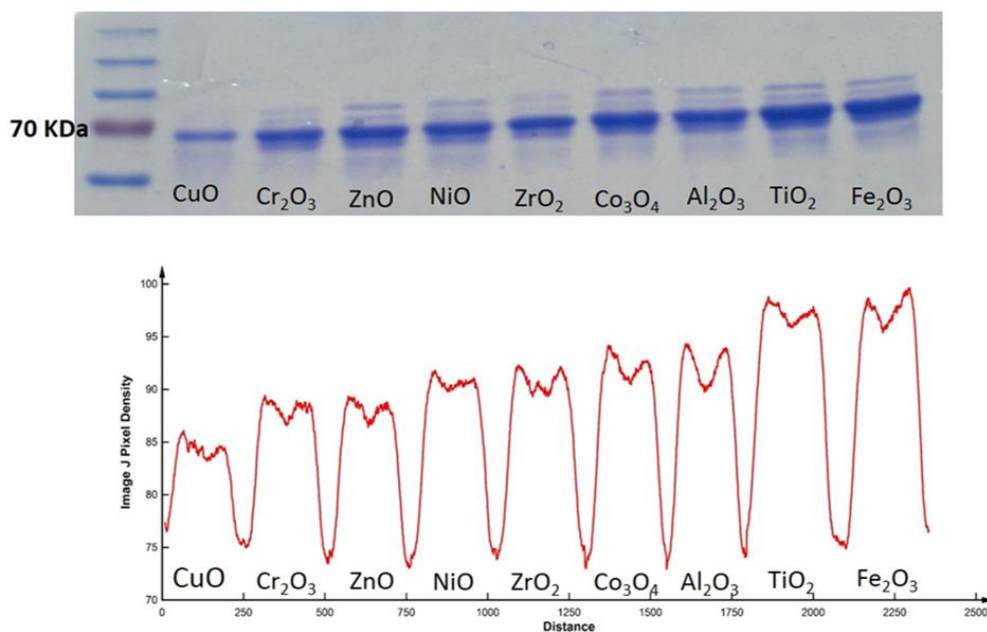
Nanoparticle adsorbed protein; the corona protein follows the trend in toxicity, with the highest thickness of adsorbed protein being present on the least lethal nanoparticle.

3.2.6 ROS assay using reduction of DCFDA

10,000 cells were seeded per well in a 96 well plate and allowed to attach overnight. Cells are washed and stained with $20\mu M$ DCFDA (2',7'-dichlorofluorescin diacetate), a fluorogenic dye that measures hydroxyl, peroxyl and other ROS activity within the cell, for 4 hours. Cells were washed again and incubated with nanoparticle dispersion to deliver select doses of exposure for 1 hour. Cells were washed for a final time and the plate was read under an excitation wavelength of 535nm. ROS intensity was plotted against dose for assessment of ROS as a potential descriptor to metal oxide nanoparticle induced toxicity on A549 cells (**Figure 6**)

Figure 7 - Percentage of DCFDA oxidation is plotted against Dose exposure of metal oxide nanoparticles
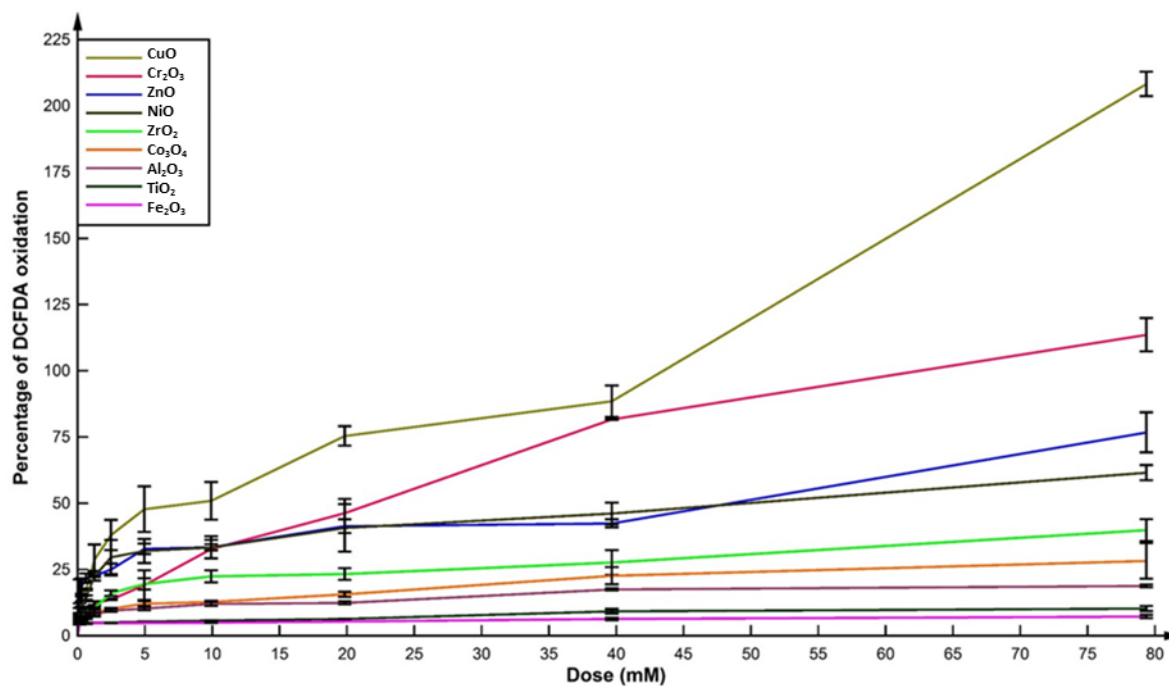
Total ROS generated also follows the trend in toxicity, with the highest levels achieved with the most lethal nanoparticle.

3.3 Results

3.3.1 Evaluation of Protein corona and ROS as descriptors of trend in toxicity incurred by metal oxide nanoparticles on A549 cells.

Image J, NIH is used to plot the densitometry profile of the resolved corona bands. The gray value or pixel density is then tabulated as in **Table 7** and tested for its potency as a toxicity descriptor. Further experiments have also been carried out by quantifying protein corona by dynamic light scattering (DLS) techniques to show that these could also be used in future as a potential descriptor (**Figure 8**).

Table 7 - R^2 for the response curve is calculated for protein corona and ROS as descriptors

log(1/LD50)	NPs	Total ROS generation across the range of doses assayed for (Computed by Dplot)	x', Protein Corona (Grey Value/Pixel Density)
3.891	CuO	8554.671	85.8
3.293	Cr_2O_3	5729.526	89
2.577	ZnO	3854.866	89.3
2.202	NiO	3651.924	91.6
2.185	ZrO_2	2244.778	92.3
2.118	Co_3O_4	1639.485	94.2
1.791	Al_2O_3	1234.955	94.5
1.355	TiO_2	652.0505	98.5
1.156	Fe_2O_3	484.8588	99.5
	Reference	This Paper, Martin et al., 2017	This Paper, Martin et al., 2017
R^2 computed for Linear Fit (Dplot)		0.971	0.957

Both Total ROS and protein corona prove to be good descriptors of the response curve with high correlations of over 95%

Figure 8 - Size of average protein corona tabulated against a few candidate nanoparticles

Metal oxide Nanoparticle	Size (nm)
CuO	33.2
ZnO	35.9
TiO_2	133.9
Fe_2O_3	175.3

DLS results are in tandem with SDS PAGE data generated, substantiating the discovery of thicker corona coat over less lethal nanoparticles.

3.3.2 Building the Nano-QSAR model based on ROS

log ($1/LD_{50}$) is plotted against total ROS generated. Best fit regression model is obtained by Dplot. The best fit regression model turned out to be a quadratic fit with R^2 of 0.971 (**Figure 9**)

Figure 9 - The response curve is plotted against total ROS generated
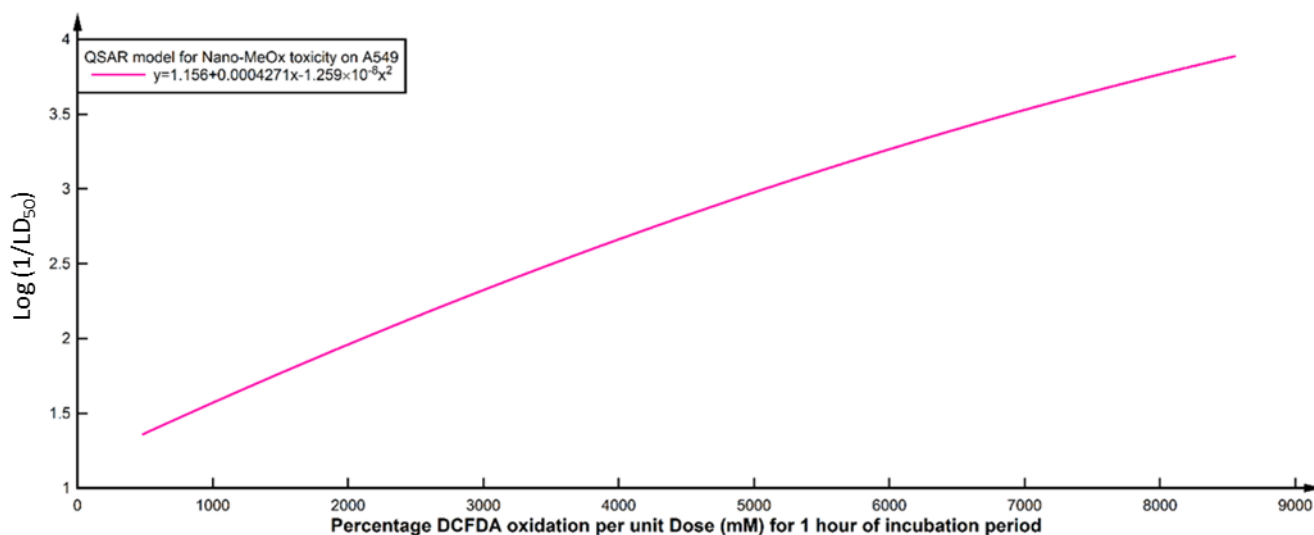
The model built thus is: log ($1/LD_{50}$) = $1.156 + 0.000427x - 1.259(10^{-8})\,x^2$

where x is the total ROS generated quantified through DCFDA oxidation for 1 hour of metal oxide nanoparticle exposure.

3.4 Discussion

Through our research work, we have discovered a consistent trend of toxicity induced by metal oxide nanoparticles on alveolar type 2 cells using A549 cell line as a model. This trend is as follows: $CuO> Cr_2O_3>ZnO> NiO> ZrO_2> Co_3O_4> Al_2O_3>TiO_2>Fe_2O_3$. This was in sync with other reports of toxicity of metal oxide NPs on A549 cells [$CuO>TiO_2$ (Moschini *et al*., 2013), $CuO> ZnO> NiO>ZrO_2> Al_2O_3\sim TiO_2> Fe_2O_3$ (at 1mg/ml in Horie *et al*., 2012) and $CuO>ZnO>Co_3O_4>Al_2O_3\sim TiO_2\sim Fe_2O_3$ (Ivask *et al*., 2015)]. Thus, we conclude that our results are accurate and establish a trend of toxicity for metal nano-oxides on A549 cells.

The next task was to express this trend in toxicity as a function of certain descriptors that are parameters attributing to physico-chemical characteristics of metal nano-oxide particles. This would aid in developing a prediction tool for toxicity induced by metal oxide nanoparticles in alveolar type 2 cells. Our literature survey uncovered Puzyn *et al*., 2011 that had developed a nano-QSAR model to predict metal nano-oxide toxicity in *E.Coli* as a function of bond dissociation energy in the form of enthalpy of formation of gaseous cation in Kcal/mole. The mechanism basis for this model is the release of metal ions which is one of the four widely studied mechanisms of toxicity induced by metal oxide nanoparticle (Djurisic *et al*., 2015). The other mechanisms include ROS generation, nanomaterial accumulation on membrane surface and internalization of nanomaterials. Since Puzyn *et al*., 2011 already provided the characteristic values of bond dissociation energy for various metal nano-oxides, I sought to express our response curve as its function. In doing so, I discovered bond dissociation energy correlated with the response curve at 56.4%. Some additional parameters were also tested for its correlation. Mulliken electronegativity had the lowest correlation at 9.7%. Others like oxidation number stood 51.8% and total metal electronegativity per oxygen was documented at 50.2%. Surface charge is a consistent player in determining nanomaterial

accumulation on cell surface and internalization, thus we next tried to test some surface charge parameters such as zeta potential and protein corona for their potency as descriptors. Zeta potential measurements were taken at the lysosomal pH for various metal oxide nanoparticle suspensions with 10mM NaCl solution to ensure consistent conductivity for each nanoparticle dispersion (Kaszuba *et al*., 2010, Clogston and Patri, 2009). A set of samples were also assessed at 5mM dispersion (culture pH of 7.0) where we have obtained a good resolution between different toxicity levels of various nanoparticles studied. This was done using DMEM as a medium to investigate if surface charge in presence of culture media may prove to be promising as a descriptor. In both cases however, we found poor fitness to the response curve for zeta potential measurements taken. As such we conclude that parameters of only surface charge are poor descriptors of the toxicity. None of the parameters evaluated thus far reached the recommended $R^2 \geq 0.81$ for *in vitro* experiments (Kubinyi *et al*., 1993), thus the validation for bond dissociation energy, mulliken electronegativity, oxidation number, total metal electronegativity per oxygen and surface charge proved poor descriptors of the response curve for toxicity. Also, this indicated release of metal ions characterized by enthalpy of dissociation, is not a contributing mechanism of toxicity induced by metal oxide nanoparticles in alveolar cells. One major reasoning might be that alveolar cells are eukaryotic cells, whose systems are vastly different from the prokaryotic systems with the presence of membrane bound organelles; *E.Coli*, evaluated in Puzyn *et al*., 2011.

I further sought to explore other mechanisms by which metal oxide nanoparticles conferred their toxicity in hopes of testing them for fitness to our response curve. These include ROS generation, nanomaterial accumulation on membrane surface and nanomaterial internalization.

To test for nanoparticle accumulation on the cell surface, I needed to discover additional parameters known to encourage such interaction. On much literature survey, it was

found that the dynamic protein adsorbed onto the nanoparticle called the corona protein dictates its bioreactivity and thus determines the degree of surface accumulation, internalization, cellular inflammation and degradation of accumulated nanoparticles within the cell (Saptarshi *et al*., 2013). Strong coulomb type interactions between nanoparticles and charged patches of protein adsorbed onto them, dictate the level of aggregation (Treuel *et al*., 2015). Further accumulation of nanoparticles on cell surface may cause many biological responses including alteration of receptor activities.

Thus, adsorbed protein onto the nanoparticles, the 'corona protein', was eluted, and SDS PAGE analysis was carried out with equal volume of each eluent. In doing so, it was discovered that protein corona is a definitive descriptor for toxicity in the form of protein adsorption for metal nano-oxide toxicity in A549 cells. A quantitative linear mathematical model was developed to express toxicity as a function of protein corona; $Log(1/LD_{50}) = 26.367 - 0.262x$, where 'x', is a parameter that depicts the size of the protein corona. In our model we have used pixel density of corona band(s) as this descriptor. There is scope to use DLS measurements also, as they are in tandem with the pixel density. Finally, when the spent media was resolved using SDS PAGE we find a similar trend of protein depletion with exposure to increasing toxicity conferring nanoparticles. It is possible that the degree of internalization of protein is in trend with toxicity, with more internalization at higher toxicity. It could be a reason why higher lethality causing nanoparticles have less protein coat adsorbed onto them, since there may be less protein available for adsorption in the closed system of *in vitro* evaluation. So, whether protein corona is in actual a determinant of toxicity or just an indicator of toxicity is to be further investigated. How quickly the nanoparticle adsorbs the biological fluid it meets and how quickly the so formed corona particles are internalized need to be understood before conclusively placing protein corona as the descriptor.

Our study has considered total protein corona, which is both, the loosely bound and the well adsorbed proteins that elute only upon a denaturant treatment (Winzen *et al*., 2015). Soft protein corona measured by DLS and hard protein eluted and run on SDS-PAGE gel follow trend in toxicity, with higher coat of protein corona over less lethal nanoparticles. Hard versus soft protein corona is better understood using **Figure 10**.

Figure 10- Hard versus Soft Protein Corona
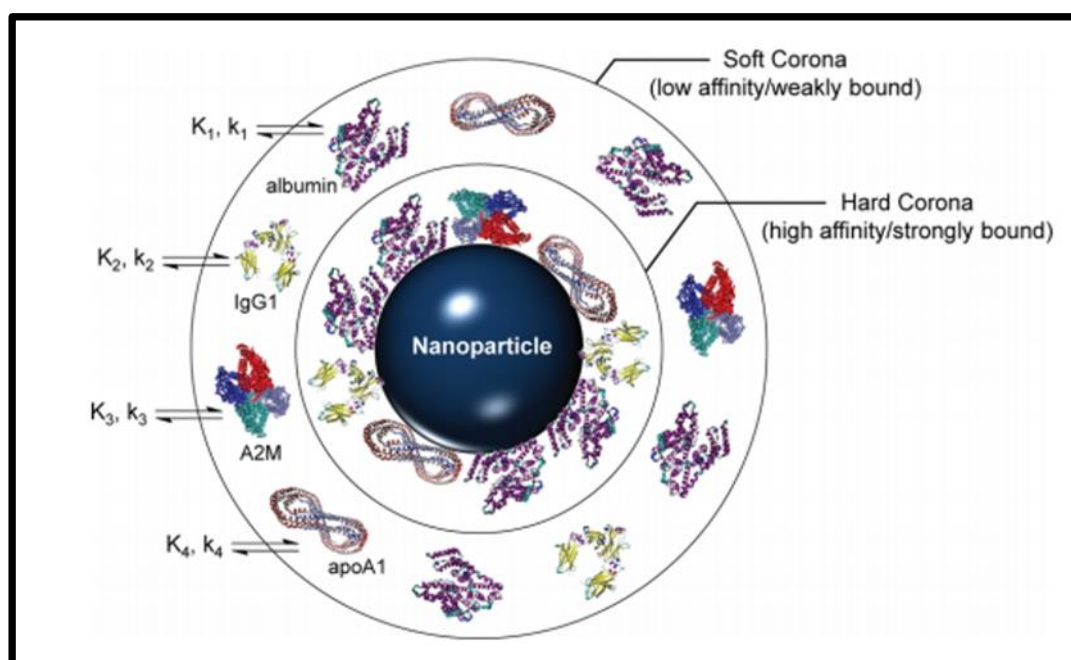
Referred from Fleischer and Payne, 2014; Adsorption of protein on to nanoparticle is a both kinetic (k) and thermodynamic (K) process. It results in modification of surface topography and composition and nanoparticle dimension. With increase in incubation time, adsorbed serum proteins (such as albumin, A2M, apoA1, IgG1) are selectively replaced by those of a higher affinity. Soft corona proteins can be dislodged from nanoparticle surface by physical processed such as sonication or centrifugation. Hard corona necessitates the use of a denaturant such as SDS to elute from the nanoparticle surface.

One validation of why the thickness of the protein corona might follow the toxicity trend could also be that, cellular uptake of nanoparticles depends on the nanoparticle directly interacting with cell membrane and its subsequent internalization through energy dependent pathways. Protein adsorption on to nanoparticles impedes the uptake efficiency by decreasing unspecific interaction between nanoparticle and the membrane (Winzen *et al.*, 2015). Serum is known to form corona coats over cationic, anionic and neutral particles (Fleischer and Payne, 2014), though our research particularly shows that the degree of adsorption and the thickness of the corona coat is a function of chemical identity of the nanoparticles.

ROS was additionally evaluated, to see if the level of oxidative stress could determine the degree of toxicity induced by metal oxide nanoparticles in A549 cells. Thus, the ROS assay was performed, and the results were highly encouraging. The trend of ROS generation followed precisely the same pattern of toxicity as we had established in our study, confirming the occurrence of ROS generation as an event before cell death in our chosen system.

When total ROS is expressed as a function of toxicity; log ($1/LD_{50}$), a quadratic function is obtained with a high correlation of about 97%. Thus, the following equation is accepted as a quantitative structure activity relationship-based model to predict metal oxide nanoparticle induced toxicity in type II alveolar cells.

$$\log (1/LD_{50}) = 1.156 + 0.000427x - 1.259(10^{-8}) x^2$$

'x' is the total ROS generated upon the first hour of incubation of nanoparticles with A549 cells. The units being percentage DCFDA oxidation per unit dose in mM of the exposing nanoparticle.

Chapter 4

Elucidation of the nature of cell death caused by metal oxide nanoparticle induced stress in A549 cells.

4.1 Introduction

There are reports of autophagic death, apoptosis and necrosis owing to metal oxide nanoparticle exposure across the spectrum of less lethal to most lethal nanoparticles. For example, ceria oxide, zinc oxide and silicon oxide nanoparticles were capable of inducing autophagy and late apoptosis in A549 cells (Yang *et al*., 2018). ZnO nanoparticles also remarkably increases the expression of pro inflammation mediators such as interleukin 8 and tumor necrosis factor-α (Yan *et al*., 2017). Copper oxide nanoparticles could cause apoptosis in A549 cells by inhibition of histone deacytylase (Kalaiarasi *et al*., 2018). They are also documented to cause autophagic death with the same cells A549 (Sun *et al*., 2012). Further in this study itself, it was found that apoptotic and necrotic like cells are an occurrence with the exposure to ZnO nanoparticles (Chap 1, Fig 6A). Since cellular stress is a highly multi factorial process, it is possible that dose and time dependent results vary as per experimental designs. However, the trend of toxicity remains constant (Loret *et al*., 2016).

This study also discovered a definite trend in toxicity which is determined by ROS generation and indicated by protein corona (Chap 3). Among the investigated metal oxide nanoparticles, the trend established by this study was $CuO> Cr_2O_3>ZnO> NiO> ZrO_2> Co_3O_4> Al_2O_3>TiO_2>Fe_2O_3$. There was thus, a possibility to predict the nature of cell death following nanoparticle-cell interactions with respect to dose and incubation period. Degree of toxicity ultimately courses the nature of cell death. For example, necrosis, is often a consequence of the cell's failure to programme death owing to the toxic disruption of significant cellular functions (Orrenius *et al*., 2010). Programmed modes of cell death such as apoptosis, autophagy and pyroptosis for example, display intricate signaling cross talks that often involve ATP, modulation of calcium homeostasis, increased generation of reactive oxygen species and involvement of crucial proteins such as calpains, proteases, endonucleases and caspases (Plattner and Verkhratsky, 2016). The dying cells are usually

identified and engulfed by macrophages and destroyed to avoid inflammation and disruption of surrounding tissue (Cocco and Ucker, 2001).

In contrast, Necrosis, is characterized by cellular swelling and bursting of intercellular contents, loss of ionic balance and incitation of inflammatory responses in the surrounding tissue (Fulda *et al*., 2010). Autophagy is seen in all eukaryotes and it is characterized by the formation of autophagic vacuoles following lysosomal degradation. It is ATP dependent and cell protective, in that protein aggregates are recycled for repair (Tsukahara *et al*., 2014). Light chain 3 (LC3) is a crucial protein necessary for the formation of autophagosome and its cleavage to LC3 B I and II is usually associated with starvation induced autophagic activity and autophagy mediated cell death (Tanida *et al*., 2008). As such LC3B is a well-studied marker for autophagy (Meyer *et al*., 2013).

Further High mobility group box protein (HMGB1) is a nuclear protein which facilitates transcription of genes associated with proliferation in response to stress. Also, upregulation of HMGB1 is associated with Beclin dependent autophagy. While oxidized HMGB1induces apoptosis by the caspase 3/9 intrinsic pathway (Tang *et al*., 2010). Expression of cyclin B1, a regulatory protein in cell cycle can also be tested to check for apoptosis. Cyclin B1 is crucial for mitosis (Strauss *et al*., 2012) and with cdk1, it coordinates G2/M progression (Wang *et al*., 2014). Down regulation of cyclin B1 is often associated with G2/M arrest (Scaife 2004), and G2/M arrest often routes in apoptosis (Di Paola, 2002).

Propidium iodide (PI) is a fluorescent dye that binds to DNA in dead cells, it is not permeated in live cells with intact membranes, as such it can be used to detect necrosis (Crowley *et al*., 2016). Since apoptosis is characterized by DNA fragmentation and thus structural differences such as N, 2N and 4N can be cell sorted and counted through flow cytometry to aid in cell cycle analysis (Riccardi and Nicoletti, 2006). Propidium iodide

staining and propidium iodide aided flow cytometry can be used to resolve the percentage of cells progressing through apoptosis, necrosis and autophagy. Thus, giving an insightful overview of the modes of cell death at play, in response to candidate nanoparticles across the toxicity trend as a function of dose and incubation time.

In addition, JC1 (5,5′,6,6′-tetrachloro-1,1′,3,3′-tetraethylbenzimidazolylcarbocyanine iodide), a cationic dye could also be used to investigate nature of cell death particularly apoptosis. Since mitochondrial membrane dysfunction characterized by its depolarization leads to apoptosis (Grubb and Lawen, 2003). JC1 exhibits a green fluorescence at lower mitochondrial membrane potential and a red fluorescence at higher potential. Thus, the ratio of red to green intensities is directly proportional to the strength of mitochondrial potential (Perelman *et al*., 2012). A higher intensity of red fluorescence indicates intact mitochondria with well-preserved membranal integrity. Conversely a higher intensity of the green fluorescence indicates a membrane disruption, that typically is observed with leaching of ions into the mitochondria (Petit *et al*., 1990).

The discussed methods should investigate the nature of cell death and remark on a possible trend with respect to the toxicity of the metal oxide nanoparticles. In chapter 1, it was discovered that phosphorylation of eIF2α and expression of Hsp70 follows the trend in toxicity, with higher expression for exposure to less lethal nanoparticle. For investigation into nature of cell death, it would be important to test if expression of p-eIF2α and Hsp70 is crucial to stress tolerance and if their expression also follows the trend in toxicity. Expression of p-eIF2α and Hsp70 as stress revival strategies to nanoparticle mediated toxicity has never been explored. Thus, they could be developed into novel stress revival strategies.

4.2 Methods

4.2.1 Materials

Common laboratory reagents were acquired from Himedia (India) and Sigma Aldrich (USA) and antibodies were obtained from Cell Signaling (USA), Biolegend (USA) and Abcam (USA). Propidium Iodide stain was secured from MP biochemicals. JC1 fluorescent dye was procured through Sigma Aldrich. Human A549 cells were obtained from National Centre for Cell Sciences, India. Characterized nanoparticles of ZnO and TiO_2 were obtained through Sigma, Aldrich (USA). ZrO_2 nanoparticles utilized were synthesized and characterized, with details in chapter 3.

4.2.2   Cell Culture

A549 cells propagated *in vitro* were perpetuated with 10% FBS conditioned DMEM (5% CO_2 at 37°C). In all investigations, cells were charged with nanoparticles at 80% confluence, unless otherwise mentioned.

4.2.3 Charging of Nanoparticles

ZnO, ZrO_2 and TiO_2 NPs were dispensed from closest stock concentration to avoid aggregation as detailed in chapter 3.

4.2.4 Western Blot Analysis to investigate the nature of cell death

After cell lysate (40 µg) was resolved by 10% SDS-PAGE the western blot was carried out as per Sarkar *et al*., 2007. In brief, the PVDF membranes were washed with tris-buffered saline followed by blocking with 5% non-fat dried milk or 3% BSA as was suited. The membranes were incubated at 4˚C overnight with primary target specific antibodies for LC3B (Cell Signaling- 1:500), HMGB1 (Biolegend- 1:500), Cyclin B1 (Cell Signaling- 1:1000), Hsp 70 (Sigma Aldrich- 1:4000), eIF2α (Cell Signaling- 1:2000), eIF2α-P (Cell Signaling- 1:1000) and β-Actin (Cell Signaling- 1:2000). The membranes were then incubated with secondary antibodies coupled to horseradish peroxidase for optimised time periods at room temperature. The membranes were washed in combinations of TBS and TBST at room temperature. Immunoreactivities were detected by ECL reagents (Amersham GE Healthcare). Expression of target proteins was normalized to β- Actin.

4.2.5. Propidium Iodide Staining for Necrotic cells

Cells are harvested and aliquoted up to 1×10^6 cells/100 µL into FACS tubes. After 2 washes with PBS, centrifugation at 300g was carried out for 5 minutes. Wash solution is decanted, and cells are resuspended in 100µl of flow cytometry staining buffer (10 µg/mL PI in PBS stored at 4 °C in the dark). Flow cytometer settings are adjusted for PI with 5 - 10 µL of PI staining solution added to a control tube of unstained cells. Incubation of 10 minutes is provided in the dark. PI fluorescence is determined using FL-2 or FL-3 channel with a FACS instrument. Data is acquired for unstained cells and single color positive controls. 5 - 10 µL of PI staining solution is added to each sample prior to analysis. Stop count is set on the viable cells from a dot-plot of forward scatter versus PI. Results are analyzed as per instrument settings.

4.2.6 Propidium Iodide Aided Cell cycle analysis

Cells are harvested and washed with PBS. This is followed by fixing with cold 70% ethanol. After 30 minutes of incubation, cells are washed twice with PBS. Centrifugation at 850g is carried out and cells are treated with 50 µl of a 100 µg/ml sock of RNase. 200 µl of PI is added (from 50 µg/ml stock solution). Analysis of results is carried out by first measuring the forward scatter (FS) and side scatter (SS) to identify single cells. Pulse processing is used to exclude cell doublets from the analysis. PI has a maximum emission of 605 nm and is measured with a suitable bandpass filter.

4.2.7 Detection of Mitochondrial membrane potential using JC1

Cells are harvested. JC-1 was dissolved in 100 mM Tris, pH 8.2 as per manufacturer's instructions to a working concentration of 2.5µM with an incubation of 15 minutes at room temperature. Cells were passed through a cell strainer (Becton Dickinson) before FACS analysis. Laser used for excitation was 488 nm (Gallios) and filters: 525/50 (FL1 green) and 585/42 nm (FL3 red). Data were processed by FlowJo v7.6.4.

4.3 Results

4.3.1 LC3B Analysis by Western Blot

Expression of LC3B as detected in the cell lysate followed the trend in toxicity established in chapter 3. At 24 hours of ZnO exposure, LC3B expression reached a maximum of 4.53 times as compared to the control expression for the documented 0.62 mM. While for incubation with ZrO_2, at the same dose point, the expression peaked at 5.75 times the basal expression. The highest observed expression was recorded for TiO_2 presentation at 0.62mM with 10.73 times the minimal expression (**Figure 1A**).

The same pattern was found to emerge when investigated for an increased incubation period of 48 hours. At 0.62mM of the documented dose, ZnO exposure observed 5.33 times the LC3B expression as that of the basal control value. ZrO_2 recorded 20.06 times and TiO_2 measured 28.44 times that of the minimal control expression. Densitometric analysis was carried out by ImageJ, NIH and plotted in **Figure 1B**.

Figure 1A – Western Blot Analysis of LC3B
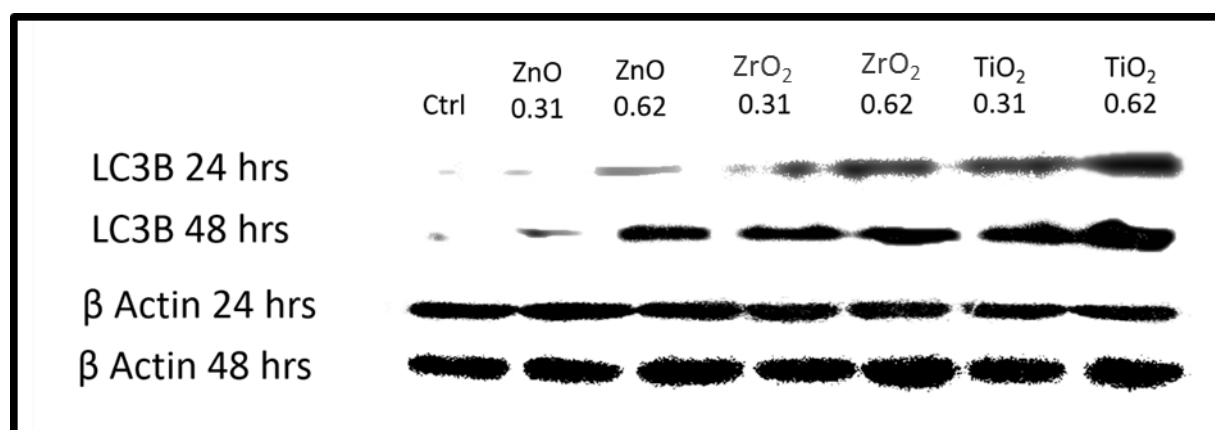
Western Blotting and chemiluminescent detection were used to target LC3B. The expression was normalized by using β-Actin as the internal control.

Figure 1B- Densitometric Analysis of LC3B, normalized to β-Actin
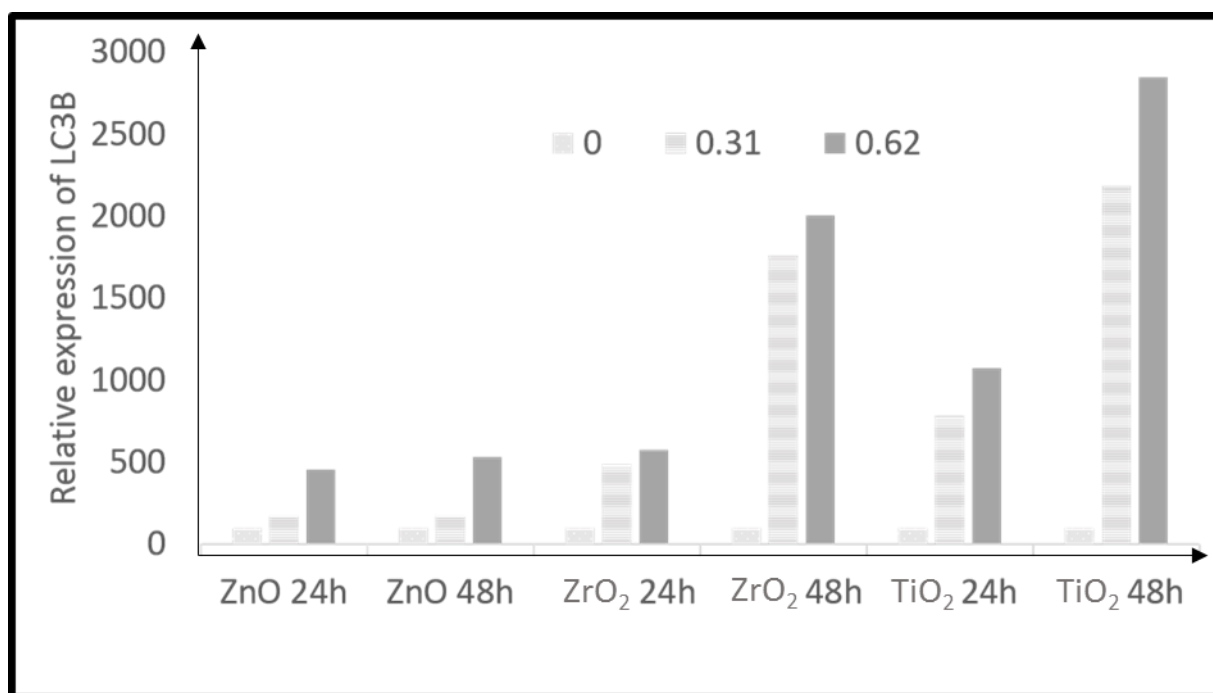
LC3B expression follows the trend in toxicity with ZnO having the least expression, while TiO$_2$ exposure has the most expression, in the candidate group where the toxicity follows the order of ZnO>ZrO$_2$>TiO$_2$. P values are ZnO 24h- 0.034 (*), ZnO 48h- 0.038 (*), ZrO$_2$ 24h- 0.012 (*), ZrO$_2$ 48h- 0.0027(**), TiO$_2$ 24h- 0.0067 (**), TiO$_2$ 48h- 0.0018 (**).

4.3.2. Western Blot Analysis of HMGB1

With ZnO treatment for both 24 and 48 hours, HMGB1 expression decreases with increasing dose (mM). At 0.31, 0.434 and 0.62 mM for 24 hours, the expression recorded, 0.37, 0.12 and 0.00007 times (insignificant) that of the basal expression. Only at the initial

exposure dose of 0.15mM, the expression slightly increased to 1.09 times that of the control, which is negligible. At 48 hours, the expression was 0.86, 0.22, 0 and 0 times the control expression for doses 0.15, 0.31, 0.434 and 0.62mM.

With exposure to TiO_2, for both 24 and 48 hours, HMGB1 expression increases with increasing dose (mM). This contrasts with results obtained on ZnO presentation. At 24 hours the increase was more pronounced and seems to slow down with further incubation to 48 hours. TiO_2 subjection at 24 hours, documented an increase of 3.73, 5.29, 5.73 and 9.52 times that of the control expression for doses, 0.15, 0.31, 0.434 and 0.62mM. At 48 hours, TiO_2 treatment recorded, 1.47, 2.86, 3.25 and 4.69 times the control expression for doses 0.15, 0.31, 0.434 and 0.62mM (**Figure 2A**). The densitometric analysis is provided in **Figure 2B**.

Figure 2A − Western Blot analysis of HMGB1
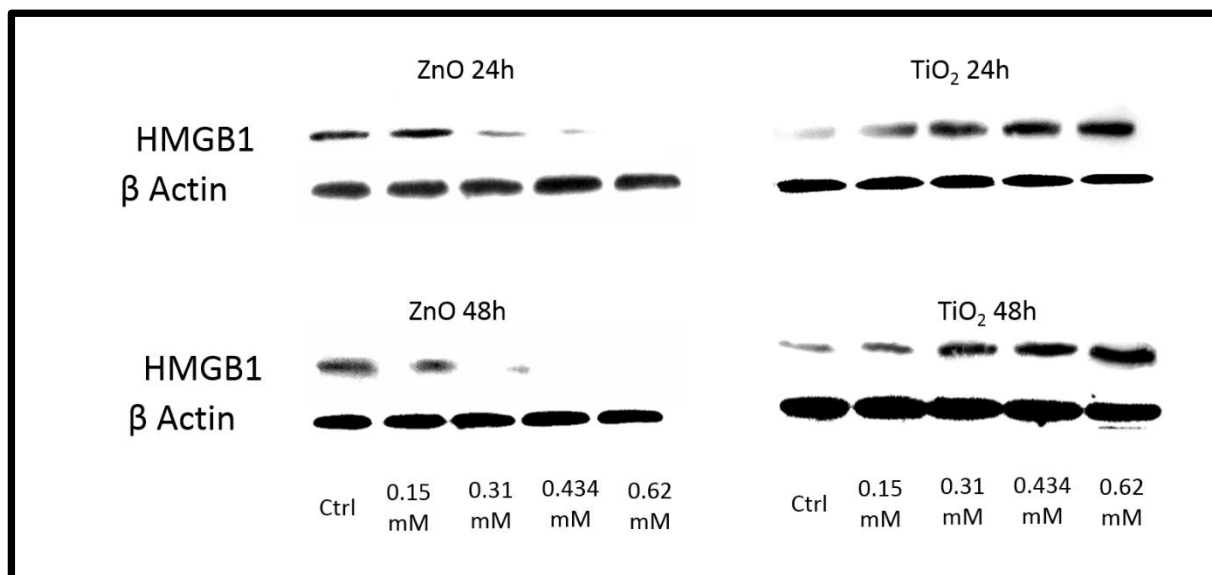
The expression of HMGB1 is normalized using β-Actin as internal control.

Figure 2B- The densitometric analysis of HMGB1 expression
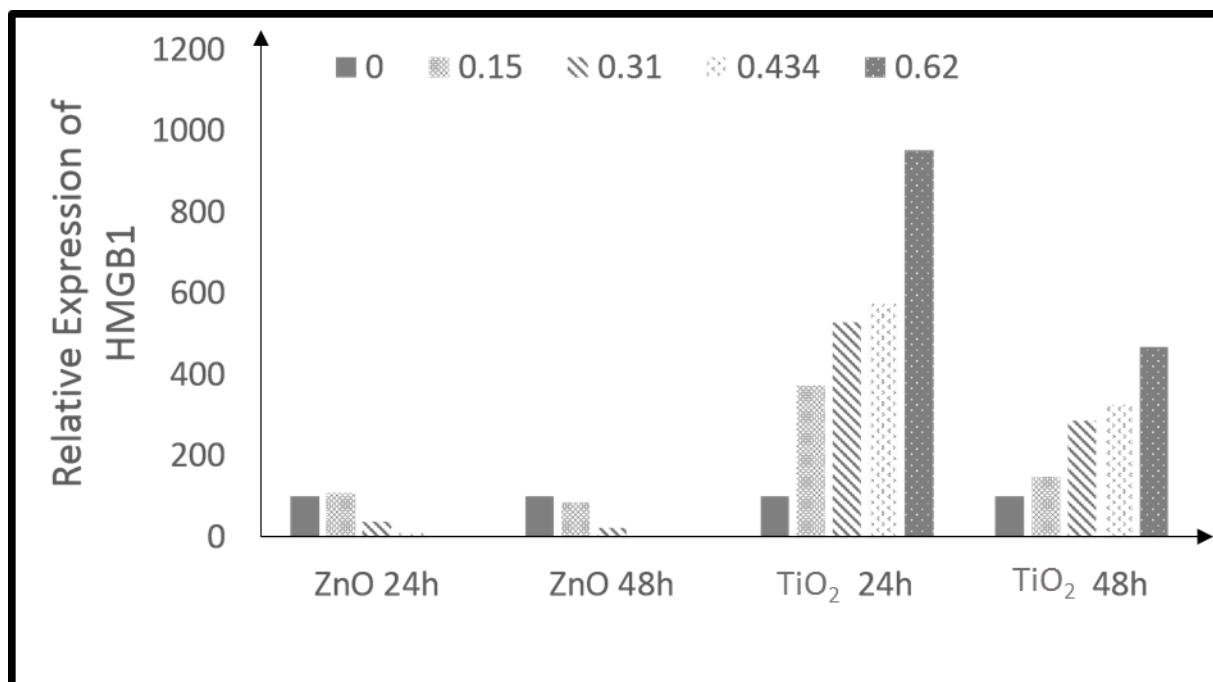
P values are ZnO 24h- 0.0067 (**), ZnO 48h- 0.0080 (**), TiO$_2$ 24h- 0.0021 (**), TiO$_2$ 48h- 0.0037 (**).

4.3.3. Western Blot Analysis of CyclinB1

For ZnO presentation, Cyclin B1 expression decreased with increase in dose (mM) for both 24 and 48 hours. At 0.31 and 0.62 mM, the expression dipped to 0.6 and 0.34 times that of the control value for 24 hours. At 48 hours, doses, 0.31 and 0.62 mM recorded 0.12 and 0.04 times that of basal value, suggesting Cyclin B1 decreases with increase in dose and time of incubation with ZnO nanoparticles.

On the other hand, 24 hours of TiO$_2$ treatment, is documented with a decrease in Cyclin B1 for 0.31mM and further increase at 0.62mM with values of 0.12 and 0.33 times the basal value. Further incubation up till 48 hours, records 0.17 and 0.036 times the control value for doses 0.31 and 0.62mM, suggesting TiO$_2$ exposure exhibits the cycling of Cyclin

B1 protein in the cell lysate. At 0.31mM, with increase in exposure, Cyclin B1 increases slightly, while at 0.62mM, there is a decrease of Cyclin B1 with increase in dose of exposure (**Figure 3A**). Densitometric analysis is provided in **Figure 3B**.

Figure 3 A- Western Blot Analysis of CyclinB1
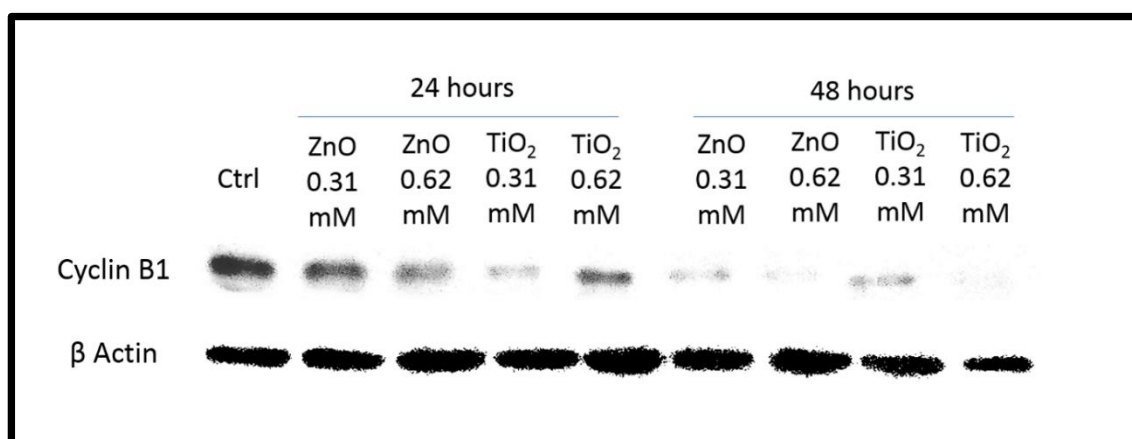
Cyclin B1 expression is normalized to β-Actin as the internal control.

Figure 3 B- Densitometric Analysis of Cyclin B1 expression
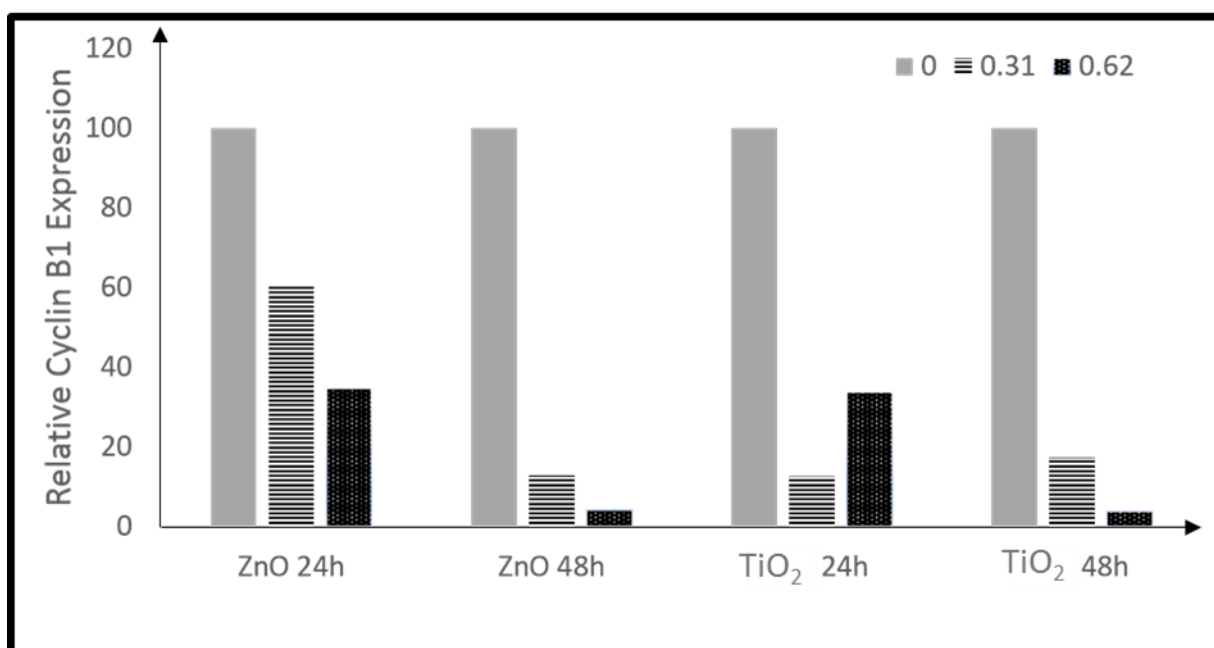
P values are ZnO 24h- 0.0057 (**), ZnO 48h- 0.00068 (***), TiO$_2$ 24h- 0.0038 (**), TiO$_2$ 48h- 0.0026 (**).

4.3.4 Western Blot Analysis of Hsp70 and p-eIF2α

Since the toxicity trend is consistent with the expression of the key molecules evaluated so far, it was imperative to investigate the expressions of Hsp70 and p-eIF2α. In chapter 2, the expression of these targets was discovered to be among the significant differences between cells exposed to ZnO (more lethal) and TiO$_2$ nanoparticles (less lethal). If indeed the trend extends to more metal oxide nanoparticles, a candidate particle whose toxicity is in between ZnO and that of TiO$_2$, should hypothetically also document an intermediate expression of Hsp70 and p-eIF2α. To test this ZrO$_2$ (log(1/LD$_{50}$) = 2.185) was chosen, as its toxicity was mid-way between TiO$_2$ (log(1/LD$_{50}$) = 1.355) and ZnO (log(1/LD$_{50}$) = 2.577) nanoparticles.

With ZnO NP exposure at 24 hours, Hsp 70 increases to 1.562 times of control value at 0.15mM and thereafter decreases to 0.95, 0.88 and 0 times at 0.31, 0.434 and 0.62mM respectively. At 48 hours, Hsp70 continues to decrease from its basal value with expression recorded, 0.95, 0.89, 0.84 and 0.78 times of control value at doses 0.15, 0.31, 0.434 and 0.62mM. ZrO$_2$ treatment at 24 hours documents increase in Hsp70 at both 24 and 48 hours, though the expression is higher for the first 24 hours of exposure. At 24 hours, doses 0.15, 0.31, 0.434 and 0.62mM document 1.52, 1.73, 1.76 and 2.05 times control expression. At 48 hours, the same exposure doses, record expression values relative to control as 1.13, 1.14, 1.7 and begins to dip to 1.25 respectively.

TiO$_2$ subjection increases Hsp70 for both 24 and 48 hours. The respective values for corresponding doses is higher than with both ZrO$_2$ and ZnO treatment. At 24 hours, for doses

0.15, 0.31, 0.434 and 0.62mM, the recorded expression values relative to control are 1.9, 3.18, 3.94 and 6.31 respectively. For the same doses at 48 hours, the expression of Hsp70 dips but continues the trend of increasing expression with increasing dose. The expression values relative to basal expression are 1.11, 1.31, 1.74 and 1.92 for corresponding doses of 0.15, 0.31, 0.434 and 0.62 mM. **Figure 4A** documents western blot analysis for Hsp70. **Figure 4B** is the corresponding densitometric analysis.

Figure 4 A- Western Blot Analysis for Hsp70
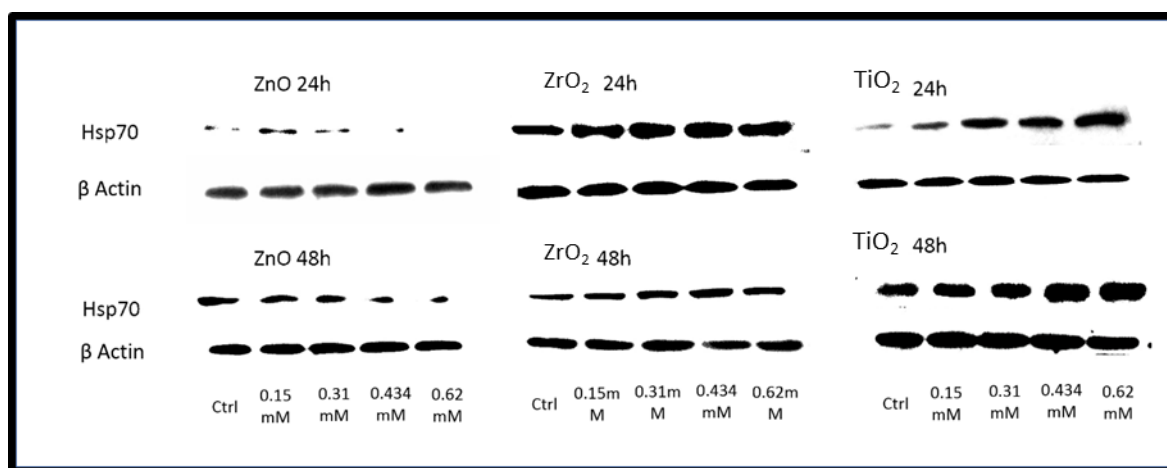
The expression of Hsp70 is normalized to β-Actin as the internal control.

Figure 4 B- Densitometric Analysis of Hsp70

P values are ZnO 24h- 0.021 (*), ZnO 48h- 0.034 (*), ZrO$_2$ 24h- 0.019 (*), ZrO$_2$ 48h- 0.0267, TiO$_2$ 24h- 0.0037 (**), TiO$_2$ 48h- 0.028 (*).

Remarkably, p-eIF2α also follows the trend in toxicity. Doses evaluated for this investigation include 0.31 and 0.62 mM. ZnO treatment documents increase in the phosphorylated form of eIF2α at 24 hours with 0.31 and 0.62mM recording 4.26 and 7.34 times basal expression. Though at 48 hours, the expression increases at 0.31mM with 3.97 times control value and decreases at 0.62mM with 2.6 times control value.

ZrO$_2$ presentation at 24 hours documents 3.25 and 7.22 basal times for doses 0.31 and 0.62mM. With further increase in exposure to 48 hours, the expression changes to 4.29 and 4.31 basal times for the same doses respectively. TiO$_2$ treatment exhibits the highest expression values documented. At both 24 and 48 hours, the values of p-eIF2α increases with increase in dose of exposure. At 24 hours, 0.31 and 0.62mM dose record an expression of 2.55 and 6.53 basal times, while for 48 hours, the same doses, are measured with 6.94 and 7.36 basal times expression (**Figure 5A**). Densitometric analysis is provided in **Figure 5B**.

Figure 5 A- Western Blot analysis of p-eIF2α for ZnO and TiO$_2$ exposure.

Figure 5B- Western Blot Analysis of p-eIF2α for ZrO$_2$ exposure
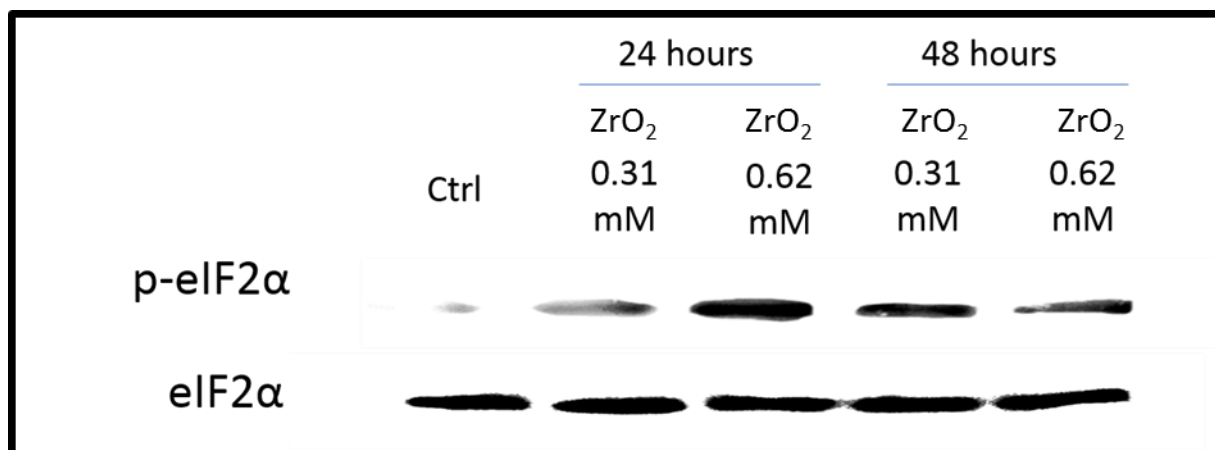
For Figures 5A and 5B; p-eIF2α is normalized to eIF2α as the internal control. eIF2α expression was checked to be like β Actin.

Figure 5C – Densitometric Analysis for p-eIF2α expression
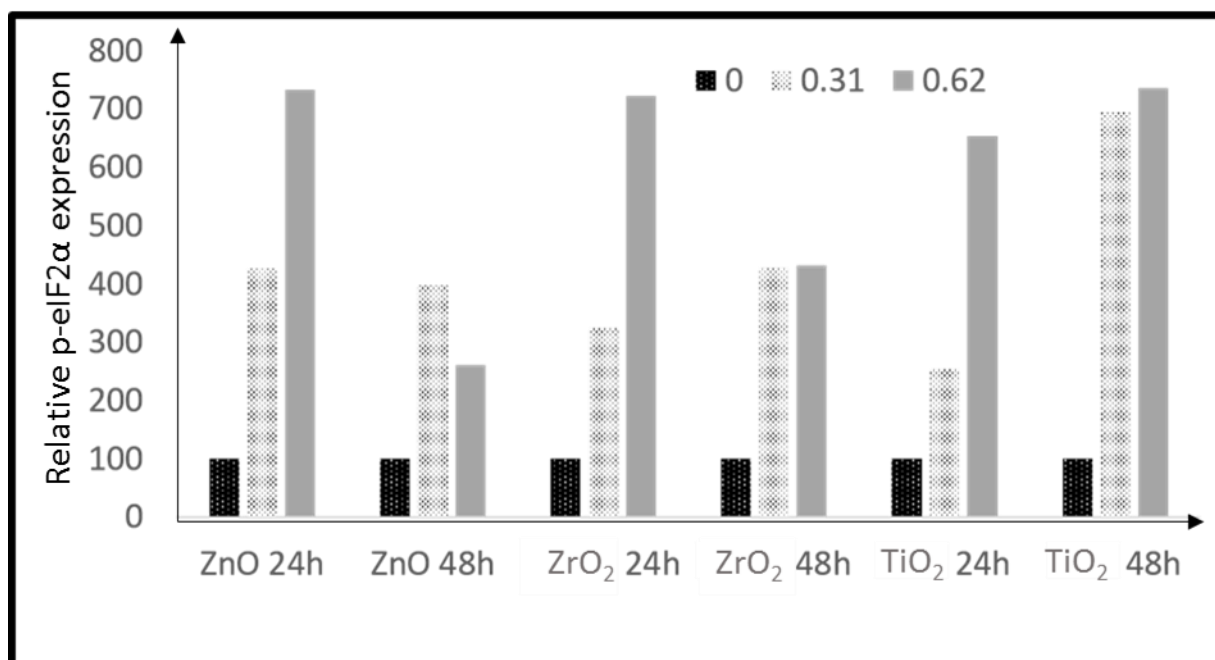
P values are, ZnO 24h- 0.0023 (**), ZnO 48h- 0.0045 (**), ZrO$_2$ 24h- 0.0031 (**), ZrO$_2$ 48h- 0.0067 (**), TiO$_2$ 24h- 0.00067 (***), TiO$_2$ 48h- 0.0017 (**).

4.3.5. Propidium Iodide Staining aided counting of necrotic cells

Doses evaluated are 0.15, 0.31 and 0.62mM for two incubation periods 24 and 48 hours. Control records non-viable cells or cells with damaged membranes at 7.3% for 24 hours and 8.5% for 48 hours respectively.

At doses 0.15, 0.31 and 0.62mM and for 24 hours, ZnO treatment documented 23, 36.8 and 48.2% of propidium iodide stained cells. At 48 hours, these values increased to 30.3, 39.3 and 75.5% respectively. For ZrO_2 presentation, at 24 hours the values were 20.2, 35 and 41.5 for doses 0.15, 0.31 and 0.62mM. With further increase in incubation time to 48 hours these values, increased to 34.5, 41.1 and 44 severally. Finally, TiO_2 exposure observed the least percentages of necrotic cells with documented values of 15, 19 and 35.6% for 24 hours and 32.2, 36.8, and 41.8% for doses 0.15, 0.31 and 0.62 mM individually.

In general, with increase in incubation time, percentage of membrane damaged cells have increased. Though at any incubation period and for any given dose of exposure the percentage of necrotic cells follow the trend in toxicity with ZnO> ZrO_2>TiO_2 (**Figure 6A-C**).

Figure 6A- Propidium Iodide Staining for Quantification of Necrotic cells with ZnO
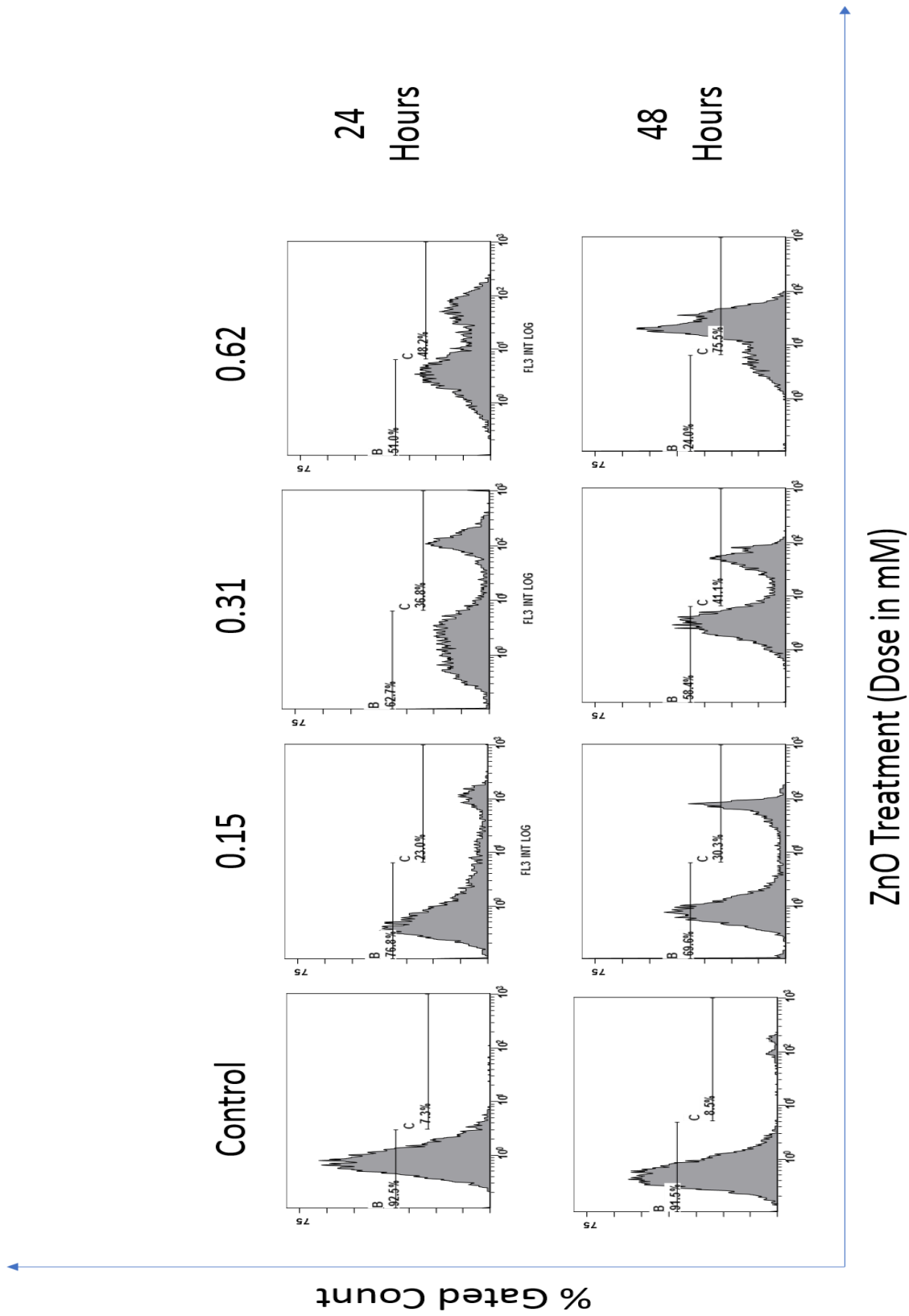
Figure 6B- Propidium Iodide Staining for Quantification of Necrotic cells with ZrO_2
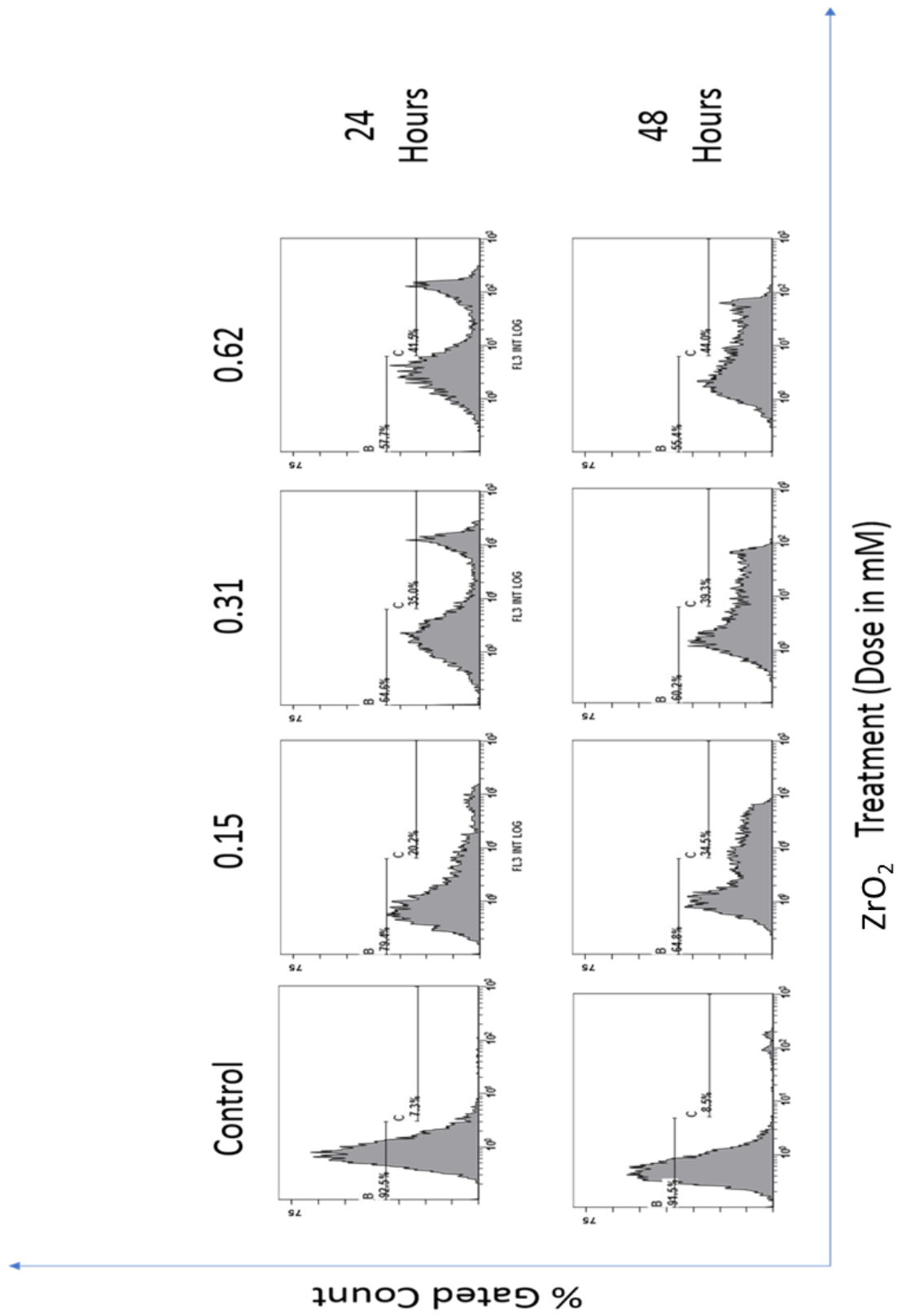
Gate C represents Necrotic cells.

Figure 6C- Propidium Iodide Staining for Quantification of Necrotic cells with TiO$_2$
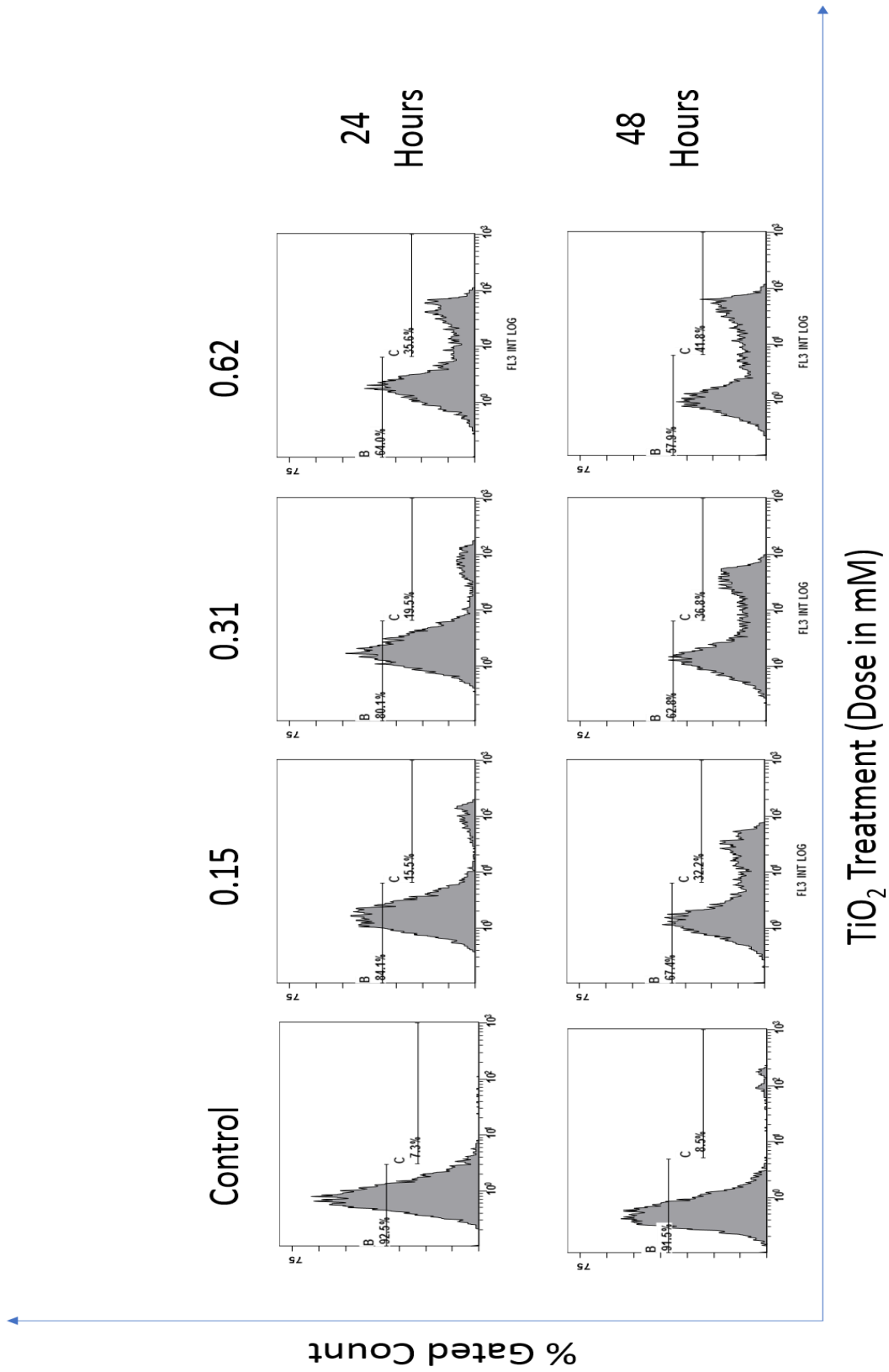
Gate C represents Necrotic cells.

4.3.6 Propidium Iodide aided cell cycle analysis by flow cytometry

Gate E represents percentage of cells with DNA less than 2N. Gate D represents 2N DNA containing cells (G_0/G1 phase). Gate F (S phase) – G (G_2/M phase) represent proportion of cells with 2N-4N, which are about to enter mitotic phase.

All experiments were carried in triplicate and the results bared consistency. Standard deviation reported errors of under 5%. The average data set is discussed herein. The control cells at 24 hours, noted 58.8% cells in G_0/G_1 phase, while the gate E (cells with fragmented DNA) sorted 5.1% at 48 hours. Majority of cells for the incubation periods documented, observed 15.7% to 23.6% of cells in the S phase, sorted through gate F. G_2/M at 24 hours, recorded 18.8 and 11.7 % for 24 and 48 hours respectively.

At both 24 and 48 hours of incubation with ZnO, the percentage of single stranded DNA increased. Highest values recorded at 24 hours was 39.5% at 0.62mM and 39.6% for 48 hours at 0.62mM. Proportion of cells progressing through G_2/M dipped. At 24 hours it dropped from a control value of 18.8% to 2.8%. At 48 hours, the depreciation was from a basal value of 11.7% to 3.4%.

Subjection to ZrO_2 nanoparticles remarkably increased the percentage of quiescent cells from 58.8% to 61.6% at 24 hours at 0.62mM. At 48 hours, the increase was from the basal value of 59.5% to 60.04% at 0.62mM. At 24 hours, percentage of single stranded DNA increased to 23.9% at 0.62mM of exposing dose. The same trend was noted at 48 hours, with 35.1% at 0.62mM. One other observation would be that the percentage of cells progressing through G_2/M further decreased and was observed between 3.6% and 1.1% at 24 and 48 hours for the highest dose evaluated is the study being 0.62mM.

Exposure to TiO_2, displayed the highest percentage of cells in the quiescent stage. With 0.62mM, at 24 hours the proportions reached 78.8% and at 48 hours it was recorded at

75.5%. Cells progressing through G_2/M were recorded at 8.5% and 9.4%, for 24 and 48 hours for an exposing dose of 0.62mM. Percentage of single stranded DNA did not increase much beyond the basal control value for both 24 and 48 hours.

The results show fragmentation of DNA followed the trend $ZnO>ZrO_2>TiO_2$ with ZnO exposure indicating a G_2/M arrest, consistent with apoptosis. Quiescent population of cells followed the trend $TiO_2>ZrO_2>ZnO$ (**Figure 7A-C**). Quiescence noted with G_0/G_1 arrest is a usual paradigm with autophagic pathways.

Figure 7A- Cell Cycle Analysis for ZnO treatment
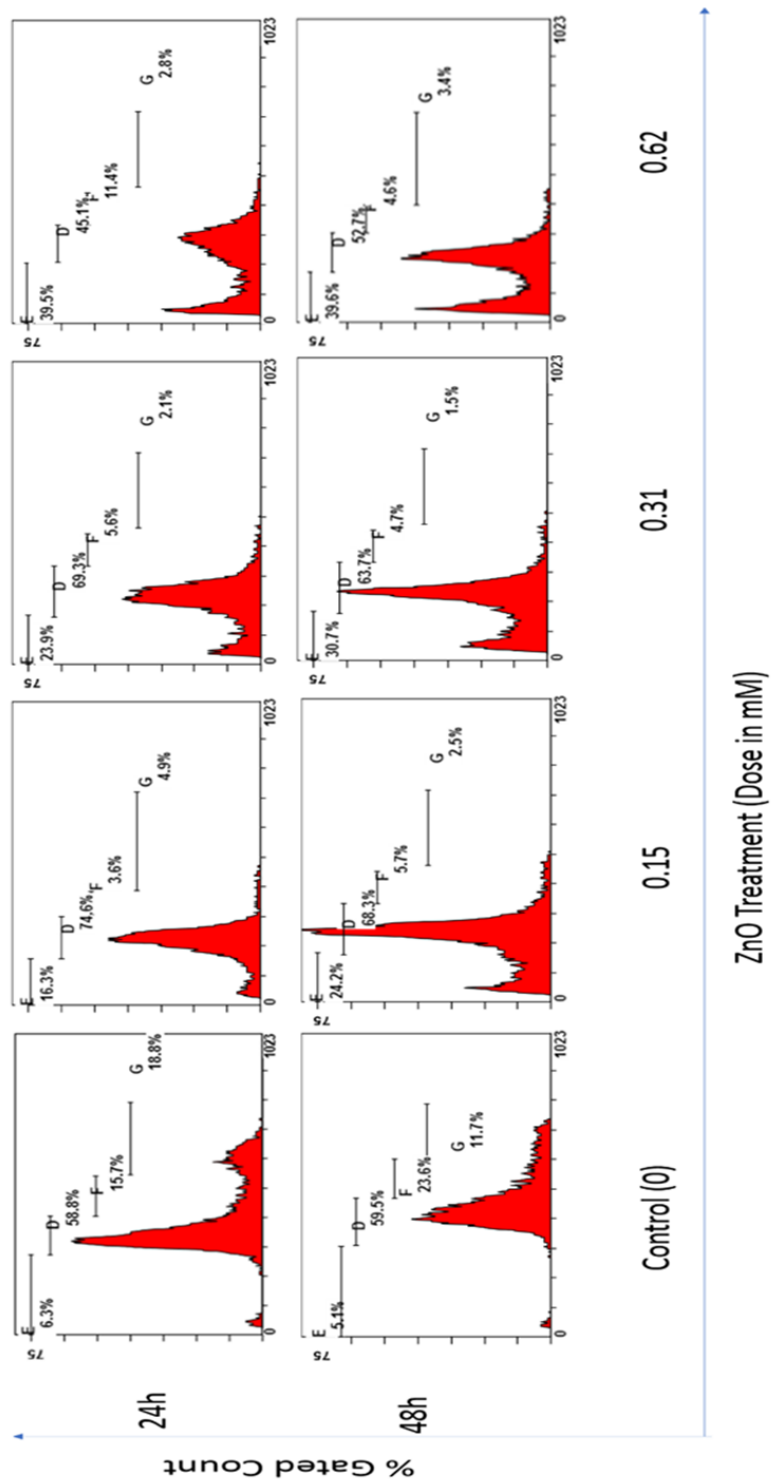
Doses evaluated 0 (control), 0.15, 0.31 and 0.62mM. Incubation periods investigated; 24 and 48 hours.

Figure 7B- Cell Cycle Analysis for ZrO₂ treatment
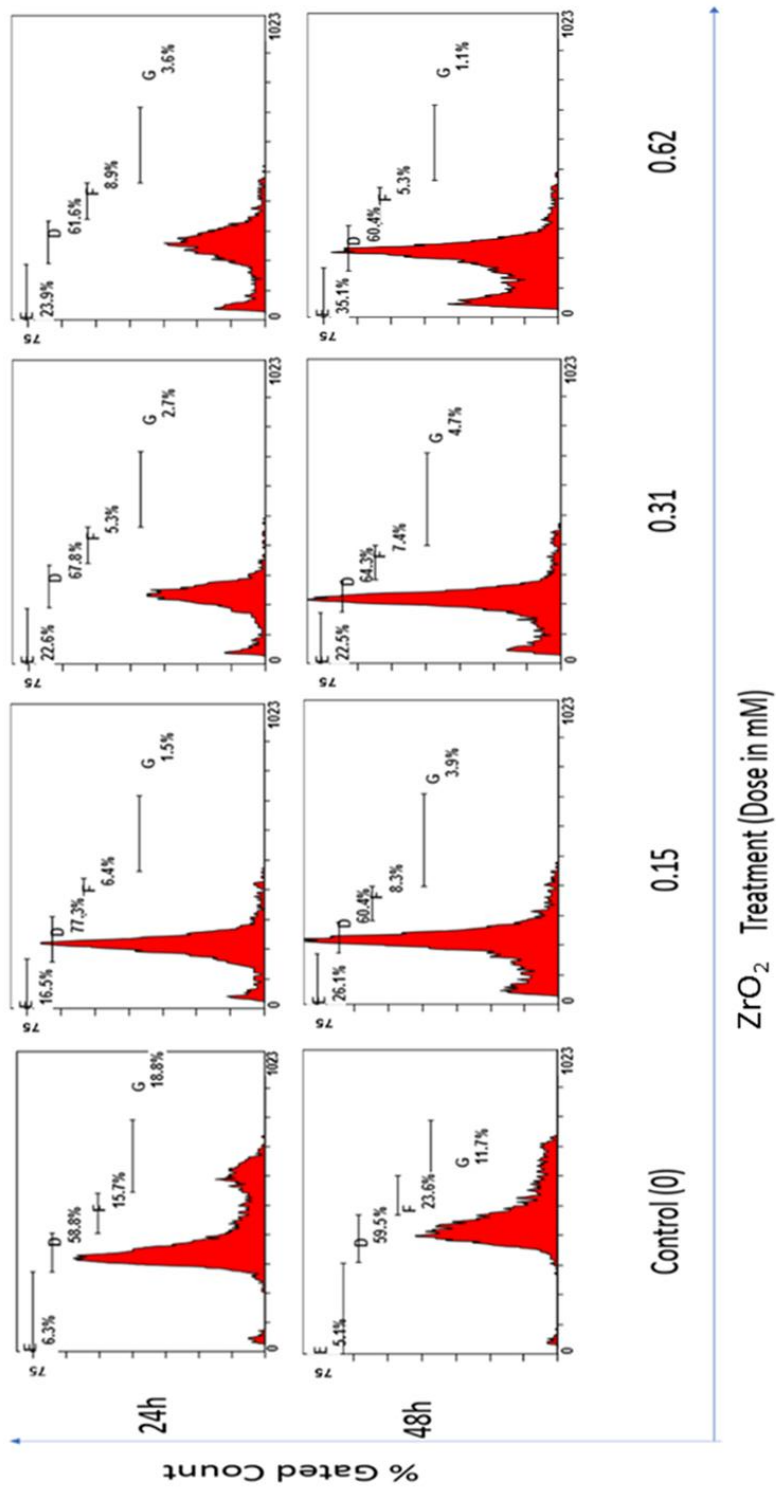
Doses evaluated 0 (control), 0.15, 0.31 and 0.62mM. Incubation periods investigated; 24 and 48 hours.

Figure 7C- Cell Cycle Analysis for TiO$_2$ treatment
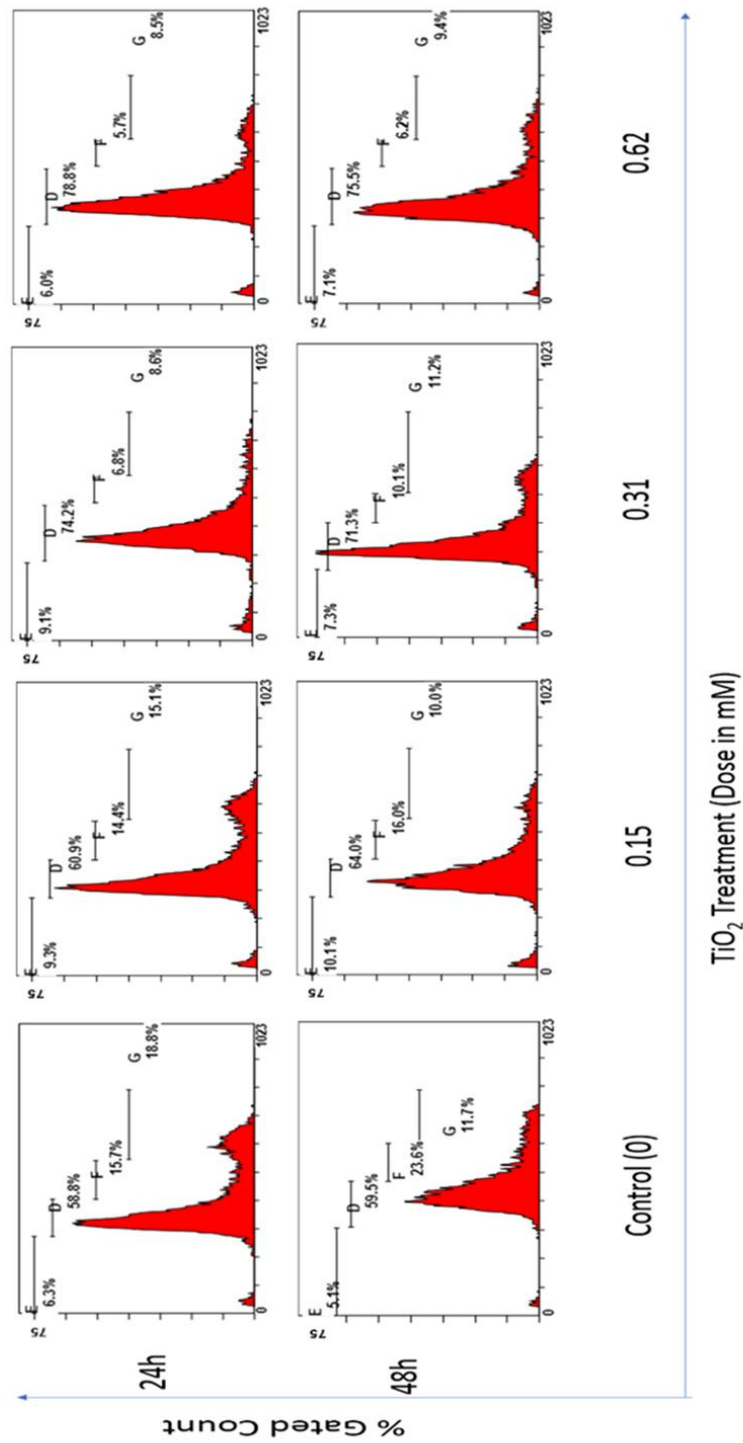
Doses evaluated 0 (control), 0.15, 0.31 and 0.62mM. Incubation periods investigated; 24 and 48 hours

4.3.7 JC1 aided quantification of mitochondrial membrane potential

Green fluorescence of JC1 is due to the depolarized mitochondrial membrane. ZnO treatment has the highest percentage of depolarization. FL1 scintillations at 24 hours measure 58.1, 60.4 and 70.5% at doses 0.15, 0.31 and 0.62mM. At 48 hours, this further increases to 59.6, 64.1 and 73 respectively.

ZrO_2 presentation results in FL1 gated counts at 44.9, 50.1 and 58.4% for 24 hours with doses 0.15, 0.31 and 0.62mM. Corresponding values of gated cell proportions for 48 hours are 48.5, 53.8 and 61.9% respectively. TiO_2 exposure leads to FL1 counts of 22.3, 31.8 and 35.3% at 24 hours. Further incubation up till 48 hours documents 24.5, 33.1 and 39.1% for respective doses.

The results (**Figure 8A-C**), measure membrane depolarization of mitochondria in the order of $ZnO > ZrO_2 > TiO_2$.

Figure 8A- Degree of mitochondrial membrane depolarization for ZnO treatment
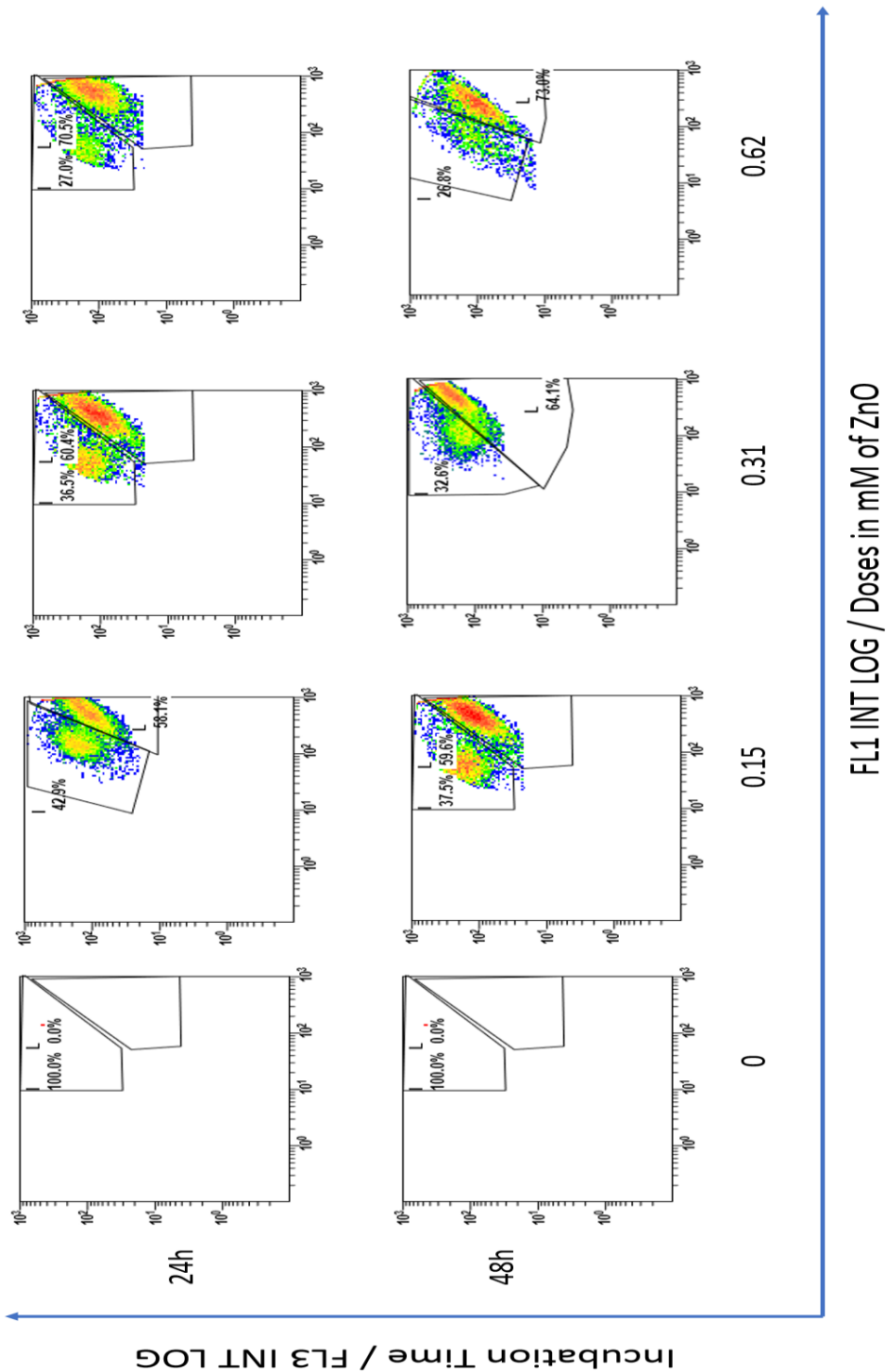
FL1 sorts green fluorescence emitted by JC1 present in low concentration (low membrane potential/depolarization). FL3 sorts red fluorescence emitted by J-aggregates present at high concentration of JC1 (high membrane potential).

Figure 8B- Degree of mitochondrial membrane depolarization for ZrO_2 treatment
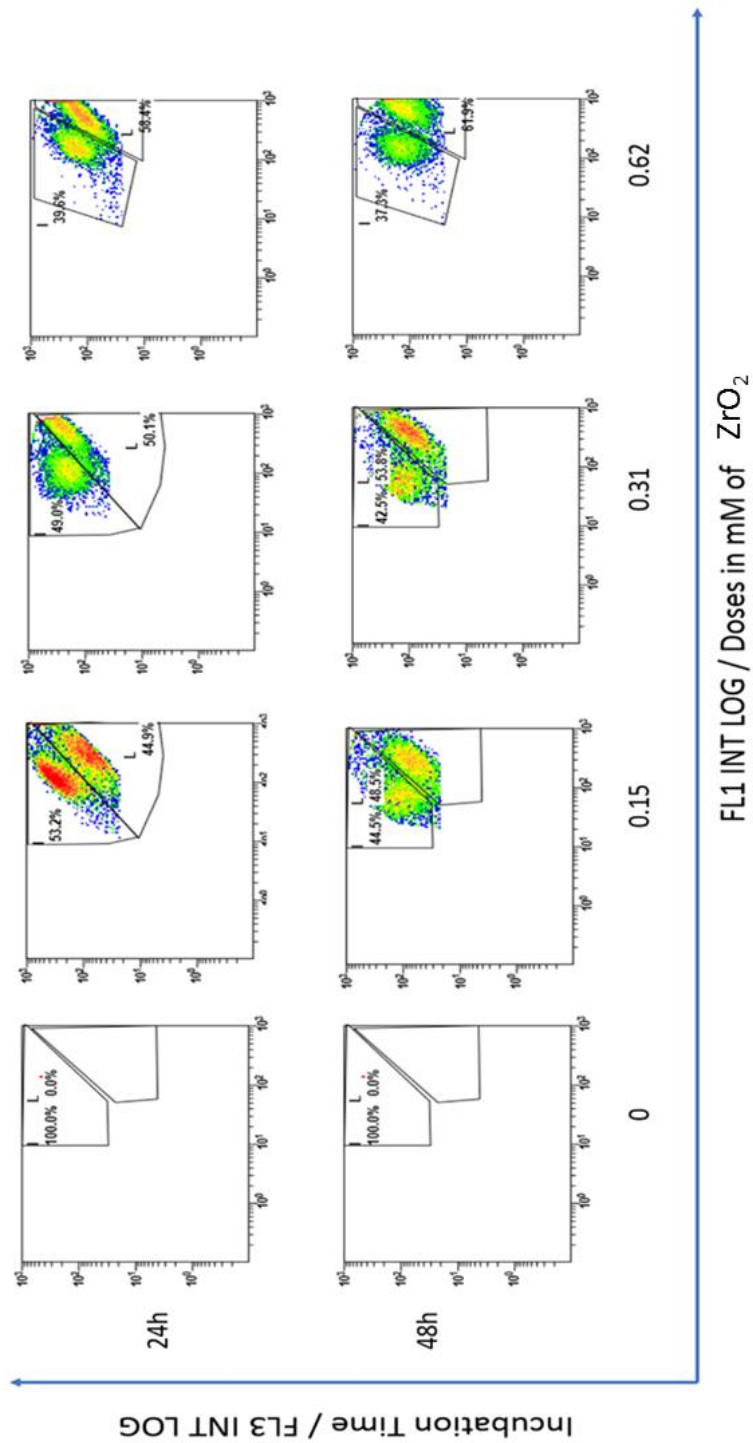
FL3 sorts red fluorescence emitted by J-aggregates present at high concentration of JC1 (high membrane potential).

Figure 8C- Degree of mitochondrial membrane depolarization for TiO₂ treatment
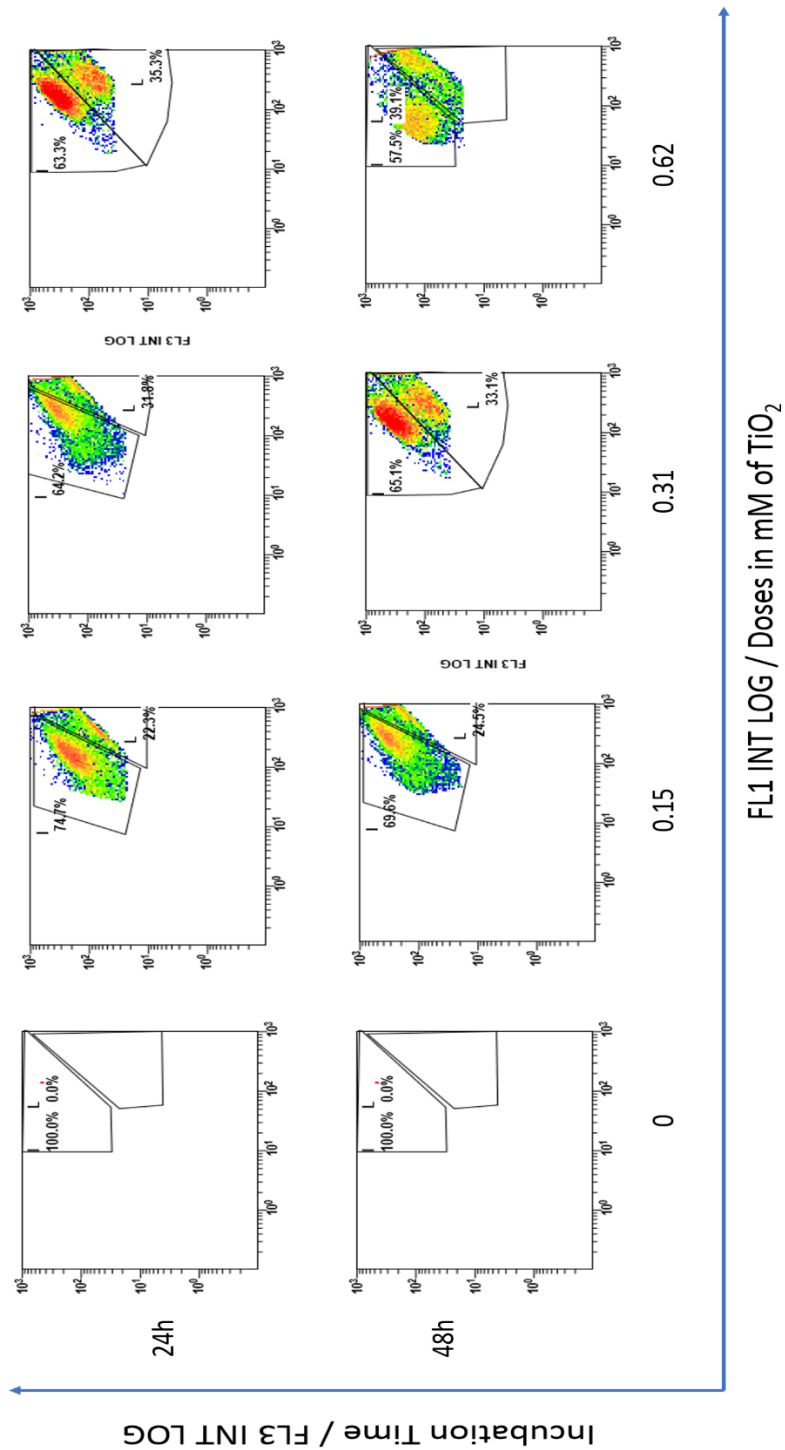
FL1 sorts green fluorescence emitted by JC1 present in low concentration (low membrane potential/depolarization). FL3 sorts red fluorescence emitted by J-aggregates present at high concentration of JC1 (high membrane potential).

4.4 DISCUSSION

LC3B expression indicate greater autophagic processes with exposure to TiO_2 as compared to ZrO_2 or ZnO. HMGB1 documents higher expression with TiO_2 treatment against ZnO. Propidium Iodide binding is pronounced in the order of $ZnO>ZrO_2>TiO_2$. Cyclin B1 results and cell cycle analysis using propidium iodide, suggest G_2/M arrest and apoptosis, in the order of $ZnO>ZrO_2>TiO_2$. Further cell cycle analysis also indicates, G_0/G_1 arrest and increased quiescent duration associated with autophagy in the order of $TiO_2>ZrO_2>ZnO$.

Hsp70 and p-eIF2α were previously shown to increase in expression with decreasing trend in toxicity. With further evaluation on ZrO_2, a candidate whose toxicity follows $TiO_2<ZrO_2<ZnO$, the expression of Hsp70 and p-eIF2α stays true in the order of $TiO_2>ZrO_2>ZnO$. JC1 data further substantiates membrane depolarization associated with necrosis and apoptosis in the order of $ZnO>ZrO_2>TiO_2$. These findings corroborate the contribution to toxic tolerance by Hsp70 and p-eIF2α and remark a necrotic or apoptotic death following exposure to higher lethal metal oxide nanoparticles.

I have thus, concluded that cell death owing to metal oxide nanoparticles switches as a function of cellular stress. During the phase of exposure, nanoparticles adsorb protein along the nasal septa, respiratory trachea and alveolus. Essentially protein adsorbed on to nanoparticle, called protein corona dictates cell-nanoparticle interactions (Saptarshi *et al*., 2013).

The interaction induces toxicity by many mechanisms. ROS generation aiding oxidative stress is a significant factor in metal oxide nanoparticle induced toxicity on A549 cells. Although oxidant generating tendencies are poor indicators of actual cell death (Sun *et al*., 2012). Presence of atmospheric irradiation by Sun such as UV is also a significant

contributor (Numano *et al*., 2014). Common suspects like variation in shape, size, surface properties, chemical nature, electronic properties and crystallinity of the nanoparticles also modulate the level of toxicity (Altunbek *et al*., 2014, Hsiao *et al*., 2011). Additionally, how experiments are conducted to investigate the level of toxicity also contribute to the level of toxic stress detected. Toxicity levels are usually more pronounced when conducted in serum free media as compared to *in vitro* experiments conducted with 5% or 10 % serum (Hsiao *et al*., 2013).

It is noted that, contribution to toxicity by metal ions were consistently insignificant to the overall level of toxic stress generated (Chapter 3). This discourages metal ion release as a significant player in metal oxide nanoparticle induced toxicity on A549 cells.

Internalization of metal oxide nanoparticles was universally documented with all metal oxide nanoparticle exposure on A549. Though the degree of uptake and dissolution thereafter, both might play a role in dictating the level of toxicity (Vandebriel *et al*., 2012).

The fourth well studied mechanism of nanoparticle toxicity as per Djurisic *et al*., 2015 is accumulation of nanoparticle on membrane surface, on which there aren't any reports thus far, so whether this mechanism contributes in realizing the stress is unclear. Though we have shown in chapter 3, that protein corona, a contributor to nanoparticle adhesion and accumulation to cell surface does follow the trend in toxicity.

There are also reports of autophagic death, apoptosis and necrosis owing to metal oxide nanoparticle exposure across the spectrum of less lethal to most lethal nanoparticles. I would like to highlight that cellular stress is highly multi factorial process. Dose and time dependent results vary as per experimental designs, though the trend of toxicity remains constant (Loret *et al*., 2016). I hypothesize that probably cell fate in terms of which signaling cascades get activated and ultimately the type of cell death maybe a function of the total level

of cellular stress. If a cell is capable of repair, it is likely to start the process of autophagy to clear out the damaged biomolecules. If the nanoparticle being exposed to is lethal; the cell is likely switched fate to death and the preferred mode of death is apoptosis to avoid inflammation among neighboring cells. Both autophagy and apoptosis are ATP dependent modes of cell death (Glick *et al*., 2010). If the level of insult is too overwhelming that the cell is unable to program apoptosis, it is likely to die of necrosis, which involves rapid swelling and bursting of cellular contents. I believe, a switching of cell death occurs depending on the intensity of total cellular stress. Most unforgiving insults result in necrosis, insults unable to be repaired end in apoptosis, while prolonged state of stress on a cell in the repair cascade, is likely to route through autophagy. Cytokine release is indicative of some level of proliferation and repair initiation. Cells secreting cytokine, may well be in the repair phase, thereby likely to die of autophagy if the insult continues unchecked.

The following model is built to enumerate mechanism of metal oxide nanoparticle induced stress in A549 cells based on literature survey and results furnished in this thesis.

4.4.1. ROS in low doses induces mitogenic processes.

Metal oxide nanoparticles (MeOx) undergo fenton reaction and other processes of dissolution in releasing ions including metal cation (Me+), hydroxyl radical (OH`), hydroxyl anion (OH-), oxygen (O2) and superoxide anion (O2-) (Manke *et al*., 2013). Metal oxide nanoparticles encounter cells along with protein corona (Cedervall *et al*., 2007). MeOx-corona can be internalized in A549 cells through many routes depending upon the properties of MeOx and the corona. These paths include; Phagocytosis, Pinocytosis, Caveolin mediated endocytosis, Clathrin mediated endocytosis, other endocytic pathways and diffusion (Yameen *et al*., 2014) as shown in **Figure 9**. The endocytosed particle may further undergo dissolution

owing to pH drop and proteolytic action, once the endosome fuses with the lysosome.
Naturally occurring radicals generated during mitochondrial respiration along with radicals released extracellularly are converted by NADPH dependent oxidases (Nox) to H_2O_2. Further, activation of GPCR and Receptor tyrosine kinase (RTK) in the presence of a growth factor also aids Nox conversion to H_2O_2 through PI3K and Rac activation. Extracellular H_2O_2 generated is passively translocated through aquaporins into the cytoplasm. Further GPCR and RTK signaling triggers SRC (non-receptor protein tyrosine kinase) mediated inactivation of peroxidases such as Prx1. This inhibits conversion of H_2O_2 into water. The net result is an increased and localized presence of H_2O_2 which then crosses a redox threshold and inactivates tyrosine phosphatases such as Protein tyrosine phosphatase (PTP) by oxidation. The oxidized enzyme is unable to dephosphorylate active proteins involved in several signaling cascades such as MAP kinase pathway, switching ON processes such as cellular growth, proliferation, differentiation and transformation (Finkel 2011). Thus, small dose of ROS, that could still be converted into H_2O_2 triggers cell growth and repair mechanisms.

Figure 9 – Low Intensity of ROS leads to mitogenic response.
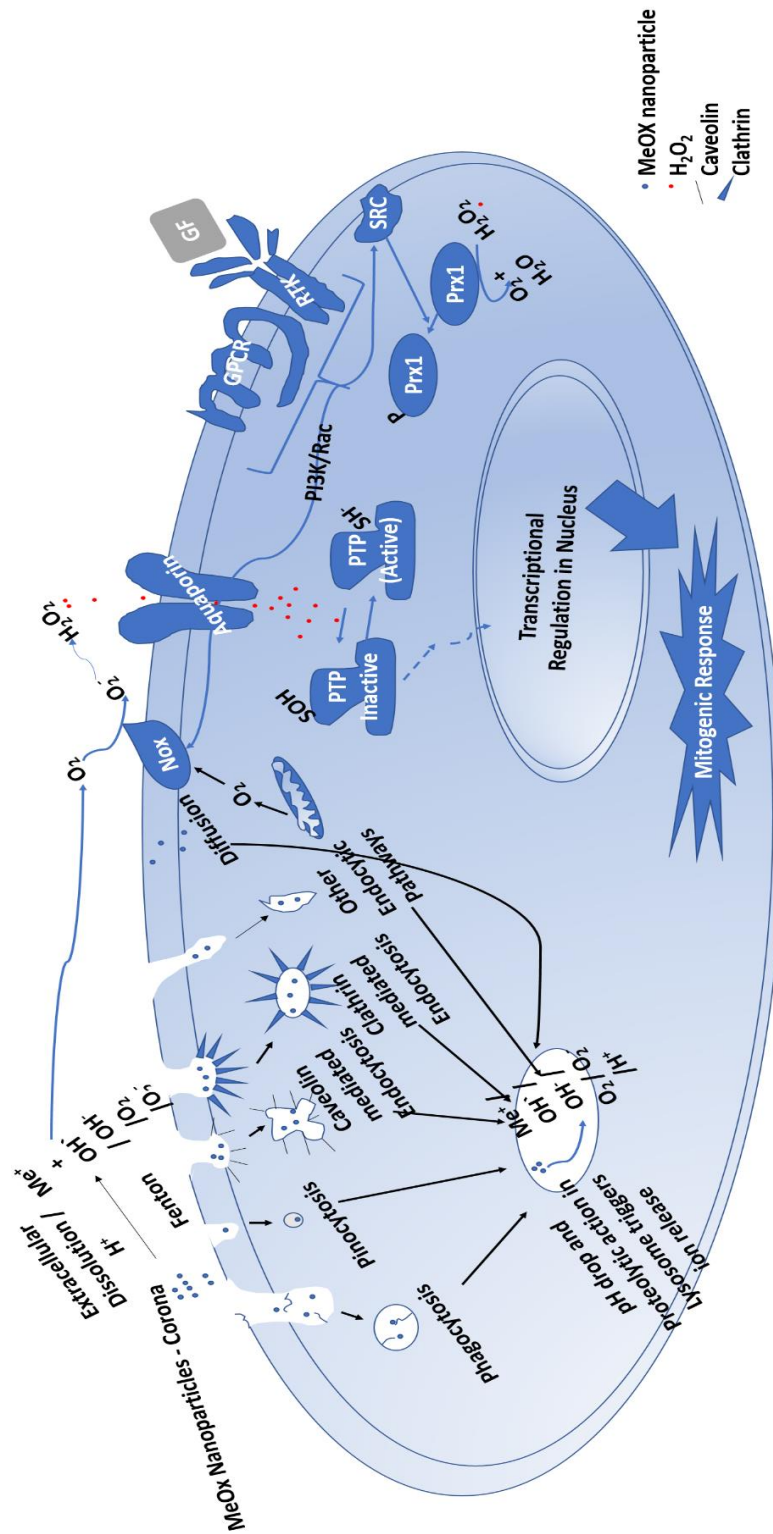
Adopted from Martin and Sarkar, 2017

4.4.2. ROS in higher doses arrests mitogenic processes

Stern *et al*. 2012 describes how auto phagosomes can directly form from lysosomes as ROS increases. Alternatively, an increased accumulation of ions within the lysosome, delivers the necessary osmotic shock needed for intracellular outburst of the lysosome releasing its ionic contents (**Figure 10**). Not only the presence of highly reactive free radicals cause damage to cellular biomolecules by random binding and disruption of activity, but the redox balance is upset. This prolongs the reduced form of tyrosine phosphatase. There by, inhibiting most growth and mitogenic processes. Depending on the level of uncontrolled ROS, cell cycle arrest or even cell death could follow, if random biomolecule damage continues unchecked in a state of inhibited growth.

Figure 10 – ROS at high intensity causes oxidative stress.
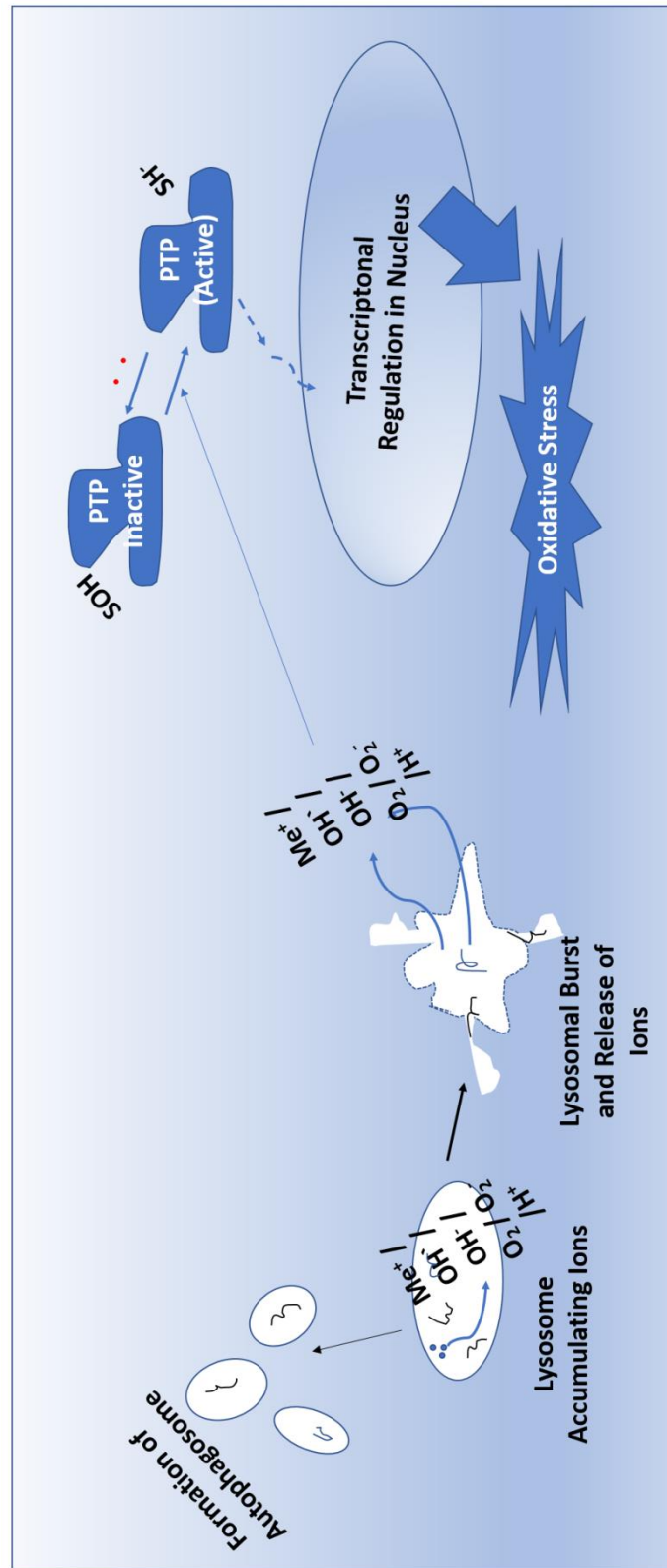
Adopted from Martin and Sarkar, 2017

4.4.3. Switching of Cell death among cells treated with metal oxide nanoparticles.

Through our literature survey, we see all three widely studies modes of cell death; Autophagy, Apoptosis and Necrosis reported along the trend of less lethal to more lethal metal oxide nanoparticles. Our model predicts the total intensity of oxidative stress could essentially stimulate the fate of cell (**Figure 11**). At low stress exposure for low incubation time, autophagy ensues. PI3-III-ATG6 mediated membrane nucleation is followed by formation of autophagosome in a depleted Bax/Bak environment. Reduced levels of ATG6 and ATG5 aid repair, while increased levels of ATG6 and ATG5 in an increasing Bcl2/XL environment leads to autophagic death. Encountered stress deemed beyond repair, routes in programmed cell death through apoptosis. This is characterized by an increasing Bax/Bak system and caspase activation, resulting in the formation of apoptotic bodies. Sudden and unmanageable stress, especially in conditions of ATP depletion ends in necrosis. Bursting of cellular contents and consequent tissue inflammation is seen (Saraste 1999, Tsujimoto 1997, Nicotera and Melino, 2004).

Figure 11- Switching of Cell death as a function of total stress.
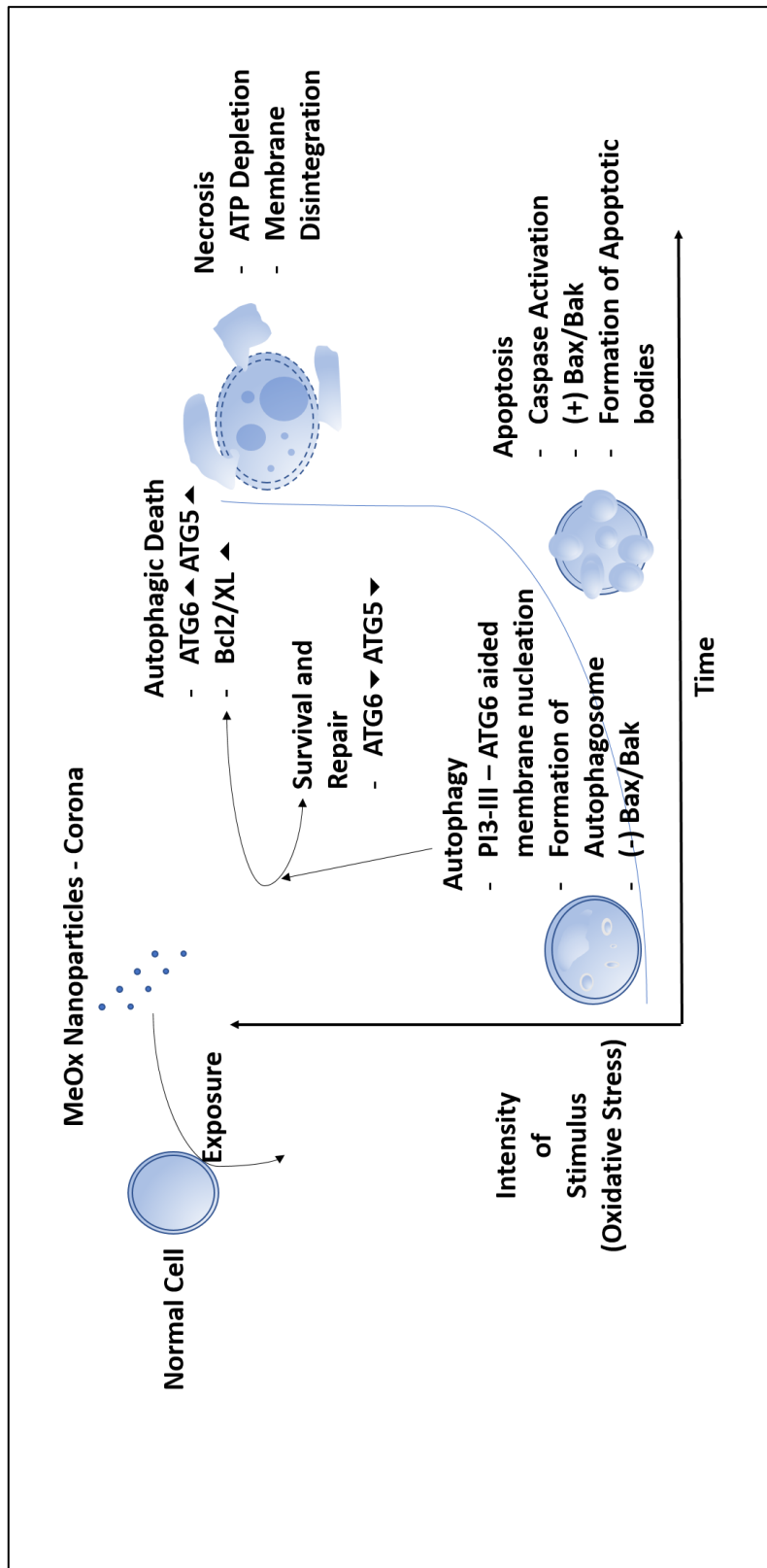
Adopted from Martin and Sarkar, 2017

5.0 CONCLUSION

ZnO nanoparticles are more lethal to A549 cells than TiO_2 nanoparticles. Increased incubation with TiO_2 NPs improves viability. This may be because of a number reasons as discovered in this research study. These include upregulation of HMGB1 that might aid in repair. Increased cdc42 expression, leads to filopodial spikes on the cell surface that eases migration. This may make the cells capable of surviving higher doses of exposure, by enabling them to escape the zone of stress. These reports are novel and have immense potential to be developed further in stress revival strategies against metal oxide nanoparticle toxicity.

TiO_2 treatment is also characterized by epithelial to mesenchymal transition not documented in ZnO exposure. This allied with increased duration of expression in Hsp70 and p-eIF2α helps alleviate metal oxide nanoparticle induced stress. As these mechanisms increase tolerance to dose by 20 times. These are also novel findings and add to the growing discoveries in this study which could be developed into therapeutic solutions.

The world is increasing in its use of nanoparticle ingenuity and human exposure thus becomes inevitable. Metal oxide nanoparticles are the largest class of commercially utilized nanoparticles. Aerosolized matter particularly adds to the raising pollution exacerbating associated pulmonary dysfunctions. These facts place a huge need for development of approaches to alleviate stress induced by metal oxide nanoparticles. As such, my research that now includes several molecular solutions to stress revival may well prove a pivotal point in medical history in the field of nanotoxicology. Therefore, it has scope for future development, both in the risk assessment of existing nanoparticles and in the design of safe manufactured nanoparticles.

One major concern in the field of nanotoxicology has also been the amalgamation of existing knowledge into tools to predict degrees of toxicity over the thousands of new molecules that are being tested for commercial applications every year. Expensive wet lab testing and large screening is not only time consuming but also impractical. This thus necessitates the development of tools to predict accurately the toxicity of nanoparticles based on physico-chemical parameters that do not require much experimentation to establish. The mechanism by which nanoparticles induce the stress is also crucial information, as only the understanding of nanoparticle-cell interaction provides scope to discover new drug targets and to develop future solutions to lung dysfunction. In this effort, many quantitative structure activity relationship-based models have been developed. But there is none to accurately establish a mechanism of toxicity in pulmonary alveolar type II cells or to predict the level of stress articulated on these cells by different metal oxide nanoparticles.

For the first time, through this study, accurate descriptors of toxicity for metal oxide nanoparticle induced stress in alveolar type II cells have been discovered. These are reactive oxygen species and protein corona. They also shed much needed light into the mechanism of this toxicity. Through this study, it is evident that metal ion release characterized by bond dissociation energy is a poor contributor to this process. Generation of ROS, internalization of ions and possibly accumulation on cell surface are significant contributors.

A quantitative structure activity relationship-based model is built to predict accurately the toxicity based on generation of total ROS and protein corona. The trend in toxicity for some of the commonly used nanoparticles are as follows:

$CuO > Cr_2O_3 > ZnO > NiO > ZrO_2 > Co_3O_4 > Al_2O_3 > TiO_2 > Fe_2O_3$
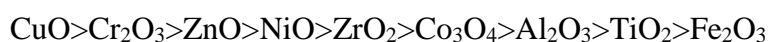
The nature of cell death is rather dynamic. It is a function of total cellular stress as proved by multitudes of experiments carried in the last chapter. The most unforgiving insults

route in necrosis, followed by apoptosis and autophagy. This substantiates the observation of many researchers (literature survey), that document all these modes of cell death across the spectrum of less lethal to highly lethal nanoparticles.

Cells prefer repair through release of cytokines and formation of autophagosomes to engulf damage molecules and trigger the synthesis of new ones. This is especially true for cells experiencing a low intensity of ROS (reactive oxygen species). They experience mitogenic responses by a cascade of signaling.

When the intensity of ROS increases by a certain threshold, reduction of protein tyrosine phosphatases occurs in the cytoplasm by a redox shift. This activates the protein tyrosine phosphatases resulting in transcriptional regulation that ultimately overwhelms the cell by oxidative stress. With further increase in dose and incubation time, the cells where autophagosomes have already formed, route through autophagic cell death.

When cells experience lethal ROS initially without a chance to mount any mitogenic responses, activation of p53 may lead to cell cycle arrest or even cell death by apoptosis. Dying and dead cells are present as apoptotic bodies and are recognized by macrophages and internalized to avoid inflammatory responses in the surrounding tissue environment.

It is also possible, that the cells experience enormous amount of stress probably due to exponential internalization of nanoparticles and maybe ion release and therefore may never have time to mount an ATP dependent defense to secure the neighboring cells. A huge disruption of osmotic balance particularly may result in bursting of the cellular contents leading to necrosis and inflammation in the surrounding tissue.

Thus, metal oxide nanoparticle exposure to alveolar type II cells may route in any of the types of cell death if the stress overwhelms the cellular defenses. Though the type of cell

death depends on how quickly and how much in intensity of stress the cell is exposed to. In other words, dose and time of exposure to toxic agent ultimately dictate the fate of the cell.

6.0 FUTURE SCOPE

- SDS PAGE and mass spectrometry analysis of the differential protein expression between less lethal and highly lethal nanoparticle candidates.

- Investigation of G_0/G_1 associated autophagy in metal oxide nanoparticle induced stress.

- Testing a wider range of characterized nanoparticles for accuracy of toxicity prediction using the QSAR tool built.

- Devising therapeutic strategies to alleviate metal oxide nanoparticle induced stress by targeting the lead molecules discovered in this study.

- Expanding studies to actual industrial samples such as effluents and discharges and building future models for combination of metal oxide nanoparticles.

PUBLICATIONS

1. **_Ansie Martin_** and Angshuman Sarkar (2018). Epithelial to Mesenchymal transition, eIF2α phosphorylation and Hsp70 expression enable greater tolerance in A549 cells to TiO$_2$ over ZnO nanoparticles. Manuscript number- SREP-18-02014C. (**Accepted** at **Scientific Reports, Nature**)

2. (As corresponding and first author) Book Chapter; **_Ansie Martin_** and Angshuman Sarkar (2018). '_In-vitro_ toxicity testing of nanomaterials, Cell Culture', ISBN 978-953-51-6440-1, **Intech Open, UK**.

3. (As co-corresponding author and first author) Detailed Review- **_Martin, A_**., & Sarkar, A. (2017). Overview on biological implications of metal oxide nanoparticle exposure to human alveolar A549 cell line. **Nanotoxicology**, 11(6), 713-724.

4. (As Co-First Author) Santimano, M. C., **_Martin, A_**., Kowshik, M., & Sarkar, A. (2013). Zinc oxide nanoparticles cause morphological changes in human A549 cell line through alteration in the expression pattern of small GTPases at mRNA level. **J. Bionanosci**, 7, 300-306.

5. (As corresponding author and first author) Mini Review- **_Ansie Martin_** and Angshuman Sarkar, Cellular migration as a Stress Relieving Strategy to Nanotoxicology, 2018, **Int J cell Sci & Mol Biol**. 2018; 4(2): 555634. DOI: 10.19080/IJCSMB.2018.04.555634002.

6. Joshi, R. S., Mukherjee, D. D., Chakrabarty, S., **_Martin, A_**., Jadhao, M., Chakrabarti, G., ... & Ghosh, S. K. (2018). Unveiling the Potential of Unfused Bichromophoric Naphthalimide to Induce Cytotoxicity by Binding to Tubulin: Breaks Monotony of Naphthalimides as Conventional Intercalators. **The Journal of Physical Chemistry B**.

7. Pathan, J., *Martin, A*., Chowdhury, R., Chakrabarty, D., & Sarkar, A. (2015). Russell's viper venom affects regulation of small GTPases and causes nuclear damage. **Toxicon**, 108, 216-225.

PUBLICATIONS UNDER REVIEW

1. 'QSAR model to predict metal oxide nanoparticle induced toxicity in A549 cells.

CONFERENCES ATTENDED

1. (Poster) Ansie Martin and Angshuman Sarkar. QSAR modelling to predict metal nano-oxide toxicity in A549 cells and common patterns that reveal the biological mechanism of the ensuing stress. "The Dynamic Cell: The Molecules and Networks to Form and Function", ICCB 2018, CCMB, 27th – 31st January 2018.

2. (Oral Talk) Ansie Martin, Subhenjit Hazra, Narendra Nath Ghosh and Angshuman Sarkar, Development of a QSAR model to predict metal nano-oxide toxicity on alveolar cells; "Trends in Cell and Molecular Biology", BITS Goa, 19th-21st December 2015

3. (Poster) Ansie Martin, Subhenjit Hazra, Narendra Nath Ghosh and Angshuman Sarkar, Evaluation of metal nano-oxide stress in building a Nano QSAR model for prediction of toxicity; "23rd International Conference on Current Trends in Computational Chemistry (CCTCC)", JSU, Jackson, Mississippi, USA

4. (Poster) Ansie Martin and Angshuman Sarkar, Cellular Responses of *in vitro* cultured Human A549 Cells to Exposure of Metal Oxide Nanoparticles; XXXVIII AICBC, "Cellular Responses to Drugs", CDRI, Lucknow, P057, Pg. 74, December 10-12, 2014.

5. (Poster) Ansie Martin and Angshuman Sarkar, ZnO and TiO_2 Nanoparticles induces cytotoxicity and morphological changes in A549 cells; Third Euro Indian International conference on Nano-medicine and Tissue Engineering, Kottayam, Kerala, India, P8, pg. 98, 9-11th August 2013.

6. (Poster) C. Santimano, A. Martin, M. Kowshik and A. Sarkar., Zinc oxide nanoparticles causes' morphological alteration in human A549 cells cultured *in vitro*. XXXVI AICBC & SARGI, BARC, Mumbai, pg.167, 17th -19th Oct 2012.

REFERENCES

1. Abudayyak, M., Gurkaynak, T.A. and Özhan, G., 2017. In vitro toxicological assessment of cobalt ferrite nanoparticles in several mammalian cell types. Biological trace element research, 175(2), pp.458-465.

2. Ahamed, M., Siddiqui, M.A., Akhtar, M.J., Ahmad, I., Pant, A.B. and Alhadlaq, H.A., 2010. Genotoxic potential of copper oxide nanoparticles in human lung epithelial cells. Biochemical and biophysical research communications, 396(2), pp.578-583.

3. Ahlinder, L., Ekstrand-Hammarström, B., Geladi, P. and Österlund, L., 2013. Large uptake of titania and iron oxide nanoparticles in the nucleus of lung epithelial cells as measured by Raman imaging and multivariate classification. Biophysical journal, 105(2), pp.310-319.

4. Akhtar, M.J., Ahamed, M., Kumar, S., Khan, M.M., Ahmad, J. and Alrokayan, S.A., 2012. Zinc oxide nanoparticles selectively induce apoptosis in human cancer cells through reactive oxygen species. International journal of nanomedicine, 7, p.845.

5. Akhtar, M.J., Kumar, S., Alhadlaq, H.A., Alrokayan, S.A., Abu-Salah, K.M. and Ahamed, M., 2016. Dose-dependent genotoxicity of copper oxide nanoparticles stimulated by reactive oxygen species in human lung epithelial cells. Toxicology and industrial health, 32(5), pp.809-821.

6. Alinovi, R., Goldoni, M., Pinelli, S., Ravanetti, F., Galetti, M., Pelosi, G., De Palma, G., Apostoli, P., Cacchioli, A., Mutti, A. and Mozzoni, P., 2017. Titanium dioxide aggregating nanoparticles induce autophagy and under-expression of microRNA 21 and 30a in A549 cell line: A comparative study with cobalt (II, III) oxide nanoparticles. Toxicology in Vitro, 42, pp.76-85.

7. Altunbek, M., Baysal, A. and Çulha, M., 2014. Influence of surface properties of zinc oxide nanoparticles on their cytotoxicity. Colloids and Surfaces B: Biointerfaces, 121, pp.106-113.

8. Andl, C. D., Mizushima, T., Oyama, K., Bowser, M., Nakagawa, H., & Rustgi, A. K. (2004). EGFR-induced cell migration is mediated predominantly by the JAK-STAT pathway in primary esophageal keratinocytes. American Journal of Physiology-Gastrointestinal and Liver Physiology, 287(6), G1227-G1237.

9. Andujar, P., Simon-Deckers, A., Galateau-Sallé, F., Fayard, B., Beaune, G., Clin, B., ... & Boczkowski, J. (2014). Role of metal oxide nanoparticles in histopathological changes observed in the lung of welders. Particle and fibre toxicology, 11(1), 23.

10. Anoopkumar-Dukie, S., Carey, J. B., Conere, T., O'sullivan, E., Van Pelt, F. N., & Allshire, A. (2005). Resazurin assay of radiation response in cultured cells. The British journal of radiology, 78(934), 945-947.

11. Armand, L., Biola-Clier, M., Bobyk, L., Collin-Faure, V., Diemer, H., Strub, J.M., Cianferani, S., Van Dorsselaer, A., Herlin-Boime, N., Rabilloud, T. and Carriere, M., 2016. Molecular responses of alveolar epithelial A549 cells to chronic exposure to titanium dioxide nanoparticles: A proteomic view. Journal of proteomics, 134, pp.163-173.

12. Baird, T. (2014). *Novel targets of eiF2 kinases determine cell fate during the integrated stress response* (Doctoral dissertation).

13. Bend, J.R., Serabjit-Singh, C.J. and Philpot, R.M., 1985. The pulmonary uptake, accumulation, and metabolism of xenobiotics. Annual review of pharmacology and toxicology, 25(1), pp.97-125.

14. Berg, J.M., Romoser, A.A., Figueroa, D.E., West, C.S. and Sayes, C.M., 2013. Comparative cytological responses of lung epithelial and pleural mesothelial cells following in vitro exposure to nanoscale SiO 2. Toxicology in Vitro, 27(1), pp.24-33.

15. Berndt, J. D., Clay, M. R., Langenberg, T., & Halloran, M. C. (2008). Rho-kinase and myosin II affect dynamic neural crest cell behaviors during epithelial to mesenchymal transition in vivo. Developmental biology, 324(2), 236-244.

16. Bhabra, G., Sood, A., Fisher, B., Cartwright, L., Saunders, M., Evans, W.H., Surprenant, A., Lopez-Castejon, G., Mann, S., Davis, S.A. and Hails, L.A., 2009. Nanoparticles can cause DNA damage across a cellular barrier. Nature nanotechnology, 4(12), pp.876-883.

17. Bihari, P., Vippola, M., Schultes, S., Praetner, M., Khandoga, A. G., Reichel, C. A., ... & Krombach, F. (2008). Optimized dispersion of nanoparticles for biological in vitro and in vivo studies. Particle and fibre toxicology, 5(1), 14.

18. Biola-Clier, M., Beal, D., Caillat, S., Libert, S., Armand, L., Herlin-Boime, N., Sauvaigo, S., Douki, T. and Carrière, M., 2016. Comparison of the DNA damage response in BEAS-2B and A549 cells exposed to titanium dioxide nanoparticles. Mutagenesis, 32(1), pp.161-172.

19. Bishop, A.L. and Alan, H.A.L.L., 2000. Rho GTPases and their effector proteins. Biochemical Journal, 348(2), pp.241-255.

20. Bombin, S., LeFebvre, M., Sherwood, J., Xu, Y., Bao, Y. and Ramonell, K.M., 2015. Developmental and reproductive effects of iron oxide nanoparticles in Arabidopsis thaliana. International journal of molecular sciences, 16(10), pp.24174-24193.

21. Boyles, M.S., Ranninger, C., Reischl, R., Rurik, M., Tessadri, R., Kohlbacher, O., Duschl, A. and Huber, C.G., 2016. Copper oxide nanoparticle toxicity profiling using untargeted metabolomics. Particle and fibre toxicology, 13(1), p.49.

22. Braig, M., Lee, S., Loddenkemper, C., Rudolph, C., Peters, A.H., Schlegelberger, B., Stein, H., Dörken, B., Jenuwein, T. and Schmitt, C.A., 2005. Oncogene-induced senescence as an initial barrier in lymphoma development. Nature, 436(7051), pp.660-665.

23. Branzei, D. and Foiani, M., 2008. Regulation of DNA repair throughout the cell cycle. Nature reviews. Molecular cell biology, 9(4), p.297.

24. Castranova, V., Rabovsky, J., Tucker, J.H. and Miles, P.R., 1988. The alveolar type II epithelial cell: a multifunctional pneumocyte. Toxicology and applied pharmacology, 93(3), pp.472-483.

25. Castranova, V., Wright, J.R., Colby, H.D. and Miles, P.R., 1983. Ascorbate uptake by isolated rat alveolar macrophages and type II cells. Journal of Applied Physiology, 54(1), pp.208-214.

26. Cedervall, T., Lynch, I., Lindman, S., Berggård, T., Thulin, E., Nilsson, H., Dawson, K.A. and Linse, S., 2007. Understanding the nanoparticle–protein corona using methods to quantify exchange rates and affinities of proteins for nanoparticles. Proceedings of the National Academy of Sciences, 104(7), pp.2050-2055.

27. Chatterjee, N. and Walker, G.C., 2017. Mechanisms of DNA damage, repair, and mutagenesis. Environmental and Molecular Mutagenesis.

28. Chen, J. J., & London, I. M. (1995). Regulation of protein synthesis by heme-regulated eIF-2α kinase. Trends in biochemical sciences, 20(3), 105-108.

29. Clements, J.A., 1957. Surface tension of lung extracts. Proceedings of the Society for Experimental Biology and Medicine, 95(1), pp.170-172.

30. Clements, J.A., Brown, E.S. and Johnson, R.P., 1958. Pulmonary surface tension and the mucus lining of the lungs: some theoretical considerations. Journal of applied physiology, 12(2), pp.262-268.

31. Clogston, J. D., & Patri, A. K. (2009). Measuring Zeta Potential of Nanoparticles. *Nanotechnology Characterization Laboratory*.

32. Cocco, R. E., & Ucker, D. S. (2001). Distinct modes of macrophage recognition for apoptotic and necrotic cells are not specified exclusively by phosphatidylserine exposure. *Molecular biology of the cell*, *12*(4), 919-930.

33. Collado, M., Gil, J., Efeyan, A., Guerra, C., Schuhmacher, A.J., Barradas, M., Benguría, A., Zaballos, A., Flores, J.M., Barbacid, M. and Beach, D., 2005. Tumour biology: senescence in premalignant tumours. Nature, 436(7051), pp.642-642.

34. Corradi, S., Gonzalez, L., Thomassen, L.C., Bilaničová, D., Birkedal, R.K., Pojana, G., Marcomini, A., Jensen, K.A., Leyns, L. and Kirsch-Volders, M., 2012. Influence of serum on in situ proliferation and genotoxicity in A549 human lung cells exposed to nanomaterials. Mutation Research/Genetic Toxicology and Environmental Mutagenesis, 745(1), pp.21-27.

35. Crapo, J.D., Young, S.L., Fram, E.K., Pinkerton, K.E., Barry, B.E. and Crapo, R.O., 1983. Morphometric Characteristics of Cells in the Alveolar Region of Mammalian Lungs 1–3. American Review of Respiratory Disease, 128(2P2), pp.S42-S46.

36. Cronholm, P., Karlsson, H.L., Hedberg, J., Lowe, T.A., Winnberg, L., Elihn, K., Wallinder, I.O. and Möller, L., 2013. Intracellular uptake and toxicity of Ag and CuO nanoparticles: a comparison between nanoparticles and their corresponding metal ions. Small, 9(7), pp.970-982.

37. Crowley, L. C., Scott, A. P., Marfell, B. J., Boughaba, J. A., Chojnowski, G., & Waterhouse, N. J. (2016). Measuring cell death by propidium iodide uptake and flow cytometry. *Cold Spring Harbor Protocols*, *2016*(7), pdb-prot087163.

38. DeFea, K. A. (2013). Arrestins in actin reorganization and cell migration. In Progress in molecular biology and translational science (Vol. 118, pp. 205-222). Academic Press.

39. DiPaola, R. S. (2002). To arrest or not to G2-M Cell-cycle arrest: commentary re: AK Tyagi et al., Silibinin strongly synergizes human prostate carcinoma DU145 cells to doxorubicin-induced growth inhibition, G2-M arrest, and apoptosis. Clin. Cancer Res., 8: 3512–3519, 2002. *Clinical cancer research*, *8*(11), 3311-3314.

40. Djurišić, A.B., Leung, Y.H., Ng, A., Xu, X.Y., Lee, P.K. and Degger, N., 2015. Toxicity of metal oxide nanoparticles: mechanisms, characterization, and avoiding experimental artefacts. Small, 11(1), pp.26-44.

41. Dubey, A., Goswami, M., Yadav, K., & Chaudhary, D. (2015). Oxidative stress and nano-toxicity induced by TiO2 and ZnO on WAG cell line. *PLoS One*, *10*(5), e0127493.

42. El Yamani, N., Collins, A.R., Rundén-Pran, E., Fjellsbø, L.M., Shaposhnikov, S., Zienolddiny, S. and Dusinska, M., 2016. In vitro genotoxicity testing of four reference metal nanomaterials, titanium dioxide, zinc oxide, cerium oxide and silver: towards reliable hazard assessment. Mutagenesis, 32(1), pp.117-126.

43. El-Battawy, K. A. (2008). Resazurin reduction test as a tool for assessment of rabbit semen quality. In 9th World Rabbit Congress, Verona (Italy) (pp. 349-52).

44. Elmore, S., 2007. Apoptosis: a review of programmed cell death. Toxicologic pathology, 35(4), pp.495-516.

45. Elsabahy, M. and Wooley, K.L., 2013. Cytokines as biomarkers of nanoparticle immunotoxicity. Chemical Society Reviews, 42(12), pp.5552-5576.

46. Elsaesser, A. and Howard, C.V., 2012. Toxicology of nanoparticles. Advanced drug delivery reviews, 64(2), pp.129-137.

47. El-Said, K.S., Ali, E.M., Kanehira, K. and Taniguchi, A., 2014. Molecular mechanism of DNA damage induced by titanium dioxide nanoparticles in toll-like receptor 3 or 4 expressing human hepatocarcinoma cell lines. Journal of nanobiotechnology, 12(1), p.48.

48. Etienne-Manneville, S., & Hall, A. (2002). Rho GTPases in cell biology. Nature, 420(6916), 629.

49. Evans, C. G., Chang, L., & Gestwicki, J. E. (2010). Heat shock protein 70 (hsp70) as an emerging drug target. *Journal of medicinal chemistry*, *53*(12), 4585-4602.

50. Falcaro, P., Ricco, R., Yazdi, A., Imaz, I., Furukawa, S., Maspoch, D., Ameloot, R., Evans, J.D. and Doonan, C.J., 2016. Application of metal and metal oxide nanoparticles@ MOFs. Coordination Chemistry Reviews, 307, pp.237-254.

51. Fede, C., Millino, C., Pacchioni, B., Celegato, B., Compagnin, C., Martini, P., Selvestrel, F., Mancin, F., Celotti, L., Lanfranchi, G. and Mognato, M., 2014. Altered Gene Transcription in Human Cells Treated with Ludox® Silica Nanoparticles. International journal of environmental research and public health, 11(9), pp.8867-8890.

52. Feng, N., Ma, X., Wei, X., Zhang, J., Dong, A., Jin, M., ... & Guo, X. (2014). Common variants in PERK, JNK, BIP and XBP1 genes are associated with the risk of prediabetes or diabetes-related phenotypes in a Chinese population. *Chinese medical journal*, *127*(13), 2438-2444.

53. Finkel, T., 2011. Signal transduction by reactive oxygen species. The Journal of cell biology, 194(1), pp.7-15.

54. Fleischer, C. C., & Payne, C. K. (2014). Nanoparticle–cell interactions: molecular structure of the protein corona and cellular outcomes. *Accounts of chemical research*, *47*(8), 2651-2659.

55. Foster, K.A., Oster, C.G., Mayer, M.M., Avery, M.L. and Audus, K.L., 1998. Characterization of the A549 cell line as a type II pulmonary epithelial cell model for drug metabolism. Experimental cell research, 243(2), pp.359-366.

56. Frijns, E., Verstraelen, S., Stoehr, L.C., Van Laer, J., Jacobs, A., Peters, J., Tirez, K., Boyles, M.S.P., Geppert, M., Madl, P. and Nelissen, I., 2017. A Novel Exposure System Termed NAVETTA for In Vitro Laminar Flow Electrodeposition of Nanoaerosol and Evaluation of Immune Effects in Human Lung Reporter Cells. Environmental Science & Technology, 51(9), pp.5259-5269.

57. Fukui, H., Horie, M., Endoh, S., Kato, H., Fujita, K., Nishio, K., Komaba, L.K., Maru, J., Miyauhi, A., Nakamura, A. and Kinugasa, S., 2012. Association of zinc ion release and oxidative stress induced by intratracheal instillation of ZnO nanoparticles to rat lung. Chemico-biological interactions, 198(1), pp.29-37.

58. Fulda, S., Gorman, A. M., Hori, O., & Samali, A. (2010). Cellular stress responses: cell survival and cell death. *International journal of cell biology*, *2010*.

59. Gajewicz, A., Cronin, M. T., Rasulev, B., Leszczynski, J., & Puzyn, T. (2014). Novel approach for efficient predictions properties of large pool of nanomaterials based on limited set of species: nano-read-across. Nanotechnology, 26(1), 015701.

60. Gajewicz, A., Schaeublin, N., Rasulev, B., Hussain, S., Leszczynska, D., Puzyn, T., & Leszczynski, J. (2015). Towards understanding mechanisms governing cytotoxicity of metal oxides nanoparticles: Hints from nano-QSAR studies. *Nanotoxicology*, *9*(3), 313-325.

61. Gavard, J., & Gutkind, J. S. (2008). Protein kinase C-related kinase and ROCK are required for thrombin-induced endothelial cell permeability downstream from Gα12/13 and Gα11/q. Journal of Biological Chemistry, 283(44), 29888-29896.

62. Giard, D.J., Aaronson, S.A., Todaro, G.J., Arnstein, P., Kersey, J.H., Dosik, H. and Parks, W.P., 1973. In vitro cultivation of human tumors: establishment of cell lines derived from a series of solid tumors. Journal of the National Cancer Institute, 51(5), pp.1417-1423.

63. Gillette, J.R., Davis, D.C. and Sasame, H.A., 1972. Cytochrome P-450 and its role in drug metabolism. Annual review of pharmacology, 12(1), pp.57-84.

64. Glick, D., Barth, S. and Macleod, K.F., 2010. Autophagy: cellular and molecular mechanisms. The Journal of pathology, 221(1), pp.3-12.

65. Gonzalez, L., De Santis Puzzonia, M., Ricci, R., Aureli, F., Guarguaglini, G., Cubadda, F., Leyns, L., Cundari, E. and Kirsch-Volders, M., 2015. Amorphous silica nanoparticles alter microtubule dynamics and cell migration. Nanotoxicology, 9(6), pp.729-736.

66. Gregersen, N., & Bross, P. (2010). Protein misfolding and cellular stress: an overview. In *Protein Misfolding and Cellular Stress in Disease and Aging* (pp. 3-23). Humana Press, Totowa, NJ.

67. Grover, J., Patel, P. N., Carnelio, S., Chandrashekar, C., Shergill, A. K., & Solomon, M. C. (2015). Comparison of glycogen content, basement membrane integrity and mitotic index in stages of oral dysplasia progression to cancer and in oral lichen-lichenoid reactions: a histochemical study. *Journal of Advanced Medical and Dental Sciences Research*, *3*(3), 3.

68. Guadagnini, R., Moreau, K., Hussain, S., Marano, F. and Boland, S., 2015. Toxicity evaluation of engineered nanoparticles for medical applications using pulmonary epithelial cells. Nanotoxicology, 9(sup1), pp.25-32.

69. Guo, F., Velu, C. S., Grimes, H. L., & Zheng, Y. (2009). Rho GTPase Cdc42 is essential for B-lymphocyte development and activation. Blood, 114(14), 2909-2916.

70. Guo, S., Shen, X., Yan, G., Ma, D., Bai, X., Li, S., & Jiang, Y. (2009). A MAP kinase dependent feedback mechanism controls Rho1 GTPase and actin distribution in yeast. *PLoS One*, *4*(6), e6089.

71. Haies, D.M., Gil, J. and Weibel, E.R., 1981. Morphometric Study of Rat Lung Cells: I. Numerical and Dimensional Characteristics of Parenchymal Cell Population 1, 2. American Review of Respiratory Disease, 123(5), pp.533-541.

72. Hall, A. (1998). Rho GTPases and the actin cytoskeleton. *Science*, *279*(5350), 509-514.

73. Hanagata, N., Zhuang, F., Connolly, S., Li, J., Ogawa, N. and Xu, M., 2011. Molecular responses of human lung epithelial cells to the toxicity of copper oxide nanoparticles inferred from whole genome expression analysis. ACS nano, 5(12), pp.9326-9338.

74. Hanot-Roy, M., Tubeuf, E., Guilbert, A., Bado-Nilles, A., Vigneron, P., Trouiller, B., Braun, A. and Lacroix, G., 2016. Oxidative stress pathways involved in cytotoxicity and genotoxicity of titanium dioxide (TiO$_2$) nanoparticles on cells constitutive of alveolo-capillary barrier in vitro. Toxicology in vitro, 33, pp.125-135.

75. Hao, X., Wang, H., Liu, W., Liu, S., Peng, Z., Sun, Y., Zhao, J., Jiang, Q. and Liu, H., 2016. Enhanced expression levels of aquaporin-1 and aquaporin-4 in A549 cells exposed to silicon dioxide. Molecular Medicine Reports, 14(3), pp.2101-2106.

76. Hayden, M. S., & Ghosh, S. (2008). Shared principles in NF-κB signaling. *Cell*, *132*(3), 344-362.

77. Hazra, S., Ghosh, B. K., Patra, M. K., Jani, R. K., Vadera, S. R., & Ghosh, N. N. (2015). A novel 'one-pot' synthetic method for preparation of (Ni0. 65Zn0. 35Fe2O4) x–(BaFe12O19) 1− x nanocomposites and study of their microwave absorption and magnetic properties. Powder Technology, 279, 10-17.

78. Hazra, S., Patra, M. K., Vadera, S. R., & Ghosh, N. N. (2012). A Novel But Simple "One-Pot" Synthetic Route for Preparation of (NiFe2O4) x–(BaFe12O19) 1− x Composites. Journal of the American Ceramic Society, 95(1), 60-63.

79. Hedberg, Y., Gustafsson, J., Karlsson, H.L., Möller, L. and Wallinder, I.O., 2010. Bioaccessibility, bioavailability and toxicity of commercially relevant iron-and chromium-based particles: in vitro studies with an inhalation perspective. Particle and fibre toxicology, 7(1), p.23.

80. Heim, J., Felder, E., Tahir, M.N., Kaltbeitzel, A., Heinrich, U.R., Brochhausen, C., Mailänder, V., Tremel, W. and Brieger, J., 2015. Genotoxic effects of zinc oxide nanoparticles. Nanoscale, 7(19), pp.8931-8938.

81. Hinnebusch, A. G. (1994). Translational control of GCN4: an in vivo barometer of initiation-factor activity. Trends in biochemical sciences, 19(10), 409-414.

82. Ho, C. Y., Powell, R. W., & Liley, P. E. (1972). Thermal conductivity of the elements. Journal of Physical and Chemical Reference Data, 1(2), 279-421.

83. Horie, M., Fujita, K., Kato, H., Endoh, S., Nishio, K., Komaba, L. K., ... & Niki, E. (2012). Association of the physical and chemical properties and the cytotoxicity of metal oxide nanoparticles: metal ion release, adsorption ability and specific surface area. *Metallomics*, *4*(4), 350-360.

84. Horie, M., Kato, H., Fujita, K., Endoh, S. and Iwahashi, H., 2011. In vitro evaluation of cellular response induced by manufactured nanoparticles. Chemical research in toxicology, 25(3), pp.605-619.

85. Horie, M., Nishio, K., Fujita, K., Endoh, S., Miyauchi, A., Saito, Y., Iwahashi, H., Yamamoto, K., Murayama, H., Nakano, H. and Nanashima, N., 2009. Protein adsorption of ultrafine metal oxide and its influence on cytotoxicity toward cultured cells. Chemical research in toxicology, 22(3), pp.543-553.

86. Horie, M., Nishio, K., Kato, H., Endoh, S., Fujita, K., Nakamura, A., Hagihara, Y., Yoshida, Y. and Iwahashi, H., 2014. Evaluation of cellular effects of silicon dioxide nanoparticles. Toxicology mechanisms and methods, 24(3), pp.196-203.

87. Hsiao, I.L. and Huang, Y.J., 2011. Effects of various physicochemical characteristics on the toxicities of ZnO and TiO_2 nanoparticles toward human lung epithelial cells. Science of the Total Environment, 409(7), pp.1219-1228.

88. Hsiao, I.L. and Huang, Y.J., 2013. Effects of serum on cytotoxicity of nano-and micro-sized ZnO particles. Journal of Nanoparticle Research, 15(9), p.1829.

89. Huang, F., Khvorova, A., Marshall, W., & Sorkin, A. (2004). Analysis of clathrin-mediated endocytosis of epidermal growth factor receptor by RNA interference. Journal of Biological Chemistry, 279(16), 16657-16661.

90. Huang, X. and Darzynkiewicz, Z., 2006. Cytometric assessment of histone H2AX phosphorylation: a reporter of DNA damage. DNA Repair Protocols: Mammalian Systems, pp.73-80.

91. Huang, Y.W., Wu, C.H. and Aronstam, R.S., 2010. Toxicity of transition metal oxide nanoparticles: recent insights from in vitro studies. Materials, 3(10), pp.4842-4859.

92. Ito, A., Shinkai, M., Honda, H. and Kobayashi, T., 2005. Medical application of functionalized magnetic nanoparticles. Journal of bioscience and bioengineering, 100(1), pp.1-11.

93. Ivask, A., Titma, T., Visnapuu, M., Vija, H., Kakinen, A., Sihtmae, M., ... & Shimmo, R. (2015). Toxicity of 11 metal oxide nanoparticles to three mammalian cell types in vitro. Current topics in medicinal chemistry, 15(18), 1914-1929.

94. JC Seagrave, K.J., 2000. Multiple modes of responses to air pollution particulate materials in A549 alveolar type II cells. Inhalation toxicology, 12(sup4), pp.247-260.

95. Johar, D., 2017. Cytoskeletal remodeling and regulation of cell fate in the hypertensive neonatal pulmonary artery in response to stress. Journal of Cellular Physiology.

96. Jones, T. and Mansfield, T.A., 1982. Studies on dry matter partitioning and distribution of 14C-labelled assimilates in plants of Phleum pratense exposed to SO2 pollution. Environmental Pollution Series A, Ecological and Biological, 28(3), pp.199-207.

97. Kalaiarasi, A., Sankar, R., Anusha, C., Saravanan, K., Aarthy, K., Karthic, S., ... & Ravikumar, V. (2018). Copper oxide nanoparticles induce anticancer activity in A549 lung cancer cells by inhibition of histone deacetylase. *Biotechnology letters*, *40*(2), 249-256.

98. Kalluri, R., & Weinberg, R. A. (2009). The basics of epithelial-mesenchymal transition. The Journal of clinical investigation, 119(6), 1420-1428.

99. Kansara, K., Patel, P., Shah, D., Shukla, R.K., Singh, S., Kumar, A. and Dhawan, A., 2015. TiO_2 nanoparticles induce DNA double strand breaks and cell cycle arrest in human alveolar cells. Environmental and molecular mutagenesis, 56(2), pp.204-217.

100.   Kar, S., Gajewicz, A., Puzyn, T., Roy, K., & Leszczynski, J. (2014). Periodic table-based descriptors to encode cytotoxicity profile of metal oxide nanoparticles: A mechanistic QSTR approach. Ecotoxicology and environmental safety, 107, 162-169.

101.   Karlsson, H.L., Cronholm, P., Gustafsson, J. and Moller, L., 2008. Copper oxide nanoparticles are highly toxic: a comparison between metal oxide nanoparticles and carbon nanotubes. Chemical research in toxicology, 21(9), pp.1726-1732.

102.   Karlsson, H.L., Gustafsson, J., Cronholm, P. and Möller, L., 2009. Size-dependent toxicity of metal oxide particles—a comparison between nano-and micrometer size. Toxicology letters, 188(2), pp.112-118.

103.   Kaszuba, M., Corbett, J., Watson, F. M., & Jones, A. (2010). High-concentration zeta potential measurements using light-scattering techniques. Philosophical Transactions of the Royal Society of London A: Mathematical, Physical and Engineering Sciences, 368(1927), 4439-4451.

104.   Kedersha, N., & Anderson, P. (2002). Stress granules: sites of mRNA triage that regulate mRNA stability and translatability.

105.   Kepp, O., Semeraro, M., Bravo-San Pedro, J. M., Bloy, N., Buqué, A., Huang, X., ... & Galluzzi, L. (2015, August). eIF2α phosphorylation as a biomarker of immunogenic cell death. In Seminars in cancer biology (Vol. 33, pp. 86-92). Academic Press.

106.   Kermanizadeh, A., Jantzen, K., Ward, M.B., Durhuus, J.A., Juel Rasmussen, L., Loft, S. and Møller, P., 2017. Nanomaterial induced cell death in pulmonary and hepatic cells following exposure to three different metallic materials: the role of autophagy and apoptosis. Nanotoxicology, (just-accepted), pp.1-49.

107.   Kim, E., Jeon, W.B., Kim, S. and Lee, S.K., 2014. Decrease of reactive oxygen species-related biomarkers in the tissue-mimic 3D spheroid culture of human lung cells exposed to zinc oxide nanoparticles. Journal of nanoscience and nanotechnology, 14(5), pp.3356-3365.

108.   Kim, I.S., Baek, M. and Choi, S.J., 2010. Comparative cytotoxicity of Al_2O_3, CeO_2, TiO_2 and ZnO nanoparticles to human lung cells. Journal of nanoscience and nanotechnology, 10(5), pp.3453-3458.

109.   Kimball, S. R. (1999). Eukaryotic initiation factor eIF2. The international journal of biochemistry & cell biology, 31(1), 25-29.

110.   Kozma, R., Ahmed, S., Best, A., & Lim, L. (1996). The GTPase-activating protein n-chimaerin cooperates with Rac1 and Cdc42Hs to induce the formation of lamellipodia and filopodia. Molecular and Cellular Biology, 16(9), 5069-5080.

111.   Kubinyi, H. (Ed.). (1993). 3D QSAR in drug design: volume 1: theory methods and applications (Vol. 1). Springer Science & Business Media.

112.   Kuku, G. and Culha, M., 2017. Investigating the Origins of Toxic Response in TiO_2 Nanoparticle-Treated Cells. Nanomaterials, 7(4), p.83.

113.   Kumar, A., Dailey, L.A., Swedrowska, M., Siow, R., Mann, G.E., Vizcay-Barrena, G., Arno, M., Mudway, I.S. and Forbes, B., 2016. Quantifying the magnitude of the oxygen artefact inherent in culturing airway cells under atmospheric oxygen versus physiological levels. FEBS letters, 590(2), pp.258-269.

114.   Laemmli, U. K. (1970). Cleavage of structural proteins during the assembly of the head of bacteriophage T4. nature, 227(5259), 680.

115.   Lai, X., Wei, Y., Zhao, H., Chen, S., Bu, X., Lu, F., Qu, D., Yao, L., Zheng, J. and Zhang, J., 2015. The effect of Fe2O3 and ZnO nanoparticles on cytotoxicity and glucose metabolism in lung epithelial cells. Journal of Applied Toxicology, 35(6), pp.651-664.

116.   Lawrence, T. (2009). The nuclear factor NF-κB pathway in inflammation. *Cold Spring Harbor perspectives in biology*, a001651.

117.   Lenz, A.G., Karg, E., Brendel, E., Hinze-Heyn, H., Maier, K.L., Eickelberg, O., Stoeger, T. and Schmid, O., 2013. Inflammatory and oxidative stress responses of an alveolar epithelial cell line to airborne zinc oxide nanoparticles at the air-liquid interface: a comparison with conventional, submerged cell-culture conditions. BioMed research international, 2013.

118.   Leszczynski, J. (2010). Bionanoscience: nano meets bio at the interface. Nature nanotechnology, 5(9), 633.

119.   Li, X., Zhang, C., Bian, Q., Gao, N., Zhang, X., Meng, Q., Wu, S., Wang, S., Xia, Y. and Chen, R., 2016. Integrative functional transcriptomic analyses implicate specific molecular pathways in pulmonary toxicity from exposure to aluminum oxide nanoparticles. Nanotoxicology, 10(7), pp.957-969.

120.   Lieber, M., Todaro, G., Smith, B., Szakal, A. and Nelson-Rees, W., 1976. A continuous tumor-cell line from a human lung carcinoma with properties of type II alveolar epithelial cells. International Journal of Cancer, 17(1), pp.62-70.

121.   Lim, C.H., 2015. Toxicity of two different sized lanthanum oxides in cultured cells and Sprague-Dawley rats. Toxicological research, 31(2), p.181.

122.   Lloyd, K.A., 2013. A scientific review: mechanisms of valproate-mediated teratogenesis. Bioscience Horizons, 6(10.1093).

123.   Loret, T., Peyret, E., Dubreuil, M., Aguerre-Chariol, O., Bressot, C., le Bihan, O., Amodeo, T., Trouiller, B., Braun, A., Egles, C. and Lacroix, G., 2016. Air-liquid interface exposure to aerosols of poorly soluble nanomaterials induces different biological activation levels compared to exposure to suspensions. Particle and Fibre Toxicology, 13(1), p.58.

124.   Lu, G. W., & Gao, P. (2010). Emulsions and microemulsions for topical and transdermal drug delivery. In *Handbook of Non-Invasive Drug Delivery Systems* (pp. 59-94).

125.   Lu, S., Zhang, W., Zhang, R., Liu, P., Wang, Q., Shang, Y., Wu, M., Donaldson, K. and Wang, Q., 2015. Comparison of cellular toxicity caused by ambient ultrafine particles and engineered metal oxide nanoparticles. Particle and fibre toxicology, 12(1), p.5.

126.   Ly, J. D., Grubb, D. R., & Lawen, A. (2003). The mitochondrial membrane potential ($\Delta\psi$m) in apoptosis; an update. *Apoptosis*, *8*(2), 115-128.

127.   Manke, A., Wang, L. and Rojanasakul, Y., 2013. Mechanisms of nanoparticle-induced oxidative stress and toxicity. BioMed research international, 2013.

128.   Martin, A., & Sarkar, A. (2017). Overview on biological implications of metal oxide nanoparticle exposure to human alveolar A549 cell line. *Nanotoxicology*, *11*(6), 713-724.

129.   Martindale, J.L. and Holbrook, N.J., 2002. Cellular response to oxidative stress: signaling for suicide and survival. Journal of cellular physiology, 192(1), pp.1-15.

130.   Maser, E., Schulz, M., Sauer, U.G., Wiemann, M., Ma-Hock, L., Wohlleben, W., Hartwig, A. and Landsiedel, R., 2015. In vitro and in vivo genotoxicity investigations of differently sized amorphous SiO 2 nanomaterials. Mutation Research/Genetic Toxicology and Environmental Mutagenesis, 794, pp.57-74.

131.   Mason, R.J., Williams, M.C., Widdicombe, J.H., Sanders, M.J., Misfeldt, D.S. and Berry, L.C., 1982. Transepithelial transport by pulmonary alveolar type II cells in primary culture. Proceedings of the National Academy of Sciences, 79(19), pp.6033-6037.

132.   Mayer, M. P., & Bukau, B. (2005). Hsp70 chaperones: cellular functions and molecular mechanism. *Cellular and molecular life sciences*, *62*(6), 670.

133.   McClain, D. A., & Edelman, G. M. (1980). Density-dependent stimulation and inhibition of cell growth by agents that disrupt microtubules. Proceedings of the National Academy of Sciences, 77(5), 2748-2752.

134.   McMahon, M., Samali, A., & Chevet, E. (2017). Regulation of the unfolded protein response by noncoding RNA. American Journal of Physiology-Cell Physiology, 313(3), C243-C254.

135.   Medina-Reyes, E.I., Déciga-Alcaraz, A., Freyre-Fonseca, V., Delgado-Buenrostro, N.L., Flores-Flores, J.O., Gutiérrez-López, G.F., Sánchez-Pérez, Y., García-Cuéllar, C.M., Pedraza-Chaverri, J. and Chirino, Y.I., 2015. Titanium dioxide nanoparticles induce an adaptive inflammatory response and invasion and proliferation of lung epithelial cells in chorioallantoic membrane. Environmental research, 136, pp.424-434.

136.   Meurs, E., Chong, K., Galabru, J., Thomas, N. S. B., Kerr, I. M., Williams, B. R., & Hovanessian, A. G. (1990). Molecular cloning and characterization of the human double-stranded RNA-activated protein kinase induced by interferon. *Cell*, *62*(2), 379-390.

137.   Meyer, G., Czompa, A., Reboul, C., Csepanyi, E., Czegledi, A., Bak, I., ... & Lekli, I. (2013). The cellular autophagy markers Beclin-1 and LC3B-II are increased during reperfusion in fibrillated mouse hearts. *Current pharmaceutical design*, *19*(39), 6912-6918.

138.   Minchin, R.F. and Boyd, M.R., 1983. Localization of metabolic activation and deactivation systems in the lung: significance to the pulmonary toxicity of xenobiotics. Annual review of pharmacology and toxicology, 23(1), pp.217-238.

139.   Mohamed, B.M., Verma, N.K., Prina-Mello, A., Williams, Y., Davies, A.M., Bakos, G., Tormey, L., Edwards, C., Hanrahan, J., Salvati, A. and Lynch, I., 2011. Activation of stress-related signaling pathway in human cells upon SiO 2 nanoparticles exposure as an early indicator of cytotoxicity. Journal of nanobiotechnology, 9(1), p.29.

140.   Monteiller, C., Tran, L., MacNee, W., Faux, S., Jones, A., Miller, B. and Donaldson, K., 2007. The pro-inflammatory effects of low-toxicity low-solubility particles, nanoparticles and fine particles, on epithelial cells in vitro: the role of surface area. Occupational and environmental medicine, 64(9), pp.609-615.

141.   Morgan, M. J., & Liu, Z. G. (2011). Crosstalk of reactive oxygen species and NF-κB signaling. *Cell research*, *21*(1), 103.

142.   Moschini, E., Gualtieri, M., Colombo, M., Fascio, U., Camatini, M. and Mantecca, P., 2013. The modality of cell–particle interactions drives the toxicity of nanosized CuO and TiO_2 in human alveolar epithelial cells. Toxicology letters, 222(2), pp.102-116.

143.   Narayana, K., D Souza, U. J., & Rao, K. S. (2002). Effect of ribavirin on epididymal sperm count in rat. Indian journal of physiology and pharmacology, 46(1), 97-101.

144.   Nardone, L.L. and Andrews, S.B., 1979. Cell line A549 as a model of the type II pneumocyte: Phospholipid biosynthesis from native and organometallic precursors. Biochimica et Biophysica Acta (BBA)-Lipids and Lipid Metabolism, 573(2), pp.276-295.

145.   Nel, A., Xia, T., Mädler, L. and Li, N., 2006. Toxic potential of materials at the nanolevel. science, 311(5761), pp.622-627.

146.   Nicotera, P. and Melino, G., 2004. Regulation of the apoptosis–necrosis switch. Oncogene, 23(16), pp.2757-2765.

147.   Nobes, C. D., & Hall, A. (1995). Rho, rac, and cdc42 GTPases regulate the assembly of multimolecular focal complexes associated with actin stress fibers, lamellipodia, and filopodia. *Cell*, *81*(1), 53-62.

148.   Numano, T., Xu, J., Futakuchi, M., Fukamachi, K., Alexander, D. B., Furukawa, F., ... & Suzui, M. (2014). Comparative study of toxic effects of anatase and rutile type nanosized titanium dioxide particles in vivo and in vitro. *Asian Pac J Cancer Prev*, *15*(2), 929-935.

149.   Okoturo-Evans, O., Dybowska, A., Valsami-Jones, E., Cupitt, J., Gierula, M., Boobis, A.R. and Edwards, R.J., 2013. Elucidation of toxicity pathways in lung epithelial cells induced by silicon dioxide nanoparticles. PloS one, 8(9), p.e72363.

150.   O'Neill, S.J., Hoehn, S.K., Lesperance, E.S.T.H.E.R. and Klass, D.J., 1984. Functional heterogeneity of isopycnic fractions of rat alveolar macrophages. Infection and immunity, 46(1), pp.282-284.

151.   Orrenius, S., Nicotera, P., & Zhivotovsky, B. (2010). Cell death mechanisms and their implications in toxicology. *Toxicological Sciences*, *119*(1), 3-19.

152.   Panariti, A., Miserocchi, G. and Rivolta, I., 2012. The effect of nanoparticle uptake on cellular behavior: disrupting or enabling functions. Nanotechnol Sci Appl, 5, pp.87-100.

153.   Pandey, N., Dhiman, S., Srivastava, T. and Majumder, S., 2016. Transition metal oxide nanoparticles are effective in inhibiting lung cancer cell survival in the hypoxic tumor microenvironment. Chemico-biological interactions, 254, pp.221-230.

154.   Park, S., Lee, Y.K., Jung, M., Kim, K.H., Chung, N., Ahn, E.K., Lim, Y. and Lee, K.H., 2007. Cellular toxicity of various inhalable metal nanoparticles on human alveolar epithelial cells. Inhalation toxicology, 19(sup1), pp.59-65.

155.   Pattle, R.E., 1958. Properties, function, and origin of the alveolar lining layer. Proceedings of the Royal Society of London B: Biological Sciences, 148(931), pp.217-240.

156. Perelman, A., Wachtel, C., Cohen, M., Haupt, S., Shapiro, H., & Tzur, A. (2012). JC-1: alternative excitation wavelengths facilitate mitochondrial membrane potential cytometry. *Cell death & disease*, *3*(11), e430.

157. PETIT, P. X., O'CONNOR, J. E., GRUNWALD, D., & BROWN, S. C. (1990). Analysis of the membrane potential of rat-and mouse-liver mitochondria by flow cytometry and possible applications. *European journal of biochemistry*, *194*(2), 389-397.

158. Petrie, R. J., Doyle, A. D., & Yamada, K. M. (2009). Random versus directionally persistent cell migration. Nature reviews Molecular cell biology, 10(8), 538.

159. Plattner, H., & Verkhratsky, A. (2016). Inseparable tandem: evolution chooses ATP and Ca^{2+} to control life, death and cellular signaling. *Phil. Trans. R. Soc. B*, *371*(1700), 20150419.

160. Puzyn, T., Rasulev, B., Gajewicz, A., Hu, X., Dasari, T. P., Michalkova, A., ... & Leszczynski, J. (2011). Using nano-QSAR to predict the cytotoxicity of metal oxide nanoparticles. Nature nanotechnology, 6(3), 175.

161. Qin, X., Zhang, J., Wang, B., Xu, G. and Zou, Z., 2017. LAMP-2 mediates oxidative stress-dependent cell death in Zn 2+-treated lung epithelium cells. Biochemical and Biophysical Research Communications, 488(1), pp.177-181.

162. Rabilloud, T., Valette, C., & Lawrence, J. J. (1994). Sample application by in-gel rehydration improves the resolution of two-dimensional electrophoresis with immobilized pH gradients in the first dimension. Electrophoresis, 15(1), 1552-1558.

163. Ramos, A.P., Cruz, M.A., Tovani, C.B. and Ciancaglini, P., 2017. Biomedical applications of nanotechnology. Biophysical reviews, pp.1-11.

164.   Ravindran, G., Chakrabarty, D., & Sarkar, A. (2017). Cell specific stress responses of cadmium-induced cytotoxicity. *Animal Cells and Systems*, *21*(1), 23-30.

165.   Riccardi, C., & Nicoletti, I. (2006). Analysis of apoptosis by propidium iodide staining and flow cytometry. *Nature protocols*, *1*(3), 1458.

166.   Ridley, A. J., & Hall, A. (1992). The small GTP-binding protein rho regulates the assembly of focal adhesions and actin stress fibers in response to growth factors. Cell, 70(3), 389-399.

167.   Ridley, A. J., Paterson, H. F., Johnston, C. L., Diekmann, D., & Hall, A. (1992). The small GTP-binding protein rac regulates growth factor-induced membrane ruffling. Cell, 70(3), 401-410.

168.   Rogaczewska, T. and Matczak, W., 1984. Evaluation of occupational exposure to cadmium based on air analysis of the work area. I. Cadmium oxide level in the air of work areas in a cadmium and nickel cumulator factory. Medycyna pracy, 36(4), pp.273-279.

169.   Royal, I., Lamarche-Vane, N., Lamorte, L., Kaibuchi, K., & Park, M. (2000). Activation of cdc42, rac, PAK, and rho-kinase in response to hepatocyte growth factor differentially regulates epithelial cell colony spreading and dissociation. *Molecular biology of the cell*, *11*(5), 1709-1725.

170.   Sahu, D., Kannan, G.M., Tailang, M. and Vijayaraghavan, R., 2016. In Vitro Cytotoxicity of Nanoparticles: A Comparison between Particle Size and Cell Type. Journal of Nanoscience, 2016.

171.   Sanders, R.L. and Longmore, W.J., 1975. Phosphatidylglycerol in rat lung. II. Comparison of occurrence, composition, and metabolism in surfactant and residual lung fractions. Biochemistry, 14(4), pp.835-840.

172.   Santimano, M.C., Martin, A., Kowshik, M. and Sarkar, A., 2013. Zinc oxide nanoparticles cause morphological changes in human A549 cell line through alteration in the expression pattern of small GTPases at mRNA level. J. Bionanosci, 7, pp.300-306.

173.   Saptarshi, S. R., Duschl, A., & Lopata, A. L. (2013). Interaction of nanoparticles with proteins: relation to bio-reactivity of the nanoparticle. *Journal of nanobiotechnology*, *11*(1), 26.

174.   Saptarshi, S. R., Duschl, A., & Lopata, A. L. (2015). Biological reactivity of zinc oxide nanoparticles with mammalian test systems: an overview. *Nanomedicine*, *10*(13), 2075-2092.

175.   Saraste, A., 1999. Morphologic criteria and detection of apoptosis. Herz, 24(3), pp.189-195.

176.   Sarkar, A., Kulkarni, A., Chattopadhyay, S., Mogare, D., Sharma, K. K., Singh, K., & Pal, J. K. (2005). Lead-induced upregulation of the heme-regulated eukaryotic initiation factor 2α kinase is compromised by hemin in human K562 cells. *Biochimica et Biophysica Acta (BBA)-Gene Structure and Expression*, *1732*(1-3), 15-22.

177.   Sarkar, A., Parikh, N., Hearn, S. A., Fuller, M. T., Tazuke, S. I., & Schulz, C. (2007). Antagonistic roles of Rac and Rho in organizing the germ cell microenvironment. *Current biology*, *17*(14), 1253-1258.

178.   Scaife, R. M. (2004). G2 cell cycle arrest, down-regulation of cyclin B, and induction of mitotic catastrophe by the flavoprotein inhibitor diphenyleneiodonium. *Molecular cancer therapeutics*, *3*(10), 1229-1237.

179. Schaeffer, D., Somarelli, J. A., Hanna, G., Palmer, G. M., & Garcia-Blanco, M. A. (2014). Cellular migration and invasion uncoupled: Increased migration is not an inexorable consequence of EMT. *Molecular and cellular biology*, MCB-00694.

180. Schmedt, C., Green, S. R., Manche, L., Taylor, D. R., Ma, Y., & Mathews, M. B. (1995). Functional characterization of the RNA-binding domain and motif of the double-stranded RNA-dependent protein kinase DAI (PKR). Journal of molecular biology, 249(1), 29-44.

181. Semisch, A., & Hartwig, A. (2014). Copper ions interfere with the reduction of the water-soluble Tetrazolium salt-8. Chemical research in toxicology, 27(2), 169-171.

182. Semisch, A., Ohle, J., Witt, B. and Hartwig, A., 2014. Cytotoxicity and genotoxicity of nano-and microparticulate copper oxide: role of solubility and intracellular bioavailability. Particle and fibre toxicology, 11(1), p.10.

183. Shahbazi, A., Gonzalez-Olmos, R., Kopinke, F. D., Zarabadi-Poor, P., & Georgi, A. (2014). Natural and synthetic zeolites in adsorption/oxidation processes to remove surfactant molecules from water. Separation and Purification Technology, 127, 1-9.

184. Sheikh, M. S., & Fornace Jr, A. J. (2000). Death and decoy receptors and p53-mediated apoptosis. *Leukemia*, *14*(8), 1509.

185. Sidrauski, C., Acosta-Alvear, D., Khoutorsky, A., Vedantham, P., Hearn, B. R., Li, H., ... & Okreglak, V. (2013). Pharmacological brake-release of mRNA translation enhances cognitive memory. Elife, 2.

186. Sigismund, S., Argenzio, E., Tosoni, D., Cavallaro, E., Polo, S., & Di Fiore, P. P. (2008). Clathrin-mediated internalization is essential for sustained EGFR signaling but dispensable for degradation. Developmental cell, 15(2), 209-219.

187.   Singh, S., Shi, T., Duffin, R., Albrecht, C., van Berlo, D., Höhr, D., Fubini, B., Martra, G., Fenoglio, I., Borm, P.J. and Schins, R.P., 2007. Endocytosis, oxidative stress and IL-8 expression in human lung epithelial cells upon treatment with fine and ultrafine TiO_2: role of the specific surface area and of surface methylation of the particles. Toxicology and applied pharmacology, 222(2), pp.141-151.

188.   Sohaebuddin, S.K., Thevenot, P.T., Baker, D., Eaton, J.W. and Tang, L., 2010. Nanomaterial cytotoxicity is composition, size, and cell type dependent. Particle and fibre toxicology, 7(1), p.22.

189.   Soldatow, V. Y., LeCluyse, E. L., Griffith, L. G., & Rusyn, I. (2013). In vitro models for liver toxicity testing. *Toxicology research*, *2*(1), 23-39.

190.   Song, J., Du, L., Feng, Y., Wu, W. and Yan, Z., 2013. Pyroptosis induced by zinc oxide nanoparticles in A549 cells. Wei sheng yan jiu= Journal of hygiene research, 42(2), pp.273-276.

191.   Soto, K.F., Murr, L.E. and Garza, K.M., 2008. Cytotoxic responses and potential respiratory health effects of carbon and carbonaceous nanoparticulates in the Paso del Norte airshed environment. International journal of environmental research and public health, 5(1), pp.12-25.

192.   Stankiewicz, T. R., & Linseman, D. A. (2014). Rho family GTPases: key players in neuronal development, neuronal survival, and neurodegeneration. Frontiers in cellular neuroscience, 8, 314.

193.   Stern, S.T., Adiseshaiah, P.P. and Crist, R.M., 2012. Autophagy and lysosomal dysfunction as emerging mechanisms of nanomaterial toxicity. Particle and fibre toxicology, 9(1), p.20.

194.   Stoccoro, A., Di Bucchianico, S., Coppedè, F., Ponti, J., Uboldi, C., Blosi, M., Delpivo, C., Ortelli, S., Costa, A.L. and Migliore, L., 2017. Multiple endpoints to

evaluate pristine and remediated titanium dioxide nanoparticles genotoxicity in lung epithelial A549 cells. Toxicology Letters.

195. Strauss, B., Harrison, A., Coelho, P. A., Yata, K., Zernicka-Goetz, M., & Pines, J. (2018). Cyclin B1 is essential for mitosis in mouse embryos, and its nuclear export sets the time for mitosis. *J Cell Biol*, *217*(1), 179-193.

196. Stringer, B., Imrich, A. and Kobzik, L., 1996. Lung epithelial cell (A549 cells) interaction with unopsonized environmental particulates: quantitation of particle-specific binding and IL-8 production. Experimental lung research, 22(5), pp.495-508.

197. Strober, W. (2015). Trypan blue exclusion test of cell viability. *Current protocols in immunology*, *111*(1), A3-B.

198. Sun, T., Yan, Y., Zhao, Y., Guo, F. and Jiang, C., 2012. Copper oxide nanoparticles induce autophagic cell death in A549 cells. PLoS One, 7(8), p.e43442.

199. Tam, A. B., Mercado, E. L., Hoffmann, A., & Niwa, M. (2012). ER stress activates NF-κB by integrating functions of basal IKK activity, IRE1 and PERK. *PloS one*, *7*(10), e45078.

200. Tammina, S.K., Mandal, B.K., Ranjan, S. and Dasgupta, N., 2017. Cytotoxicity study of Piper nigrum seed mediated synthesized SnO 2 nanoparticles towards colorectal (HCT116) and lung cancer (A549) cell lines. Journal of Photochemistry and Photobiology B: Biology, 166, pp.158-168.

201. Tang, D., Kang, R., Livesey, K. M., Cheh, C. W., Farkas, A., Loughran, P., ... & Lotze, M. T. (2010). Endogenous HMGB1 regulates autophagy. *The Journal of cell biology*, *190*(5), 881-892.

202. Tang, Y., Wang, F., Jin, C., Liang, H., Zhong, X. and Yang, Y., 2013. Mitochondrial injury induced by nanosized titanium dioxide in A549 cells and rats. Environmental toxicology and pharmacology, 36(1), pp.66-72.

203.   Tanida, I., Ueno, T., & Kominami, E. (2008). LC3 and Autophagy. In *Autophagosome and Phagosome* (pp. 77-88). Humana Press.

204.   Teow, Y., Asharani, P.V., Hande, M.P. and Valiyaveettil, S., 2011. Health impact and safety of engineered nanomaterials. Chemical communications, 47(25), pp.7025-7038.

205.   Thongkam, W., Gerloff, K., van Berlo, D., Albrecht, C. and Schins, R.P., 2016. Oxidant generation, DNA damage and cytotoxicity by a panel of engineered nanomaterials in three different human epithelial cell lines. Mutagenesis, p.gew056.

206.   Titma, T., Shimmo, R., Siigur, J. and Kahru, A., 2016. Toxicity of antimony, copper, cobalt, manganese, titanium and zinc oxide nanoparticles for the alveolar and intestinal epithelial barrier cells in vitro. Cytotechnology, 68(6), pp.2363-2377.

207.   Tomas, A., Futter, C. E., & Eden, E. R. (2014). EGF receptor trafficking: consequences for signaling and cancer. Trends in cell biology, 24(1), 26-34.

208.   Toropov, A. A., & Toropova, A. P. (2015). Quasi-QSAR for mutagenic potential of multi-walled carbon-nanotubes. *Chemosphere*, *124*, 40-46.

209.   Toropov, A. A., & Toropova, A. P. (2015). Quasi-SMILES and nano-QFAR: United model for mutagenicity of fullerene and MWCNT under different conditions. Chemosphere, 139, 18-22.

210.   Toropova, A. P., Toropov, A. A., Rallo, R., Leszczynska, D., & Leszczynski, J. (2015). Optimal descriptor as a translator of eclectic data into prediction of cytotoxicity for metal oxide nanoparticles under different conditions. Ecotoxicology and environmental safety, 112, 39-45.

211.   Treuel, L., Docter, D., Maskos, M., & Stauber, R. H. (2015). Protein corona– from molecular adsorption to physiological complexity. Beilstein journal of nanotechnology, 6, 857.

212. Triboulet, S., Aude-Garcia, C., Armand, L., Collin-Faure, V., Chevallet, M., Diemer, H., ... & Herlin, N. (2015). Comparative proteomic analysis of the molecular responses of mouse macrophages to titanium dioxide and copper oxide nanoparticles unravels some toxic mechanisms for copper oxide nanoparticles in macrophages. PloS one, 10(4), e0124496.

213. Tsuji, J. S., Maynard, A. D., Howard, P. C., James, J. T., Lam, C. W., Warheit, D. B., & Santamaria, A. B. (2005). Research strategies for safety evaluation of nanomaterials, part IV: risk assessment of nanoparticles. *Toxicological sciences*, *89*(1), 42-50.

214. Tsujimoto, Y., 1997. Apoptosis and necrosis: intracellular ATP level as a determinant for cell death modes. Cell Death & Differentiation, 4(6).

215. Tsukahara, T., Matsuda, Y., & Haniu, H. (2014). The role of autophagy as a mechanism of toxicity induced by multi-walled carbon nanotubes in human lung cells. *International journal of molecular sciences*, *16*(1), 40-48.

216. Urner, M., Schlicker, A., Z'graggen, B. R., Stepuk, A., Booy, C., Buehler, K. P., ... & Beck-Schimmer, B. (2014). Inflammatory response of lung macrophages and epithelial cells after exposure to redox active nanoparticles: effect of solubility and antioxidant treatment. *Environmental science & technology*, *48*(23), 13960-13968.

217. Ursini, C.L., Cavallo, D., Fresegna, A.M., Ciervo, A., Maiello, R., Tassone, P., Buresti, G., Casciardi, S. and Iavicoli, S., 2014. Evaluation of cytotoxic, genotoxic and inflammatory response in human alveolar and bronchial epithelial cells exposed to titanium dioxide nanoparticles. Journal of Applied Toxicology, 34(11), pp.1209-1219.

218. Valastyan, J. S., & Lindquist, S. (2014). Mechanisms of protein-folding diseases at a glance. *Disease models & mechanisms*, *7*(1), 9-14.

219.   Vallabhapurapu, S., & Karin, M. (2009). Regulation and function of NF-κB transcription factors in the immune system. *Annual review of immunology*, *27*, 693-733.

220.   Vallyathan, V. and Shi, X., 1997. The role of oxygen free radicals in occupational and environmental lung diseases. Environmental Health Perspectives, 105(Suppl 1), p.165.

221.   Vandebriel, R. J., & De Jong, W. H. (2012). A review of mammalian toxicity of ZnO nanoparticles. *Nanotechnology, science and applications*, *5*, 61.

222.   Vandenabeele, P., Galluzzi, L., Berghe, T.V. and Kroemer, G., 2010. Molecular mechanisms of necroptosis: an ordered cellular explosion. Nature reviews. Molecular cell biology, 11(10), p.700.

223.   Verstraelen, S., Remy, S., Casals, E., De Boever, P., Witters, H., Gatti, A., Puntes, V. and Nelissen, I., 2014. Gene expression profiles reveal distinct immunological responses of cobalt and cerium dioxide nanoparticles in two in vitro lung epithelial cell models. Toxicology letters, 228(3), pp.157-169.

224.   Wallace Jr, W.E., Vallyathan, V., Keane, M.J. and Robinson, V., 1985. In vitro biologic toxicity of native and surface-modified silica and kaolin. Journal of Toxicology and Environmental Health, Part A Current Issues, 16(3-4), pp.415-424.

225.   Wang, M., Wey, S., Zhang, Y., Ye, R., & Lee, A. S. (2009). Role of the unfolded protein response regulator GRP78/BiP in development, cancer, and neurological disorders. *Antioxidants & redox signaling*, *11*(9), 2307-2316.

226.   Wang, Y., Cui, H., Zhou, J., Li, F., Wang, J., Chen, M. and Liu, Q., 2015. Cytotoxicity, DNA damage, and apoptosis induced by titanium dioxide nanoparticles in human non-small cell lung cancer A549 cells. Environmental Science and Pollution Research, 22(7), pp.5519-5530.

227.	Wang, Z., Fan, M., Candas, D., Zhang, T. Q., Qin, L., Eldridge, A., ... & Duru, N. (2014). Cyclin B1/Cdk1 coordinates mitochondrial respiration for cell-cycle G2/M progression. *Developmental cell*, *29*(2), 217-232.

228.	Wang, Z., Li, N., Zhao, J., White, J.C., Qu, P. and Xing, B., 2012. CuO nanoparticle interaction with human epithelial cells: cellular uptake, location, export, and genotoxicity. Chemical research in toxicology, 25(7), pp.1512-1521.

229.	Weichenthal, S., Dufresne, A. and Infante-Rivard, C., 2007. Indoor ultrafine particles and childhood asthma: exploring a potential public health concern. Indoor air, 17(2), pp.81-91.

230.	Welf, E. S., & Haugh, J. M. (2012). Stochastic models of cell protrusion arising from spatiotemporal signaling and adhesion dynamics. In Methods in cell biology (Vol. 110, pp. 223-241). Academic Press.

231.	WILSON, D., ZAQOUT, M., Jeong-Hoon, H.E.O., Eun-Kee, P.A.R.K., Chul-Ho, O.A.K. and Susumu, U.E.N.O., 2012. Nuclear factor-kappa b is not involved in titanium dioxideinduced inflammation. Journal of UOEH, 34(2), pp.183-191.

232.	Winzen, S., Schoettler, S., Baier, G., Rosenauer, C., Mailaender, V., Landfester, K., & Mohr, K. (2015). Complementary analysis of the hard and soft protein corona: sample preparation critically effects corona composition. *Nanoscale*, *7*(7), 2992-3001.

233.	Wörle-Knirsch, J.M., Kern, K., Schleh, C., Adelhelm, C., Feldmann, C. and Krug, H.F., 2007. Nanoparticulate vanadium oxide potentiated vanadium toxicity in human lung cells. Environmental science & technology, 41(1), pp.331-336.

234.	Yameen, B., Choi, W.I., Vilos, C., Swami, A., Shi, J. and Farokhzad, O.C., 2014. Insight into nanoparticle cellular uptake and intracellular targeting. Journal of Controlled Release, 190, pp.485-499.

235.   Yan, Z., Wang, W., Wu, Y., Wang, W., Li, B., Liang, N., & Wu, W. (2017). Zinc oxide nanoparticle-induced atherosclerotic alterations in vitro and in vivo. *International journal of nanomedicine*, *12*, 4433.

236.   Yang, T., Wu, T., Lv, L., Zhang, Z., Liu, D., Xu, J., ... & Wu, G. (2018). Ceria Oxide Nanoparticles an Ideal Carrier Given Little Stress to Cells and Rats. *Journal of Nanoscience and Nanotechnology*, *18*(6), 3865-3869.

237.   Yang, X., Liu, X., Lu, H., Zhang, X., Ma, L., Gao, R. and Zhang, Y., 2012. Real-time investigation of acute toxicity of ZnO nanoparticles on human lung epithelia with hopping probe ion conductance microscopy. Chemical research in toxicology, 25(2), pp.297-304.

238.   Yatsimirskii, K. B. (1994). Electronic structure, energy of hydration, and stability of metal aquo ions. *Theoretical and Experimental Chemistry*, *30*(1), 1-9.

239.   Yatsimirsky, A. K., Yatsimirskaya, N. T., & Kashina, S. B. (1994). Micellar catalysis and product stabilization in hydrazone formation reactions and micellar-modified determination of hydrazine and phenylhydrazine. Analytical Chemistry, 66(14), 2232-2239.

240.   Yin, Z., Zhou, Y.L., Zeng, M.H. and Kurmoo, M., 2015. The concept of mixed organic ligands in metal–organic frameworks: design, tuning and functions. Dalton Transactions, 44(12), pp.5258-5275.

241.   Zhang, J.M. and An, J., 2007. Cytokines, inflammation and pain. International anesthesiology clinics, 45(2), p.27.

242.   Zhang, W., Jiang, P., Chen, Y., Luo, P., Li, G., Zheng, B., Chen, W., Mao, Z. and Gao, C., 2016. Suppressing the cytotoxicity of CuO nanoparticles by uptake of curcumin/BSA particles. Nanoscale, 8(18), pp.9572-9582.

243.   Zhang, X., Huk, D. J., Wang, Q., Lincoln, J., & Zhao, Y. (2014). A microfluidic shear device that accommodates parallel high and low stress zones within the same culturing chamber. *Biomicrofluidics*, *8*(5), 054106.

244.   Zhang, X., Liu, G., Kang, Y., Dong, Z., Qian, Q., & Ma, X. (2013). N-cadherin expression is associated with acquisition of EMT phenotype and with enhanced invasion in erlotinib-resistant lung cancer cell lines. *PloS one*, *8*(3), e57692.

SHORT CV OF THE CANDIDATE

- 2012 to 2018 PhD with Dr. Angshuman Sarkar at the Department of Biological Sciences, Birla Institute of Technology and Science (BITS) – Pilani, K Birla Goa Campus

- 2011- Occasional Post Graduate Research (PGR) in Infection Biology with Dr. Kumar Rajakumar, Department of Infection, Immunity and Inflammation, University of Leicester (UK)

- Competitive Exams Qualified: CSIR-NET Lectureship for 2012 and 2009

GRE General Test - Score: 1340/1600 that includes, verbal-600/800 and Quantitative score-740/800. Analytical Writing score is 4.0/6.0.

TOEFL iBT Score 104/120 and GATE 2010

- 2009-2011 Molecular Biology Project with Dr. Rajan Dighe, Department of Molecular Reproduction, Development and Genetics, Indian Institute of Science (Bangalore, India)

- 2005-2009 Bachelor of Engineering in Biotechnology at Sir M Visvesvaraya Institute of Technology (Bangalore, India), 79% First Class with Distinction, MVIT Gold Medallist, Student Convener for the national symposium on 'Entrepreneurial Opportunities and IPR', part of Abhyuday 2007

- 2005 12th CBSE (Central Board of Secondary Education, India) 88% First Class with Distinction

- 2003 10th CBSE (Central Board of Secondary Education, India) 90% First Class with Distinction, Awarded Certificate of Merit by CBSE for scoring 100/100 in mathematics.

SHORT CV OF THE SUPERVISOR

Angshuman Sarkar, Ph. D., FISCB

Associate Professor, Department of Biological Science

Birla Institute of Technology & Science (BITS) Pilani,

NH17 B Bypass Road, K Birla Goa Campus, Zuarinagar,

Goa 403 726, India

Phone: 0832-2580261(Chamber) and 0832-2580756 (Res).

Email: asarkar12@gmail.com   OR   asarkar@goa.bits-pilani.ac.in

Carrier Highlights:

► Awarded 'Young Investigator' Pilot Project Grant by DBT 'Cancer Biology Mission India' in 2015.

►Awarded "Appreciation Certificate" by Memorial Sloan Sloan-Kettering Cancer Center, USA, in 2008 for outstanding leadership and commitment in the Cancer Research in 2009.

►Discovered live imaging technique of HIV in human dendritic cells and (USA) patented in 2008 with David McDonald.

►Awarded Research Associateship by Department of Cell and Molecular Biology [CWRU, Cleveland, USA in 2007.

►Offered a Fellowship by Cold Spring Harbor Laboratory (CSHL), New York, USA for Post Doctoral Training in 2003.

►Published a paper in one of the high ranking Cell Press Journal about the role of some proteins in maintaining germ line stem cells niche in 2007-2008, this paper was subsequently selected as top 20 cited papers in USA for the year 2007-2008.

►Received CSIR, fellowship by Govt. of India, New Delhi in 1999.

►Awarded 'Gold Medal' for securing first position in M.Sc. in 1999 by Nagpur University.

Some selected publications (Last 5years only):

1. Ansie Martin and **Angshuman Sarkar**, Epithelial to Mesenchymal transition, eIF2α phosphorylation and Hsp70 expression enable greater tolerance in A549 cells to TiO_2 over ZnO nanoparticles, **2018,** *Scientific Reports* (Accepted).

2. Ansie Martin and **Angshuman Sarkar**, Cellular migration as a Stress Relieving Strategy to Nanotoxicology, **2018**, *Int J cell Sci & Mol Biol*. 2018; 4(2): 555634. DOI: 10.19080/IJCSMB.2018.04.555634002.

3. Joshi RS, Mukherjee DD, Chakrabarty S, Martin A, Jadhao M, Chakrabarti G, **Sarkar A**, Ghosh SK. Unveiling the Potential of Unfused Bichromophoric Naphthalimide to Induce Cytotoxicity by Binding to Tubulin: Breaks Monotony of Naphthalimides as Conventional Intercalators. *J Phys Chem B.,* **Mar 21, 2018**. doi: 10.1021/acs.jpcb.7b10429.

4. Ansie Martin and **Angshuman Sarkar**, Overview on biological implications of metal oxide nanoparticle exposure to human alveolar A549 cell line. *Nanotoxicology*, 11(6):713-724, 2017.

5. Akriti Rastogi, **Angshuman Sarkar**, Dibakar Chakrabarty, Partial purification and identification of a metalloproteinase with anticoagulant activity from Rhizostoma pulmo (Barrel Jellyfish), *Toxicon*, 132, 29-39, 2017.

6. Jigni Pathan, Sukanta Mondal, **Angshuman Sarkar**, Dibakar Chakrabarty, Daboialectin, a C-type lectin from Russell's viper venom induces cytoskeletal damage and apoptosis in human lung cancer cells in vitro *Toxicon*, 127, 11-21 2017.

7. G. Ravindran, D. Chakrabarty and A. Sarkar. Cell specific regulation of p53 mRNA expression induced by cadmium. *Animal Cells and Systems* **(TACS) Dec. 2016,** http://dx.doi.org/10.1080/19768354.2016.1267041**.**

8. C. Chanda, **A. Sarkar**, D. Chakrabarty, Thrombolytic protein from cobra venom with anti-adhesive properties. *Arch. Biochem Biophys*. **2016 Jan 10; 590:20-26**.

9. J. Pathan, A Martin, R. Chowdhury, D. Chakrabarty **A. Sarkar**, Russell's viper venom affects regulation of small GTPases and causes nuclear damage. *Toxicon*. **2015 Dec 15;108:216-25**.

10. G. Ravindran, D. Chakrabarty and **A. Sarkar**; Cadmium toxicity alters mRNA expression of Rho-like genes in A549 cell line. *Journal of Cell and Molecular Biology*, Haliç University Press Publication, **Vol. 11 (1 & 2):13-20, 2013**.

11. C. Chanda, A**. Sarkar**, S. Sistla, and D. Chakrabarty; Anti-platelet activity of a three-finger toxin (3FTx) from Indian monocled cobra (*Naja kaouthia*) venom. *Biochem Biophys Res Commun*. 2013 Nov 22; 441 (3):550-4. doi: 10.1016/j.bbrc.2013.10.125. Epub. **2013 Oct 30.**